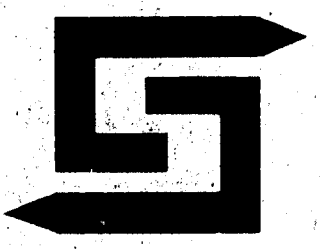

SIGNATRON®

SECURITY CLASSIFICATION OF THIS PAGE (When Data Entered)

REPORT DOCUMENTATION PAGE

READ INSTRUCTIONS BEFORE COMPLETING FORM

1. REPORT NUMBER: Report No. ECOM-76-8085-1	2. GOVT ACCESSION NO.
3. RECIPIENT'S CATALOG NUMBER	
4. TITLE (and Subtitle): Adaptive Antenna Control	5. TYPE OF REPORT & PERIOD COVERED: Interim, 25 Jun - 25 Dec 1976
6. PERFORMING ORG. REPORT NUMBER: A212	
7. AUTHOR(s): Peter Monsen, Steen Parl, John N. Pierce	8. CONTRACT OR GRANT NUMBER(s): DAAB07-76-C-8085
9. PERFORMING ORGANIZATION NAME AND ADDRESS: Signatron Inc., Lexington, MA	10. PROGRAM ELEMENT, PROJECT, TASK AREA & WORK UNIT NUMBERS: 1X763707D051702
11. CONTROLLING OFFICE NAME AND ADDRESS: US Army Electronics Command, ATTN: DRSEL-NL-RM-3, Fort Monmouth, NJ 07703	12. REPORT DATE: May 1977
	13. NUMBER OF PAGES
14. MONITORING AGENCY NAME & ADDRESS (if different from Controlling Office)	15. SECURITY CLASS. (of this report)
	15a. DECLASSIFICATION/DOWNGRADING SCHEDULE

16. DISTRIBUTION STATEMENT (of this Report)

Approved For Public Release; Distribution Unlimited

17. DISTRIBUTION STATEMENT (of the abstract entered in Block 20, if different from Report)

18. SUPPLEMENTARY NOTES

None

19. KEY WORDS (Continue on reverse side if necessary and identify by block number)

Troposcatter	Coupling Loss
Communication	Antenna
Angle Diversity	Beam Steering

20. ABSTRACT (Continue on reverse side if necessary and identify by block number)

The Adaptive Antenna Control (AAC) program seeks to improve the performance and availability of DOC troposcatter and diffraction links by means of adapting the antenna response to compensate for variations in the angle of arrival of the received radio signal. Particular emphasis is to be placed on AAC techniques which mitigate aperture-to-medium coupling loss. The program consists of a study phase, the development of AAC equipment, and a test phase. This interim technical report summaries the program activities

DD FORM 1 JAN 73 1473 EDITION OF 1 NOV 65 IS OBSOLETE

UNCLASSIFIED

SECURITY CLASSIFICATION OF THIS PAGE (When Data Entered)

20. Abstract (Continued)

during the first 6 months of the 18 month contract effort. The major accomplishments in this initial period were

identification of vertical angle diversity as the most cost and performance effective AAC technique for troposcatter systems.

identification of an electronically controlled movable feedhorn system as the most effective method of tracking angle of arrival variations in trans-horizon systems dominated by diffraction propagation.

development of a comprehensive troposcatter computer model for prediction of multipath spread, aperture to medium coupling loss, and angle diversity parameters.

The report presents the theoretical basis for the troposcatter model and presents results of multipath and aperture to medium coupling loss calculations. Experimental results, particularly for C-band systems where the multipath spread is small, are shown to be subject to large measurement errors. Coupling loss calculations agree well with experimental results however the absence of empirical data on the boresight/horizon angle of existing DCS antenna system provides a significant ambiguity.

Angle diversity augmentation is shown to be a superior approach over additional space diversity to reduce coupling loss when existing systems are converted to higher carrier frequencies. Combining techniques for angle diversity are discussed for both analog and digital systems. Performance considerations are addressed for the selected AAC technique for both diffraction and troposcatter systems.

SIGNATRON, Inc. (617) 861-1500
12 Hartwell Avenue
Lexington, Massachusetts 02173 TWX: 710-326-6323

(12)

(9) INTERIM TECHNICAL REPORT. NO. 1, 25 Jun — 25 Dec 76

(6) ADAPTIVE ANTENNA CONTROL

(15) DAAB07-76-C-8085

(14) A212

(12) 160 P.

December 22, 1976

(11) May 77

(10) Prepared By:

Peter P. Monsen,
Steen S. Parl
John N. Pierce

(16) 1X763707D345

(17) 17

(18) ECOM

(19) 76-8085-1

SIGNATRON, Inc.
12 Hartwell Avenue
Lexington, Massachusetts 02173

DDC RECEIVED SEP 21 1977 A

ACCESSION for
NTIS White Section
DDC Buff Section
UNANNOUNCED
JUSTIFICATION
Letter on file
BY
DISTRIBUTION/AVAILABILITY CODES
Dist. AVAIL. and/or SPECIAL
A

DISTRIBUTION STATEMENT A
Approved for public release;
Distribution Unlimited

Prepared For:

US Army ECOM
Ft. Monmouth
Eatontown, N.J.

323 760

Communications, Control and Information Systems

AD

TABLE OF CONTENTS

TABLE OF CONTENTS (Cont'd)

LIST OF ILLUSTRATIONS

LIST OF ILLUSTRATIONS (Cont'd)

LIST OF TABLES

SECTION 1

INTRODUCTION

This report is the first interim technical report under the Adaptive Antenna Control program, Contract No.DAAB07-76-8-85. The Adaptive Antenna Control (AAC) program is under the contract management of the Project Manager for DCS (Army) Communications Systems, Ft.Monmouth, New Jersey. ECOM, Ft.Monmouth, N.J. is responsible for technical direction of the program. SIGNATRON, Inc. of Lexington, MA with RF Systems, Inc. of Cohassett as a major subcontractor have the responsibility for executing the program tasks. This report describes the AAC program, summarizes system analysis work to date, and projects the scope and direction of future efforts. Hardware descriptions and specific design information for the implementation tasks will be provided in the AAC design report due 22 January 1977.

1.1 Need for Adaptive Antenna Control

Transhorizon radio systems within the Defense Communications System (DCS) employ both tropospheric scatter and diffraction over obstacles as primary propagation modes. Troposcatter systems suffer from short term multipath fading and long term depressions in median received signal level. The short term fading can be alleviated by the use of additional diversity. Angle of arrival diversity represents an attractive method of realizing this additional diversity as it requires no additional frequencies or antennas. Depression of the median received signal is primarily due to substandard refractive index gradients which bend the radio wave upward and increase the scattering angle and hence the path loss. This condition cannot be alleviated by a change in antenna pointing angle as the change in refractive index causes more upward bending of the radio wave but maintains the same take-off angle. Note that downward bending of the radio wave resulting

from superrefractive or ducting conditions is not a problem on troposcatter circuits because any decrease in signal due to earth blockage is more than compensated for by the decreased path loss due to a decrease in the scatter angle.

For transhorizon radio links using diffraction over an obstacle (knife-edge), superrefractive conditions are the primary cause of signal outages. A knife-edge diffraction path is characterized by either the absence of short term fading due to scattering or milder forms of short term fading due to multiple path interference conditions. Thus outages tend to be long term and are primarily produced by downward bending of the radio wave and resulting earth blockage during superrefractive conditions.

Experimental tests on a DCS diffraction system have shown these outages to exist and because of their long term nature, they represent a serious deterioration in link availability. Clearly an automatic method of varying the transmit and receive antenna beams in elevation could provide protection against these outage conditions. On the other hand the absence of a significant multipath fading phenomenon on most diffraction links suggest that additional diversity in the form of angle diversity is not of appreciable value provided adaptive antenna pointing can be accomplished.

The DCS tropospheric scatter radio systems may be faced with requirements to operate at higher carrier frequencies in certain host countries. Normally, for wide beam antennas and short paths, the additional antenna gain at a higher frequency more than offsets the increased path transmission loss. However, for longer paths and generally narrower beamwidths, at higher frequencies the aperture to medium coupling loss will reduce the effective antenna gain and a net loss will result after frequency conversion.

Adaptive antenna techniques offer the potential of mitigating coupling loss and meeting system performance requirements at higher frequencies on existing links.

1.2 AAC Approach for DCS Application

As a result of the above considerations, an adaptive antenna control system has been proposed which utilizes angle diversity on DCS troposcatter systems and antenna beam steering on DCS diffraction systems. The angle diversity system will employ dual polarized feedhorns to produce vertically displaced antenna beams which intersect at or near the half power beamwidth points. In this manner, the scattering angle and hence the path loss of the elevated beam is minimized while maintaining a significant decorrelation between the received diversity signals. For example a 168 mile path with 28' antennas at 4.46 GHz has a relative loss of 1.7 dB in the elevated beam and power correlation coefficient of 0.52. An analysis shows that almost all DCS troposcatter systems will realize significant improvement from the addition of angle diversity. In some cases the additional angle of arrival diversity may complement the existing quadruple diversity operation to produce approximately 8th order diversity in a dual space/dual frequency/dual angle configuration. In other applications dual frequency diversity systems may be upgraded to quad diversity performance by using a dual frequency/dual angle configuration. A reduction to this configuration from a conventional duplex four-frequency, four-antenna quad diversity results in the savings of two antennas which might prove to be an attractive alternative for certain links. Similarly a reduction to dual space/dual angle provides nearly quadruple diversity performance and saves two frequencies.

Performance predictions for classes of DCS links must be performed in the study as angle diversity (AD) does not yield an exact doubling of

the diversity order due to loss in the elevated beam and correlation between diversity signals. The resulting performance improvement for defined classes and the cost analysis for AD implementation will determine the cost effectiveness of this approach for each class.

For DCS diffraction systems, a mechanical means of providing antenna movement and an electronic adaptive control system for optimally pointing the antenna is proposed. Electronic steering has been judged cost ineffective because of the difficulty of providing amplitude and/or phase control of large transmitter powers (~10 kW). A mechanical design of a weatherized moveable feedhorn structure is under development by RF Systems. The AAC program will include the design of an adaptive antenna aiming system and an analysis thereof.

Within the AAC program, which is developing an angle diversity feed system and the application guidelines for using angle diversity to enhance the performance of digital troposcatter in a frequency congested environment, it is desirable and convenient to also address the effects of aperture medium of coupling loss in the S and C frequency bands in order to extend the usable range of troposcatter systems operating in these bands (e.g., TRC-170). Under the subject program, troposcatter tests to be performed at RADC for angle diversity present an opportunity to obtain empirical data to extend the theoretical model of coupling loss to higher frequencies and develop candidate techniques capable of mitigating coupling loss. Because of the likelihood that angle diversity will be used in the DCS, the suitability of angle diversity versus other candidate techniques such as multiple apertures also will be addressed to determine whether angle diversity is superior to other techniques in a joint cost performance tradeoff. As such, calculations for DCS links are

required to determine the resultant change in required system gain and system cost after frequency conversion and the introduction of each candidate technique in order identify the optimum improvement technique.

1.3 AAC Advanced Development Model

The Advanced Development Model (ADM) includes the design of an adaptive antenna control system with mechanical movement for diffraction systems and the implementation of an angle diversity subsystem for troposcatter systems. The adaptive antenna aiming system utilizes a servomechanism for antenna control and a straightforward adaptation algorithm to maximize the received power at each link terminal. It is envisioned that control information would be transmitted over an order wire channel primarily to preclude both antannas from trying to adapt simultaneously.

The ADM for a troposcatter system consists of a vertical array of two dual polarized feedhorns, additional waveguide and RF down converters for each additional diversity, and a predetection combiner for digital channel applications. The PDC combines up to four digital angle diversity signals and considers the presence of multipath by weighting each angle diversity signal with a three tap transversal filter. The output of the PDC is combined with the digital modem combination of the dual space/dual frequency diversity channels to provide up to eight order diversity. The PDC will be designed for possible operation with any linear modulation modem type, e.g., 2 PSK, QPSK, Staggered QPSK,MSK, and provides optimum combining when the modem interfaces the PDC with a one bit error signal. Although this error signal interface should be possible for any of the linear modulation modem types, the PDC can be configured in a suboptimum mode for combining without any interface signals between the modem and PDC.

The PDC concept is based on technology developed during the Megabit Digital Troposcatter Subsystem (MDTS) program and the PDC design includes 4 card types identical to those used in the MDTS modem. Interface and excellent operation of the PDC with the MDTS modem is guaranteed by the functional and design similarity between the two systems.

1.4 AAC Field Test

The RADC test bed (Youngstown-Verona, NY) to be used in the field test is a 168 mile tropospheric scatter radio system. We propose to fabricate a simplex angle diversity system using two vertical feedhorns at each of the two receiver (Verona) test link antennas. The maximum diversity complement achievable under this configuration will be eighth order for a dual space/dual frequency/dual angle (2S/2F/2A) system. A Predetection Combiner will be fabricated to provide the diversity combining function for the digital tests.

It is planned that three MDTS modems will be supplied for the digital tests. For a 2S/2F/2A configuration, one modem is required for transmission*, one modem is required to combine the conventional quad diversity channels while the PDC combines the four additional angle diversity channels, and the third modem is used at the receiver for a simultaneous comparison test of quad diversity without angle diversity.

In addition to the digital transmission tests, extensive testing of channel characteristics such as multipath spread, diversity channel correlation, aperture-to-medium coupling loss, and receiver power statistics is planned. These tests will serve to validate the performance model of the AAC Advanced Development Model and they will also be used to improve and validate the troposcatter

---

* This modem can be an MDTS modulator since reception is not required at Youngstown.

channel model. Of particular interest is an accuract prediction model for multipath spread and coupling loss which includes an assessment of the variability of these quantities as well as the median values. An examination has also begun to determine the availability of meteorological data which could be used to relate atmospheric measurements to communication parameter prediction.

Some of the primary goals of the test program include

- verification of the channel characteristics prediction model
- verification of the angle diversity performance prediction model
- measurement of channel parameters including aperature-to-medium coupling loss
- establishing the operational capability of an AD troposcatter system
- determination of equipment parameter modifications in the AAC model to improve performance and cost effectiveness
- establishing the interface capability of the AAC model with digital equipments.

The schedule for the accomplishment of the AAC tasks and field tests outlined in this section is shown in Fig. 1.1.

1.5 Report Summary

A theoretical model for troposcatter communication has been developed as the basis for prediction of multipath spread, angle diversity communication parameters, and aperture-to-medium coupling loss. The model derives from Tartarskii's original work on scattered signals due to random variations in the refractive index in the common volume defined by the antenna beams. Under a decorrelation assumption for the refractive index correlation function and a limitation on the signal bandwidth, the uncorrelated scattering

AAC

MILESTONES A212

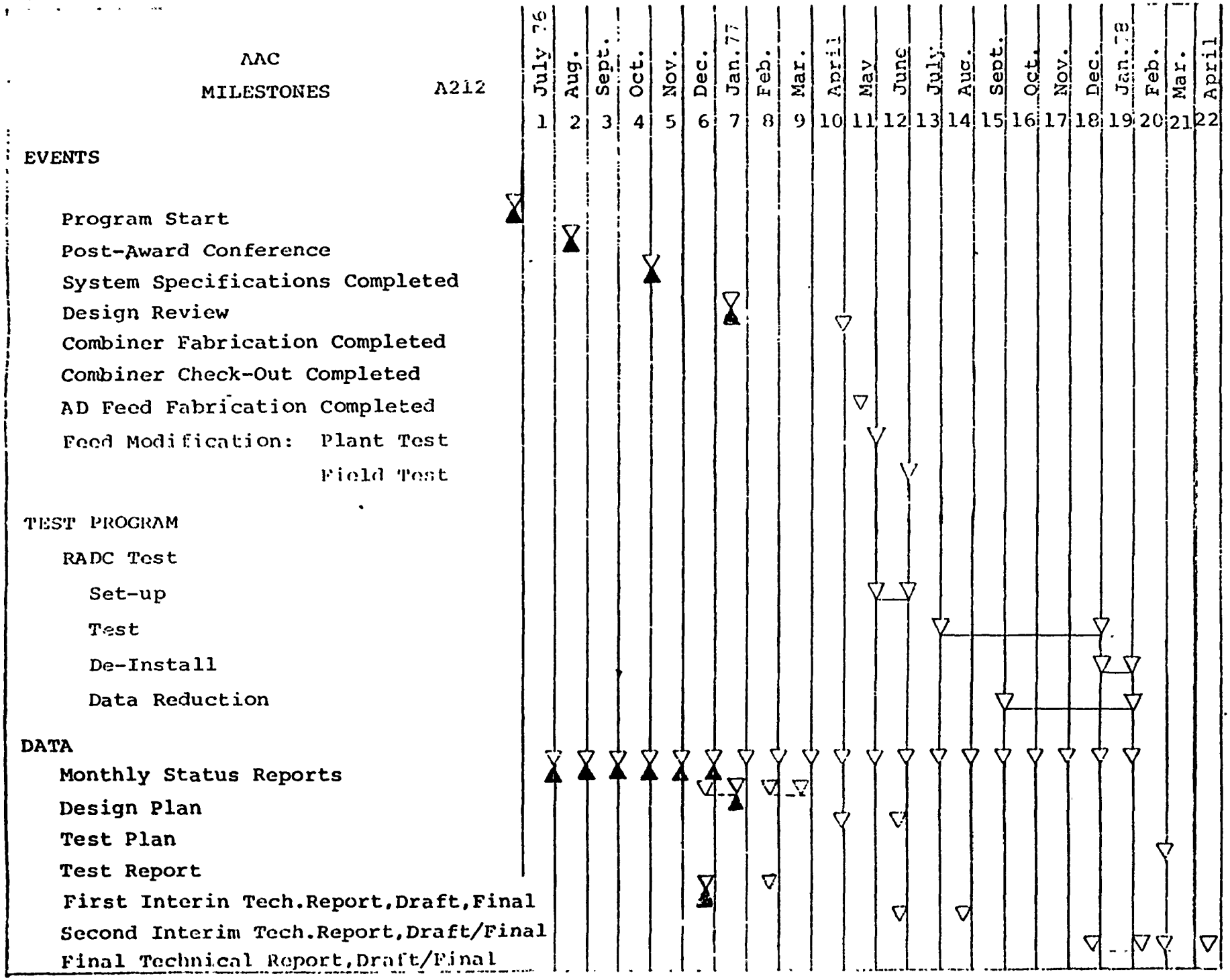

Figure 1.1

Gaussian communication model can be used to represent signal transfer over troposcatter paths. The result is that a set of L diversity channels is completely characterized by the set of cross-channel multipath profiles $Q_{\ell m}(t)$ defined by

$$\overline{h_\ell(t)h_m^*(\tau)} = \delta(t-\tau)\ Q_{\ell m}(t)$$

where $h_\ell(t)$ and $h_m(t)$ are the random troposcatter impulse responses. for the ℓth and mth diversity, respectively. For an angle diversity system where there exists significant correlation only between the main and squinted beam, three profiles; Q_{11} for the main beam, Q_{22} for the squinted beam, and Q_{12} for the product beam, are required. Section 2 presents the theoretical basis and the volume integration formulation for the determination of the profile function $Q_{\ell m}(t)$. Also in this section, formulas and asymptotic results for multipath spread and coupling loss are derived.

Accurate prediction of channel parameters in accordance with the theory of Section 2 requires an integration over the scattering volume of the antenna patterns and the refractive index spectrum. An exact calculation method for a specific refraction profile is used as the basis for the numerical integration procedure. A description of the refraction profile model and the integration geometry begins Section 3. Following this description we present and interpret computation results for multipath spread and coupling loss. Much of the discrepancy between predicted and measured multipath spread is shown to a result of measurement inaccuracy. Transmitter filter effects and prober processing inaccuracies are the most significant contributors and their effects can be dramatic when measuring small multipath widths ($2\sigma < 100$ nanoseconds). The MDTS field test data was used to compare predicted and measured multipath spreads and the results of Section 3 serve to validate the utility

of the prediction model used. Following the multipath spread calculations and data analysis, a similar set of coupling loss computations and comparison with previous empirical results has been initiated and described in Section 3. For zero take-off angles of the antenna beams the volume integration method generally predicts larger coupling loss then available semi-empirical techniques. Better agreement results when the volume integration method assumes positive take-off angles. Antenna take-off angles (the angle between the antenna boresight and the local horizon) are shown to be a significant link parameter which needs to be accurately specified for useful performance prediction. In the absence of this information it is not clear whether the prediction model is imprecise or incorrect link parameter specification is responsible for the inaccuracies. Also in this section an assessment of multi-feedhorns (angle diversity) vs. multi-antennas (space diversity) for the mitigation of aperture-to-medium coupling loss is presented. The angle diversity approach is shown to have a clear superiority from a cost/performance standpoint.

In Section 4 the methods of adaptive antenna control are introduced and evaluated. An adaptive mechanical feedhorn arrangement is recommended for diffraction links and a dual vertical feedhorn with angle diversity combining is recommended for troposcatter links. An evaluation of the potential utility of angle diversity in the DCS is provided. As an approximate guide, angle diversity produces a significant improvement if the ratio of beamwidth to scattering angle is less than 0.875. This criterion is satisfied by most DCS troposcatter systems. This section concludes with a summary of previous adaptive antenna control experiments.

Specific implementation factors for adaptive antenna control on both diffraction and troposcatter links are presented in Section 5. Diversity combiner structures for both analog and digital applications are also discussed. In Section 6, performance improvement considerations are addressed for the diffraction path. Variations in take-off angle due to fluctuations in the refractive index gradient are proportional to path distance and independent of obstacle height. For a 175 nautical mile path, realistic refractive index variations could produce a change of $\pm \frac{1}{2}^{\circ}$. Thus a fixed antenna beam system with a beamwidth less than or equal to $\frac{1}{2}^{\circ}$ could experience a complete loss of signal. The performance of angle diversity with analog transmission techniques is computed for the RADC test link. Finally, digital performance factors are considered and the proposed method of computing modem performance is indicated. A major portion of the study program within the next reporting period will entail the development of modem performance characteristics for typical and projected angle diversity links.

SECTION 2

TROPOSCATTER COMMUNICATION MODEL

In this section we develop the theoretical basis for a troposcatter communication model which will be used to relate atmospheric parameters to communication parameters and to relate system performance to the communications parameters. The atmospheric parameters of interest are those available in conventional radio-sonde measurement techniques, i.e., air pressure, temperature, and water vapor pressure as a function of height. These parameters can in turn be related to the statistical description of the refractive index fluctuations. This statistical description is used to develop the communication parameters of an equivalent random linear filter. This section concerns itself with the statistical description of this filter. Numerical computation of communication parameters such as multipath spread and antenna coupling loss are presented in Section 3. In Section 6 the methods of using these parameters to compute communication performance is addressed. The relationship between atmospheric and communication parameters and the techniques for obtaining meteorological information will be dealt with in greater detail in subsequent reports. Although the communications model is applicable to both analog and digital systems, emphasis is placed on the digital system application since the multipath effects are more pronounced on the generally wider bandwidth digital systems.

2.1 Uncorrelated Scatter (US) Channel

The troposcatter channel, viewed as a black box, has an input-output relationship identical to a randomly time-varying linear filter. Because the time variation is very slow (~ 1 Hz) compared to the large signal bandwidths (1-20 MHz), performance can be determined from an ensemble description of an equivalent random linear filter. An ensemble member characterization is shown in Fig. 2.1

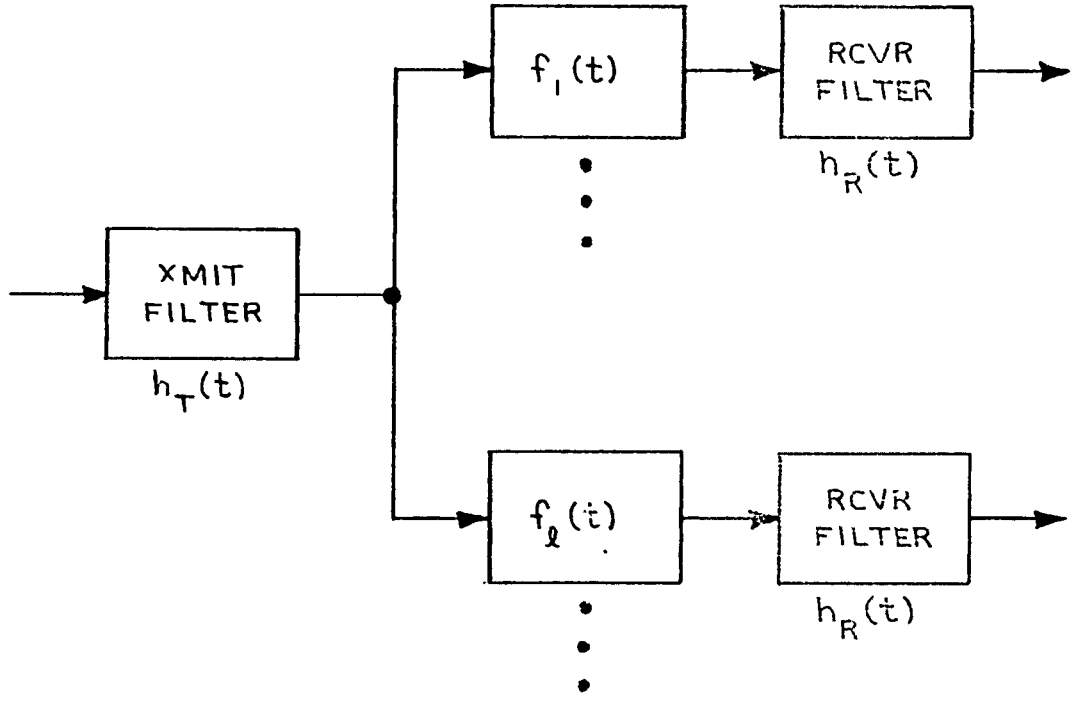

$$h_\ell(t) = h_T(t) \circledast f_\ell(t) \circledast h_R(t) \,, \quad \circledast = \text{CONVOLUTION}$$

Fig. 2.1 Troposcatter Communication Model

in terms of fixed transmit and receive filters and a random filter representing the troposcatter medium.

The composite filter is the threefold convolution*

$$h_\ell(t) = h_T(t) \circledast f_\ell(t) \circledast h_R(t) \tag{2.1}$$

where the symbol $\circledast$ denotes convolution. If we define the combined fixed filter

$$h_{TR}(t) = h_T(t) * h_R(t)$$

then

$$h_\ell(t) = \int_{-\infty}^{\infty} h_{TR}(t-u)\ f_\ell(u)\ du.$$

The impulse response $f_\ell(t)$ represents the random tropospheric scatter channel. An important communications model for this channel is the complex Gaussian uncorrelated scatter (US) channel [2.1]. This model defines $f_\ell(u)$ to be zero-mean Gaussian with uncorrelated scattering for different transmission delays, i.e.,

$$\overline{f_\ell(t)\ f_m^*(t')} = \delta(t-t')\ Q_{\ell m}(t) \tag{2.2}$$

where $Q_{\ell m}(t)$ is defined as the cross channel multipath profile. Note that for this model the composite filter has second moment

$$\overline{h_\ell(t)h_m^*(t')} = \int_{-\infty}^{\infty} h_{TR}(t-u)du \int_{-\infty}^{\infty} h_{TR}^*(t'-v)\ f_\ell(u) f_m^*(v)dv$$

$$= \int_{-\infty}^{\infty} h_{TR}(t-u)\ h_{TR}^*(t'-u)\ Q_{\ell m}(u)\ du.$$

*Complex notation to represent real bandpass signals is used throughout the report. The real impulse response is $\mathrm{Re}\{h_\ell(t)e^{j2\pi f_o t}\}$ where f_o is the carrier frequency which is assumed to be much larger than the signal bandwidth.

If the fixed filters have a maximum bandwidth* of B Hz, a sampled data representation of the composite filter is

$$h_\ell(t) = \sum_{i=-\infty}^{\infty} h_{i\ell} \text{ sinc } (t/\tau - i)$$

where

$$\tau < 1/B$$

$$h_{i\ell} = \frac{1}{\tau} \int_{-\infty}^{\infty} h_\ell(t) \text{ sinc } (t/\tau - i)\, dt = h_\ell(i\tau)$$

and

$$\text{sinc } x = \sin(\pi x)/\pi x.$$

From Nyquist's Theorem, the samples $h_{i\ell}$ are a complete representation of the multichannel filter. A complete statistical description of the communication channel is thus obtained if $h_{i\ell}$ is described statistically. A complete description for the special case of zero mean Gaussian samples is given by the second moment $\overline{h_{i\ell} h^*_{jm}}$. For the US model, this seccnd moment is

$$\overline{h_{i\ell} h^*_{jm}} = \int_{-\infty}^{\infty} h_{TR}(i\tau - u) h^*_{TR}(j\tau - u)\, Q_{\ell m}(u)\, du \qquad (2.3)$$

and for typical transmitter and receiver filters which do not significantly distort the information signal, the width of $h_{TR}(\cdot)$ is such that when $i \neq j$ the value of the correlation function is much smaller than when $i = j$. Thus to a good approximation

$$\overline{h_{i\ell} h^*_{jm}} \doteq \delta_{ij} \int_{-\infty}^{\infty} |h_{TR}(i\tau - u)|^2 Q_{\ell m}(u)\, du.$$

We will now show that for Gaussian distributed refractive index fluctuations, if a condition on the decorrelation of these fluctuations is met, the troposcatter channel is well approximated by the

* A two sided bandwidth B is used with complex notation corresponding to the RF bandwidth.

uncorrelated scatter channel and the cross channel multipath profile $Q_{\ell m}(t)$ is expressible as a volume integral with respect to the combined antenna patterns and the spectrum of the refractive index fluctuations.

Consider transmission through a particular troposcatter channel with the geometry shown in Fig. 2.2. At a scattering point $\underline{r}'$, which can be considered to be in the far field with respect to both the transmitter (T) and receiver (R), we assume an incident electric field $A_o(\underline{r}')e^{jk\underline{m}\cdot\underline{r}'}$ which is a plane wave with progration vector $k\,\underline{m}$ where $k = 2\pi f_o/c = 2\pi/\lambda$, f_o = carrier frequency, c = speed of light in the medium, and λ = wavelength. A fraction of the energy associated with the incident field is scattered in the direction $\underline{n}$ toward the receiver. The scattering mechanism can be attributed to random spatial variations in the refractive index at the point $\underline{r}'$. Let $n_1(\underline{r}')$ be the random component of the refractive index, viz.,

$$n(\underline{r}') = \bar{n}(\underline{r}') + n_1(r'),$$

then in the Appendix following we show a derivation first developed by Tatarski [2.2.] that the electric field at the receiver antenna is given by

$$e(\underline{r}) = \frac{k^2}{2\pi r}\int_V A_o(\underline{r}')n_1(\underline{r}')\, e^{jk(|\underline{r}-\underline{r}'| + \underline{m}\cdot\underline{r}')}\, d^3r'. \quad (2.4)$$

Troposcatter antennas utilize a receiving aperture typically in the form of a parabolic reflector with a feedhorn placed at the focal point. The mean field at the receiver is obtained by integrating over the receiving aperture Σ

$$E(\underline{r}) = \frac{1}{\Sigma}\iint_{\Sigma} e(\underline{r} + \underline{u})\, d\xi d\eta,$$

$$\underline{m} = \frac{\underline{r}' - \underline{s}}{|\underline{r}' - \underline{s}|}$$

$$\underline{n} = \frac{\underline{r} - \underline{r}'}{|\underline{r} - \underline{r}'|}$$

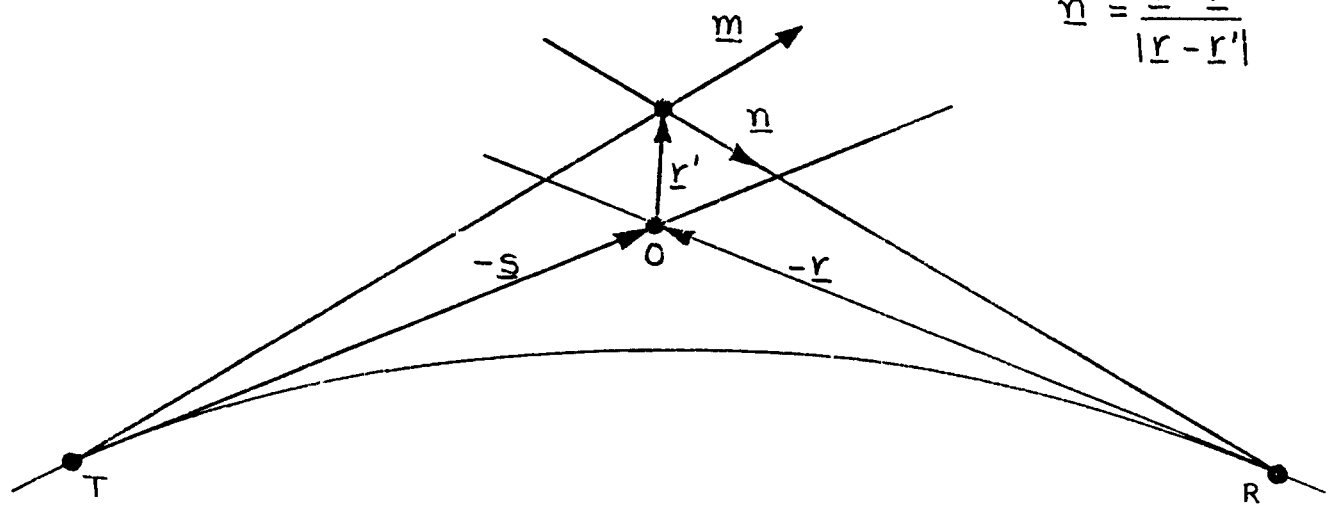

Fig. 2.2 Troposcatter Geometry

where $\underline{u}$ is in the plane of the aperture and points to the differential surface element $d\xi d\eta$. Since $r \gg u$, the effect of changing r solely impacts the exponent in (2.4). A useful Taylor series expansion is

$$|\underline{x}+\underline{u}| = x + \frac{1}{x}\,\underline{x}\cdot\underline{u} + \frac{1}{2x}\left[u^2 - \frac{1}{x^2}\,(\underline{u}\cdot\underline{u})^2\right] + \ldots$$

and if

$$\frac{ku^2}{2x} = \frac{\pi u^2}{\lambda x} \ll \pi,$$

the exponential term is well approximated by

$$e^{jk|\underline{x}+\underline{u}|} \doteq e^{jk(x + \frac{1}{x}\,\underline{x}\cdot\underline{u})} \tag{2.5}$$

If D is the receiving aperture diameter, it is easy to verify that

$$\frac{D^2}{\lambda r} \ll 1$$

for practical troposcatter parameters. The mean field is thus

$$E(\underline{r}) = \frac{k^2}{2\pi r}\int_V A_o(\underline{r}')n_1(\underline{r}')\; e^{jk(|\underline{r}-\underline{r}'|+\underline{m}\cdot\underline{r}')}d^3r'\cdot f_1(\underline{n}) \tag{2.6}$$

where

$$f_1(\underline{n}) = \frac{1}{\Sigma}\iint_\Sigma e^{+jk\underline{n}\cdot\underline{u}}\,d\xi d\eta \tag{2.7}$$

is the normalized antenna gain pattern at the receiver. In (2.6) we have suppressed the time dependence in the notation. Let $U(\underline{r}',\xi)$ represent a three dimensional delta function for the delay ξ from the transmit antenna to the source point $\underline{r}'$ and down to the receive antenna, i.e.,

$$U(\underline{r}',\xi) = \delta[|\underline{r}'-\underline{s}| + |\underline{r}-\underline{r}'| - c\xi].$$

The received field at time t, $E(\underline{r}, t)$, for an excitation $A_o(\underline{r}',t)e^{j\underline{m}\cdot\underline{r}'}$ at the source point is the superposition integral

$$E(\underline{r},t) = \frac{k^2}{2\pi r}\int_{-\infty}^{\infty} d\xi \int_V U(\underline{r}',\xi)A_o(\underline{r}',t-\xi)f_1(\underline{n})n_1(\underline{r}')e^{jk(|\underline{r}-\underline{r}'|+\underline{m}\cdot\underline{r}')}d^3r' \ .$$

The time dependence of $n_1(\underline{r}')$ is ignored since the refractive index does not change over the range of differential delays of significance in the inside integral. Since the system is linear we can combine the transmitter and receiver filters in the expression for A_o. Thus we define

$$A_o(\underline{r}',t) = \sqrt{\frac{P_T G_T}{4\pi s^2}}\ f_o(\underline{m})\ h_{TR}(t) \qquad (2.8)$$

where

P_T = transmitted power

G_T = transmitter antenna maximum power gain

s = mean distance from transmitter to common volume

$f_o(\underline{m})$ = normalized transmitter antenna pattern (see Eq. (2.7))

$h_{TR}(t) = h_T(t) \circledast h_R(t)$ = combined fixed filter response.

In an angle diversity system with one transmit beam and multiple receive beams, the mean field for the ℓth diversity is given by

$$E_\ell(\underline{r},t) = \frac{k^2}{2\pi r}\sqrt{\frac{P_T G_T}{4\pi s^2}}\int_{-\infty}^{\infty} h_{TR}(t-\xi)\,d\xi$$

$$\int_V U(\underline{r}',\xi)f_o(\underline{m})f_\ell(\underline{n})n_1(\underline{r}')e^{jk(|\underline{r}-\underline{r}'|+\underline{m}\cdot\underline{r}')}d^3r' \ . \qquad (2.9)$$

We have ignored the slight difference between r and the actual distance to an elevated common volume in the denominator of (2.9).

Also, the path length d is approximately

$$d = r + s. \tag{2.10}$$

Since (2.9) represents the mean field at the receiver for impulse function excitation, we must multiply by the antenna aperature area to obtain the sampled data impulse response. Since the aperature area is related to the receive antenna maximum power gain by $G_R = 4\pi\Sigma/\lambda^2$, we have

$$h_{i\ell} = \sqrt{\lambda^2 G_R/4\pi}\ \ E_\ell(\underline{r},\ i\tau)$$

where G_R is the receive antenna maximum power gain. For convenience let

$$P_o = \frac{P_T G_T G_R}{4\pi} = \text{free space received power per unit distance}$$

$$g_\ell(\underline{r}') = f_o(\underline{m})\, f_\ell(\underline{n}) = \text{normalized combined antenna pattern}$$

and define the smoothed volume integration in (2.9) by

$$\int_{-\infty}^{\infty} h_{TR}(i\tau-\xi)\,d\xi \int_V U(\underline{r}',\xi) \equiv \int_{V_i} \tag{2.12}$$

With these definitions, the sampled data impulse response is

$$h_{i\ell} = \frac{k\sqrt{P_o}}{2\sqrt{\pi rs}} \int_{V_i} g_\ell(\underline{r}')\, n_1(\underline{r}')\ e^{jk(|\underline{r}-\underline{r}'|+\underline{m}\cdot\underline{r}')}\, d^3r'. \tag{2.13}$$

The smoothed integration defined in (2.12) can be viewed as the weighted sum of scatter points which have transmission delays which roughly fall in the interval $[i\tau-\tau/2, i\tau+\tau/2]$. The weighting falls off as the transmission delay moves away from the midpoint $i\tau$.

The refractive index fluctuations can be reasonably approximated by a stationary zero-mean complex Gaussian process. The statistics of $h_{i\ell}$ are then completely specified in terms of the

refractive index correlation function

$$\overline{n_1(\underline{r}'+\underline{\rho})\ n_1^*(\underline{r}')} = \overline{\varphi(\underline{\rho})} \tag{2.14}$$

or its three dimensional Fourier transform, the refractive index spectrum

$$\Phi(\underline{k}) = \frac{1}{8\pi^3}\int_V \varphi(\underline{\rho})\ e^{-j\underline{k}\cdot\underline{\rho}}\ d^3\rho. \tag{2.15}$$

The correlation radius ℓ_o is defined as the radius beyond which $\varphi(\underline{\rho})$ is small compared to its maximum value.

The impulse response correlation function is

$$\overline{h_{i\ell}h_{jm}^*} = \frac{k^2 P_o}{4\pi\ r^2 s^2}\iint_{V_i V_j} g_\ell(\underline{r}')g_m^*(\underline{r}'')\varphi(r''-r')e^{jk\alpha}\ d^3r'd^3r'' \tag{2.16}$$

where

$$\alpha = |\underline{r}-\underline{r}'| - |\underline{r}-\underline{r}''| + \underline{m}(r')\cdot\underline{r}' - \underline{m}(\underline{r}'')\cdot\underline{r}''.$$

In order to reduce (2.16) further, we must either know the correlation function $\varphi(\underline{r}''-r')$ or some estimate of its correlation radius. We will show that the basis for the widely used uncorrelated scattering assumption is that the correlation radius satisfies

$$\ell_o << c/B\theta \text{ uncorrelated scatter assumption} \tag{2.17}$$

where θ is the scattering angle at the lowest point in the common volume.

Since $\theta << 1$ it follows that ℓ_o on the order of $<c/B$ satisfies the constraint, e.g., for a bandwidth of 10 MHz, the correlation radius must be on the order of 100 feet or less.

The smoothed integrals

$$\int_{V_i}\int_{V_i} \equiv \int_{-\infty}^{\infty} h_{TR}(i\tau-\xi_1)d\xi_1 \int_V U(\underline{r}_1', \xi_1) \int_{-\infty}^{\infty} h_{TR}(j\tau-\xi_2)d\xi_2 \int_V U(\underline{r}'', \xi_2)$$

reduce to two volume integrals

$$\int_{V_i}\int_{V_j} = h_{TR}\left(i\tau - x(\underline{r}')/c\right) \int_V h_{TR}\left(j\tau - x(r'')/c\right) ,$$

where x is the path distance through the source point,

$$x(\underline{r}') = |\underline{r}' - \underline{s}| + |\underline{r} - \underline{r}'| .$$

Introducing the change of variables

$$\underline{\rho} = \underline{r}'' - \underline{r}'$$

we have

$$\int_{V_i}\int_{V_j} = \int_V h_{TR}\left(i\tau - x(r')/c\right) \int_V h_{TR}\left(j\tau - x(\underline{r}' + \underline{\rho})/c\right) .$$

The distance parameter

$$x(\underline{r}'+\underline{\rho}) = |\underline{r}' + \underline{\rho} - \underline{s}| + |\underline{r} - \underline{\rho} - \underline{r}''|$$

can be reduced by using the expansion

$$|\underline{r}+\underline{u}| = \sqrt{r^2 + 2\underline{r}\cdot\underline{u} + u^2}$$

$$\doteq r\sqrt{1 + \frac{2\underline{r}\cdot\underline{u}}{r^2}} \doteq r + \underline{a}_r \cdot \underline{u}$$

where

$$\underline{a}_r = \underline{r}/r .$$

One finds

$$x(\underline{r}'+\underline{\rho}) \doteq |\underline{r}'-\underline{s}| + \underline{m}(\underline{r}') \cdot \underline{\rho} + |\underline{r} - \underline{r}'| - \underline{n}(\underline{r}') \cdot \underline{\rho}$$

$$= x(\underline{r}') + (\underline{m} - \underline{n}) \cdot \underline{\rho} \quad .$$

The second term is very small compared to the first and is of the order

$$|\underline{m}-\underline{n}| \; |\underline{\rho}| = \rho \sin \theta(\underline{r}') \doteq \rho \; \theta(\underline{r}') \doteq \rho\,\theta ,$$

where $\theta(r')$ and θ are the scattering angles at the source point r' and at the lowest point of the common volume, respectively.

Returning to the impulse correlation function, we have

$$h_{i\ell} h^*_{jm} = \frac{k^2 P_o}{4\pi r^2 s^2} \int_V h_{TR}\left(i\tau - x(\underline{r}')/c\right) g_{\ell}(\underline{r}') d^3 r'$$

$$\cdot \int_V h_{TR}\left(j\tau - x(\underline{r}')/c - \theta\rho/c\right) g_m^*(\underline{r}'+\underline{\rho}) \phi(\underline{\rho}) e^{jk\alpha} d^3\rho$$

Since the correlation distance is on the order of feet and the antenna beam pattern spans distances on the order of miles, it follows that in the second integral where $|\rho| < \ell_o$ we can make the approximation

$$g_m(\underline{r}' + \underline{\rho}) \doteq g_m(\underline{r}').$$

Also by using a Taylor series expansion as in (2.4), and since $\ell_o^2/\lambda r \ll 1$, we find we can reduce the exponent α as follows. Since

$$|\underline{r} - \underline{r}' - \underline{\rho}| \doteq |\underline{r} - \underline{r}'| - \underline{n} \cdot \underline{\rho}$$

and

$$\underline{m}(\underline{r}' + \underline{\rho}) \cdot (\underline{r}' + \underline{\rho}) \doteq \underline{m} \cdot (\underline{r}' + \underline{\rho}) ,$$

we have

$$\alpha \doteq |\underline{r}-\underline{r}'| - |\underline{r}-\underline{r}'-\underline{\rho}| + \underline{m}(\underline{r}') \cdot \underline{r}' - \underline{m}(\underline{r}' + \underline{\rho}) \cdot (\underline{r}' + \underline{\rho})$$

$$\alpha \doteq -\underline{n} \cdot \underline{\rho} + \underline{m} \cdot \underline{\rho} \ .$$

The correlation function becomes

$$\overline{h_{i\ell} h_{jm}^*} = \frac{k^2 P_o}{4\pi r^2 s^2} \int_V h_{TR}(i\tau - x/c) g_\ell(\underline{r}') g_m^*(\underline{r}') d^3 r'$$

$$\cdot \int h_{TR}(j\tau - x/c - \theta\rho/c) \phi(\underline{\rho}) e^{jk(\underline{m}-\underline{n})\cdot\rho} \, e^3\rho \qquad (2.18)$$

where x, $\underline{m}$, and $\underline{n}$ are functions of the source point $\underline{r}'$. Note in (2.18) that the second integral is a smoothed 3-dimensional Fourier transform similar to the refractive index spectrum defined in (2.15).

Now the uncorrelated scattering assumption states that the correlation radius satisfies

$$\ell_o << c/B\theta \ ,$$

hence in the second integral of (2.18) the terminal equipment impulse response varies over the delay range

$$\frac{\theta \ell_o}{c} << \frac{1}{B}$$

where B is the bandwidth. Since $h_{TR}(\cdot)$ is approximately constant over an interval small compared to a reciprocal bandwidth it can be taken outside of the second integral with the result

$$\overline{h_{i\ell} h_{jm}^*} = \frac{2\pi^2 k^2 P_o}{r^2 s^2} \int_V h_{TR}(i\tau - x/c) h_{TR}(j\tau - x/c) g_\ell(\underline{r}') g_m^*(\underline{r}') \cdot \Phi\left[k(\underline{m} - \underline{n})\right] d^3 r' \quad . \tag{2.19}$$

If we define

$$Q_{\ell m}(t) = \int U(\underline{r}', t) g_\ell(\underline{r}') g_m^*(\underline{r}') \Phi\left[k(\underline{m} - \underline{n})\right] d^3 r' \quad , \tag{2.20}$$

we can express the correlation function as

$$\overline{h_{i\ell} h_{jm}^*} = \frac{2\pi^2 k^2 P_o}{r^2 s^2} \int_{-\infty}^{\infty} h_{TR}(i\tau - t) h_{TR}(\tau - t) Q_{\ell m}(t) dt. \tag{2.21}$$

However, since (2.21) is identical in form to (2.3), it follows that $Q_{\ell m}(t)$ of (2.20) is the cross channel multipath profile defined in (2.2) for the uncorrelated scatter channel.

Thus we have established that for a refractive index correlation radius less than the ratio of the speed of light to the signal bandwidth, the uncorrelated scatter model is a good representation for troposcatter communication. Under ducting conditions or the presence of large atmospheric layers, there will be more correlation between adjacent delay cells with the result that intersymbol interference will not be as severe and implicit diversity gains will not be as large. However the ducting and large layer are typically associated with stronger received signals and thus are of less importance in predicting communication outage performance. Thus for the performance predictions to be developed in this effort, the US model with a cross channel multipath profile defined by (2.20) will be used throughout.

2.2 Troposcatter Parameters

The complex Gaussian uncorrelated scattering model for troposcatter communication is completely defined by the cross-channel multipath profile

$$\overline{f_\ell(t) f_\ell^*(t')} = \delta(t-t')\, Q_{\ell m}(t)$$

which was determined in the previous sub-section to have the form

$$Q_{\ell m}(t) = \frac{2\pi^2 k^2 P_o}{r^2 s^2} \int_V U(r', t)\, g_\ell(\underline{r}')\, g_m^*(\underline{r}')\, \Phi[k(\underline{m}-\underline{n})]\, d^3 r' \qquad (2.22)$$

where

$k = 2\pi/\lambda$, λ = wavelength

P_o = free space received power per unit distance

r = mean distance from common volume to receiver

s = mean distance from transmitter to common volume

$g_\ell(\underline{r}')$ = combined transmit/receive antenna gain characteristic for ℓth diversity channel, $g_\ell \leq 1$.

$\Phi(\cdot)$ = refractive index spectrum

$\underline{m}$ = unit vector in direction of transmit energy

$\underline{n}$ = unit vector in direction of scattered energy

$U(\underline{r}', t) = \delta(|\underline{r}'-\underline{s}| + |\underline{r}-\underline{r}'| - ct)$.

Some of the troposcatter communication parameters of interest to be computed from the cross-channel multipath profile are received signal power, 2σ multipath spread, and antenna coupling loss. The received power for the ℓth diversity channel is given by

$$P_\ell = \int_0^\infty Q_{\ell\ell}(t)\,dt$$

$$P_\ell = \frac{2\pi^2 k^2 P_o}{r^2 s^2} \int_V |g_\ell(\underline{r}')|^2 \, \Phi\,[k(\underline{m}-\underline{n})]\, d^3r' \qquad (2.23)$$

For convenience let $\ell = 1$ represent the main beam diversity branch in an angle diversity system. Then although P_1^{-1} is a measure of the absolute path loss, it will not be used in our calculations because it lacks the empirical factors present in NBS and other path loss prediction techniques. NBS Technical Note 101 [2.3] will be used for calculation of P_1^{-1}. However, the relative path loss P_1/P_ℓ determined from (2.23) will be a critical parameter in the assessment of the utility of vertical or horizontally displaced angle diversity beams. The signal-to-noise ratio for a digital system is defined as the mean received energy per bit divided the noise power in a 1 Hz bandwidth. The relationship between SNR_ℓ and the median P_ℓ in milliwatts is

$$SNR_\ell(dB) = 10 \log P_\ell + 1.6 - \left(N_F + F_L + R_B - 174\right) \qquad (2.24)$$

where

N_F = noise figure (dB)

F_L = receive antenna feeder loss (dB)

R_B = 10 log (r_B), r_B = bit rate in bits/second

1.6= dB factor converting median to mean for a Rayleigh channel .

For an analog system (2.24) defines the SNR in an RF channel bandwidth of R_BHz.

The 2σ multipath spread which determines the intermodulation distortion in an analog system and the intersymbol interference and implicit diversity in a digital system is defined by

$$2\sigma_\ell = 2\sqrt{\frac{1}{P_\ell}\int_0^\infty t^2 Q_{\ell\ell}(t)dt - \frac{1}{P_\ell^2}\left[\int_0^\infty tQ_{\ell\ell}(t)dt\right]^2} \qquad (2.25)$$

Antenna coupling loss results from an inability to collect all the scatter energy when high gain narrow beam antennas are used. Since in our definition of the combined antenna pattern $g_\ell(\underline{r}')$ the maximum gain is fixed at unity, the antenna coupling loss for the ℓth diversity branch is simply

$$C_{L\ell} = P_\ell / P_\ell (g_\ell = 1)$$

$$C_{L\ell} = \int_V |g_\ell(\underline{r}')|^2 \Phi[k(\underline{m}-\underline{n})]d^3r' / \int_V \Phi[k(\underline{m}-\underline{n})]d^3r' \qquad (2.26)$$

The refractive index spectrum to be used in these calculations is generally accepted [2.2, 2.4, 2.5] to have the form

$$\Phi[k(\underline{m}-\underline{n})] = C(z)|\underline{m}-\underline{n}|^{-n} k^{-n} \tag{2.27}$$

where $C(z)$ is a height variation which reflects the smaller mean square value of refractive index fluctuations in the thinner atmosphere at larger height values z. The unit vectors $\underline{m}$ and $\underline{n}$ have the dot product

$$\underline{m} \cdot \underline{n} = \cos \theta$$

where θ is the scatter angle at the point $\underline{r}'$. The magnitude of the vector $\underline{m} - \underline{n}$ is then

$$|\underline{m}-\underline{n}| = \sqrt{1-2 \cos \theta + 1} = 2 \sin \theta/2 \doteq \theta.$$

Thus Φ takes the form

$$\Phi = C(Z) (k\theta)^{-n} \tag{2.28}$$

The scatter parameter n is normally positive and thus its effect is to reduce the energy scatter from points with larger values of θ. Typical values of n range from unity to five with $n = 11/3$ the most commonly used.

2.3 Asymptotic Estimates

For the uncorrelated scattering channel with a refractive index spectrum of the form of (2.28), asymptotic estimates of multipath spread and coupling loss can be obtained in explicit form for the limiting case of small beamwidth. The main value of these estimates is to functionally determine the 2σ multipath spread and coupling loss C_L dependence on the effective earth radius factor K and the refractive index spectrum slope n.

The variability in 2σ and C_L can then be assessed from knowledge of the long term variations in K and n. The estimates are also useful for approximations to the actual value but for purposes of predicting median communication performance, the detailed numerical integration of the scatter volume as described in the next section is recommended for determining absolute values.

When the antenna beamwidths, $\beta_t=\beta_r=\beta$, are much smaller than the minimum scattering angle θ_o, the refractive index spectrum does not change significantly in the volume integration. The multipath profile and received power expressions become

$$Q_{\ell\ell}(t) = \frac{2\pi^2 k^{2-n}}{r^2 s^2} C_o \theta_o^{-n} \int_V U(\underline{r}',t)|g_\ell(\underline{r}')|^2 d^3r', \quad \beta<<\theta_o \tag{2.29}$$

$$P_\ell = \frac{2\pi^2 k^{2-n}}{r^2 s^2} C_o \theta_o^{-n} \int_V |g_\ell(\underline{r}')|^2 d^3r', \quad \beta<<\theta_o \tag{2.30}$$

In order to estimate the multipath spread and coupling loss, we must approximate the integrals in (2.29) and (2.30). In Fig. 2.3, four scattering points are indicated: the origin "O" corresponding to the minimum scattering angle θ_o, the point "A" which is vertically displaced a distance h from "O", the point "B" which is horizontally displaced a distance w from "O", and the point "C" which is longitudinally displaced a distance ℓ from "O". When the beam angle γ is a quarter beamwidth $\beta/4$, the points A and B correspond to half-power scatter returns relative to the return from the origin. The half-power distances are

$$h_1 = \frac{d\beta}{8} \qquad \beta<<\theta_o$$

$$w_1 = \frac{d\beta}{8} \qquad \beta<<\theta_o$$

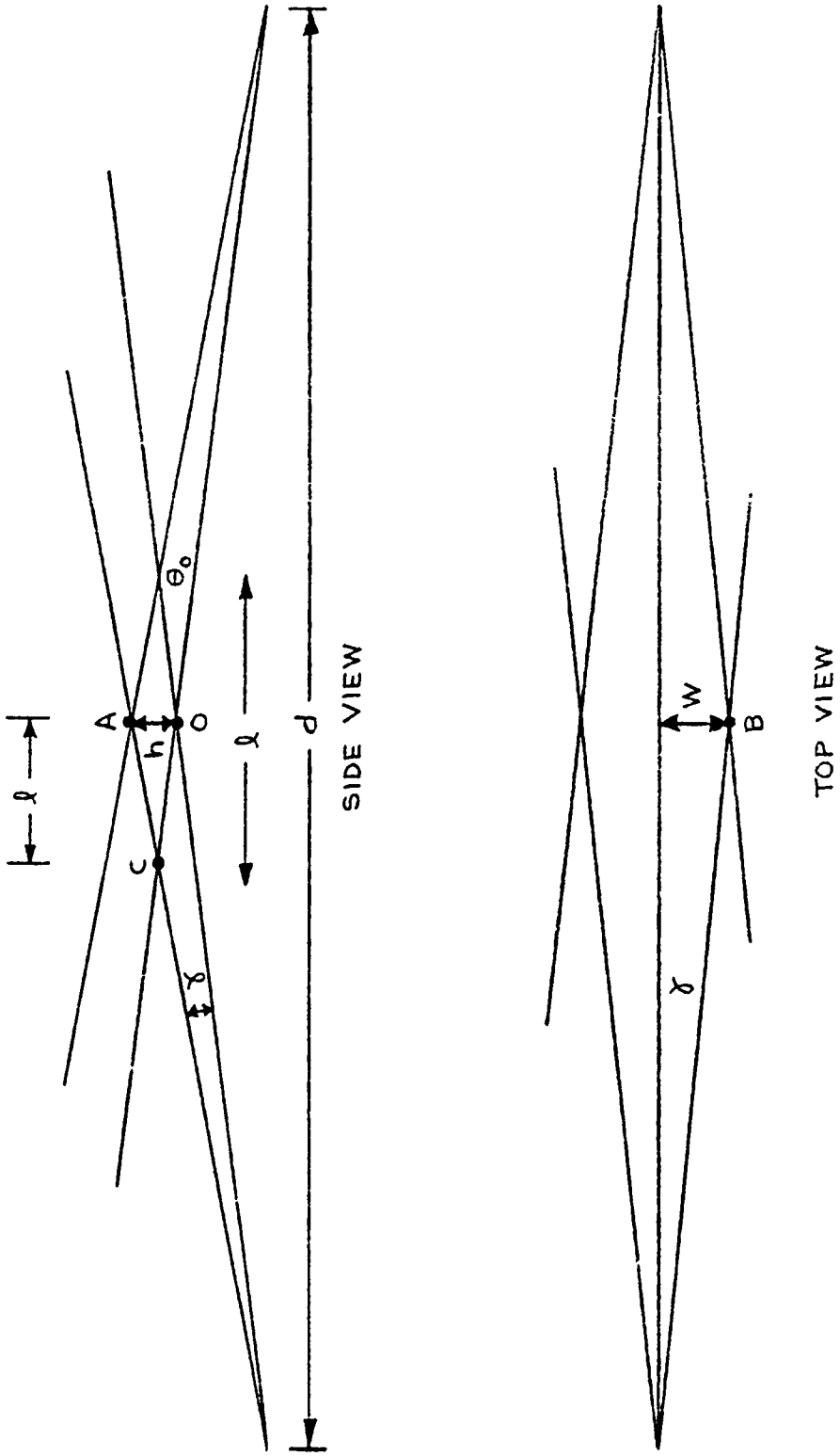

Fig. 2.3 Scatter Volume Geometry

When $\gamma = \beta/2$, the point C represents a half-power return, and the half power longitudinal distance is

$$\ell_1 = \frac{2h_1}{\theta_o+\beta/2} \doteq 2h_1/\theta_o = d\beta/4\theta_o, \quad \beta<<\theta_o$$

A reasonable assumption for the joint antenna pattern characteristic is a Gaussian fall-off in each direction from the origin except for points below the origin from which no return is made. Under this assumption the common volume integration in (2.30) is

$$V_\beta = \int_o^\infty e^{-0.69z^2/h_1^2}\,dZ \int_{-\infty}^{\infty} e^{-0.69y^2/w_1^2}\,dy \int_{-\infty}^{\infty} e^{-0.69x^2/\ell_1^2}\,dx$$

$$V_\beta = 4.85\, w_1 h_1 \ell_1 = 0.0189\, \frac{d^3\beta^3}{\theta_o} \qquad (2.31)$$

We now replace in (2.30) the free space loss per unit distance P_o by $P_T(\pi D/\lambda)^4 4\pi$, where D is the antenna reflector diameter assumed the same at each terminal and then

$$P_\ell \alpha P_T \cdot \frac{f^2}{d^4} \cdot \left(\frac{D}{\lambda}\right)^4 \cdot d^3\beta^3\theta_o^{-n-1} f^{-n}, \quad \beta << \theta_o.$$

Where the first factor is the transmit power, the second factor accounts for the isotropic free space path loss, the third factor represents the antenna gain dependence, and the last factor represents the volume integration of the refractive index inhomogeneities Since the antenna beamwidth β is approximately λ/D, after combining factors one has

$$P_\ell \alpha P_T f^{3-n} D \theta_o^{-n-1} / d, \quad \beta << \theta_o \qquad (2.32)$$

For turbulent scatter, the spectrum slope n is 11/3 which gives a $f^{-2/3}$ power fall-off with frequency and a $\theta_o^{-14/3}$ power fall-off with scatter angle.

The received power dependence indicated in (2.32) includes the coupling loss effect. We will examine this quantity separately but first we estimate the 2σ multipath spread.

The surfaces of constant delay in (2.29) are prolate spheroids. We can avoid the difficult integrations by some simple approximations. The differential delay for the points A, B, and C in Fig. 2.3 are readily computed to be

$$\Delta\tau_A = d\beta\theta_o/4c \qquad \beta<<\theta_o$$

$$\Delta\tau_B = d\beta^2/8c \qquad \beta<<\theta_o$$

$$\Delta\tau_C = d\beta\theta_o/8c \qquad \beta<<\theta_o$$

The delay shell through the point A will contribute close to the maximum power to the multipath profile. Thus to obtain an estimate of the 2σ spread, we assume a triangular shape for Q(t) with a base width of $d\beta\theta_o/2c$ seconds. The estimated spread is then

$$2\sigma = \frac{1}{2\sqrt{6}} \frac{d\beta\theta_o}{c} \qquad \beta<<\theta_o \qquad (2.33)$$

The main effect of the profile shape assumption is to fix the constant $1/2\sqrt{6}$. For narrow beam antennas the estimate (2.33) compares favorably with the predicted value from numerical integration procedures described in Section 3. For the RADC C-band test link with 0^o elevation angles, we find

$\beta = 0.0094$

$\theta_o = 0.0318$

2σ (estimated) = 55 ns.

2σ (predicted) = 44 ns. (See Section 3)

Note that for small beamwidths the multipath spread is independent of spectrum slope n and inversely proportional* to the effective earth radius factor K as $\theta_o = d/KR_o$.

The multipath estimates are generally a little larger than the values obtained by numerical integration of the common volume because in the integration the $\theta^{-n}(\underline{r}')$ fall-off with height reduces the effective multipath spread.

When the antenna beamwidths are large compared to the minimum scattering angle, the volume integration is primarily dependent on the refractive index spectrum, Φ. We have

$$Q_{\ell\ell}(t) = \frac{2\pi^2 k^2 P_o}{r^2 s^2} \int_{V(t)} C(z)\,\theta^{-n}(\underline{r}')\,d^3r', \qquad \beta \gg \theta_o \tag{2.34}$$

$$P_\ell = \frac{2\pi^2 k^2 P_o}{r^2 s^2} \int_{V} C(z)\,\theta^{-n}(\underline{r}')\,d^3r', \qquad \beta \gg \theta_o \tag{2.35}$$

The height dependence typically falls off inversely proportional to height and is not as a significant factor in the volume integration as the angle dependence. Neglecting this height dependence by setting $C(z) = C_o$, a constant, we can compute the effective scattering vclume size. Let θ_1 be the value of θ such that the scattered power is reduced by 3dB from the maximum scattered power, i.e. θ_1 solves

$$\left(\frac{\theta_1}{\theta_o}\right)^{-n} = 1/2$$

$$\text{or } \theta_1 = 2^{1/n}\theta_o$$

---

*only when the take-off angles $\phi_t = \phi_r = 0$, otherwise $\theta_o = d/KR_o + \phi_t + \phi_r$.

Now let h_1 and w_1 be the height and width shift required from the point of minimum scattering angle to produce a scattering angle of θ_1 in the respective vertical or azimuthal planes. The geometry for the determination of h_1 and w_1 is shown in Fig. 2.4. These values are easily shown to be

$$h_1 = \frac{d\theta_1}{4} - \frac{d\theta_o}{4} = \frac{d\theta_o}{4}\left(2^{1/n}-1\right) \tag{2.36}$$

$$w_1 = \frac{d\theta_o}{4}\sqrt{4^{1/n}-1} \tag{2.37}$$

The length of the scattering volume is on the order of the path length as the geometry shows that the longitutinal distance is

$$\ell_1 \sim \frac{2h_1}{\theta_1-\theta_o} = \frac{d\left(\theta_1-\theta_o\right)}{\theta_1-\theta_o} = d/2$$

To estimate the size of the scattering volume assume that the vertical and azimuthal fall-off as a function of departure from the point of minimum scattering is Gaussian distributed. If the length of the scattering volume is taken as d, the size of the volume in (2.35) becomes

$$V_{\theta_o} = d\int_o^\infty e^{-0.69z^2/h_1^2}dZ \int_{-oo}^{\infty} e^{-0.69y^2/w_1^2}dy$$

$$= d\left(\frac{1}{2}\sqrt{2\pi h_1^2/1.38}\right)\sqrt{2\pi w_1^2/1.38}$$

$$= 2.27\, dh_1w_1 = 0.14\, d^3\theta_o{}^2\left(2^{1/n}-1\right)\sqrt{4^{1/n}-1} \tag{2.38}$$

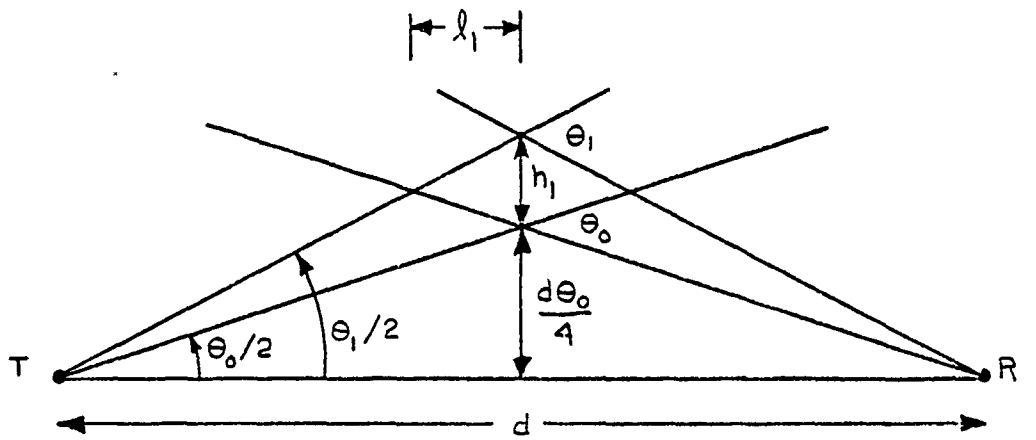

SIDE VIEW

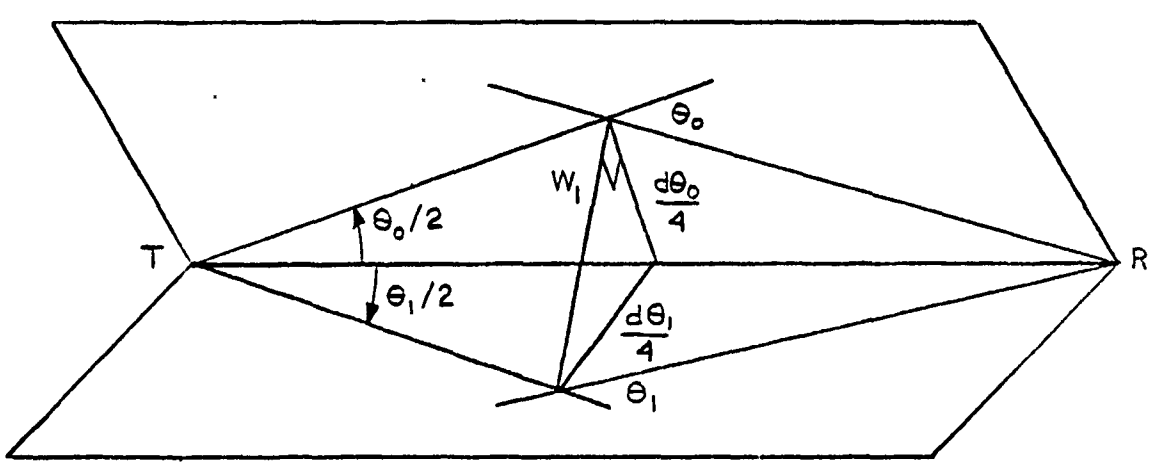

THREE DIMENSIONAL VIEW

Fig. 2.4 Scatter Volume Half-Power Dimensions

The received power is approximately

$$P = \frac{2\pi^2 k^2 P_o C}{r^2 s^2} \theta_o^{-n} V_{\theta_o} \qquad (2/39)$$

The asymptotic coupling loss for narrow beam antennas can now be estimated as the ratio of scattering volumes for the two examples considered. We have

$$C_L = \frac{\int_V \theta^{-n} d^3 r'}{\theta_o^{-n} \int |g(\underline{r}')|^2 d^3 r'} = \frac{\theta_o^{-n} V_{\theta_o}}{\theta_o^{-n} V_\beta}$$

$$C_L = 7.5 \left(2^{1/n}-1\right) \sqrt{4^{1/n}-1} \left(\frac{\theta_o}{\beta}\right)^3 , \quad \beta << \theta_o \qquad (2.40)$$

which shows that the asymptotic coupling loss varies inversely as the cube of the beamwidth when the transmitter and receiver beamwidths are constrained to be the same. For different values of transmitter and receiver beamwidths, the coupling loss is

$$C_L = 7.5 \left(2^{1/n}-1\right) \sqrt{4^{1/n}-1} \frac{\theta_o^3}{\beta_{max} \beta_{min}^2} , \quad \beta_{min} < \beta_{max} << \theta_o .$$

If one of the two antenna beams is on the order of the scattering angle, i.e. a wide beamwidth, the coupling loss at the single narrow beam antenna is

$$C_L \Big|_{\substack{\text{single} \\ \text{Antenna}}} = 7.5\left(2^{1/n}-1\right) \sqrt{4^{1/n}-1} \frac{\theta_o^2}{\beta^2}, \quad \beta << \theta_o$$

which agrees well with Gjessing's result [2.5] derived from correlation distance calculations at the receiver antenna. He found

$$C_L\Big|_{\substack{\text{single}\\ \text{Antenna}}} = \frac{5Ad^2}{\lambda^2 R_o^2}\left(2^{1/n}-1\right)\sqrt{4^{1/n}-1}$$

where

A = antenna aperature area

R_o = earth radius

Since $\beta \doteq 7\pi\lambda/6\sqrt{4A/\pi}$ and $\theta_o = d/R_o$, his result reduces to

$$C_L\Big|_{\substack{\text{single}\\ \text{Antenna}}} = 5.3\left(2^{1/n}-1\right)\sqrt{4^{1/n}-1}\ \frac{\theta_o^2}{\beta^2}$$

The difference in constant multipliers of 1.4dB less loss for Gjessing's result is due to choice of approximation functions.

As a numerical check on the coupling loss for a symmetical link, the C-band RADC test link considered in Section 3 has parameters

$\theta_o = 0.0318$

$\beta = 0.0094$

which for a spectrum slope of n = 11/3 yields a coupling loss estimate (2.40) of 15.9 dB. As will be indicated in the next section, the estimate is within the range of the numerical integration prediction technique and other semi-empirical methods examined.

2.4 References

[2.1] P.A. Bello, "Characterization of Randomly Time-Variant Linear Channels," IEEE Trans. on Communications Systems, December 1963, p. 370.

[2.2] V.I. Tatarski, "Wave Propagation in a Turbulent Medium", Translated from Russian by R.A. Silverman, McGraw-Hill, New York, NY, 1961.

[2.3] P.L. Rice, et.al., "Transmission Loss Predictions for Tropospheric Communications Circuits", NBS Tech. Note 101, US Dept. of Commerce, National Bureau of Standards, May 7, 1965.

[2.4] H.G. Booker and W.E. Gordon, "A Theory of Radio Scattering in the Troposphere", Proc. Inst. Radio Engrs., No. 38, p. 401, 1950.

[2.5] F. Villars and V.F. Weisskopf, "The Scattering of Electromagnetic Waves by Turbulent Atmospheric Fluctuations", Phys. Rev., No. 94, p. 232, 1954.

[2.6] D.T. Gjessing and K.S. McCormick, "On the Prediction of the Characteristic Parameters of Long-Distance Tropospheric Communication Links", IEEE Trans. on Communications, Vol. 22, No. 9, p. 1325, Sept. 1974.

SECTION 3

TROPOSCATTER PARAMETER PREDICTION

The theoretical basis for the uncorrelated scattering model of the troposcatter communication channel has been presented in the previous section. In this section we convert these theoretical concepts into a functional prediction technique for determining multipath spread, multipath profiles and the inherent correlation between delay cells, and aperture to medium coupling loss. The prediction technique consists of a numerical three dimensional integration of the scatter volume. An absolute reference for the main beam path loss will be determined from computerized NBS calculations* and relative power calculations for angle diversity beams will be derived from the volume integration. The volume integration is not used for the main beam path loss because it lacks the empirical data inputs in the NBS calculations.

A validation of the prediction model will be accomplished by comparing multipath predictions with measured data collected on the MDTS field tests at Rome, N.Y. in the winter of 1976. After an analysis is completed which shows good agreement between multipath predictions and measurements, a similar analysis is planned to resolve discrepancies between predicted and measured aperture - to-medium coupling loss values. Another important prediction technique output will be the cross-channel multipath profile which provides the multipath correlation data required to predict average bit error probability for adaptive digital modems.

---

*A. G. Longley, et.al.; "Prediction of Tropospheric Radio Transmission Loss over Irregular Terrain, A Computer Method, 1968", ESSA (NBS), Boulder, Colorado, July 1968.

3.1 Prediction Model

Experimental data on the delay spread on a troposcatter link are typically larger than predicted by theoretical calculations. Theoretical calculations of coupling loss also exhibit a considerable range of predicted values. These calculations are normally based on a constant gradient atmosphere as well as a series of approximations to the propagation path and the antenna pattern. The calculations presented here are exact for a specific refraction profile which has a nearly constant gradient near the surface of the (spherical) earth. This analysis is intended as the first step in resolving the discrepancy between experimental and theoretical results obtained in the past. The effect of terminal equipment filters and measurement errors will also be evaluated in the evaluation of multipath spread.

3.1.1 A Model for the Refraction Profile

In regions of tropospheric scatter it is generally acknowledged that the coefficient of refraction decreases linearly with height. We shall use a power-law model featuring an approximately linear decrease.

Let $n(R)$ be the refractive index as a function of the distance from the center of the earth. It is assumed that the atmosphere is spherically layered. The refractive index will be assumed to be of the form

$$n(R) = n_o \cdot (R_o/R)^{\gamma}.$$

In this equation R_o is the radius of the earth, $n_o = n(R_o)$ in the refractive index at the surface, and γ is a parameter determined by the refractive index gradient at the surface. γ can be related to the gradient of the coefficient of refraction (usually expressed in N-units per km) as follows

$$\Delta N \text{ [N-units/km]} = - \gamma \cdot 10^9 n_o/R_o.$$

R_o is given in meters, and n_o can be taken to be equal to 1. For the standard atmosphere the gradient is 40 N-units/km corresponding to $\gamma = 0.25$. The propagation path is naturally curved, but by a suitable transformation of the coordinate system straight-line propagation can be used. Define, in a given great-circle plane, *-coordinates:

$$R^* = R^*(R) = \frac{1}{1-\gamma} R_o^{\gamma} R^{1-\gamma}$$

$$d^* = d \quad \text{(distance along the surface)}.$$

With this definition the angular distance between two points on the surface is transformed from α to

$$\alpha^* = \alpha(1-\gamma).$$

The effective earth radius is then defined by

$$R_{eff} = R^*(R_o) = R_o/(1-\gamma).$$

This definition is justified by the following theorem

Theorem: The propagation path in the *-coordinates is a straight line.

Proof:

We refer to Fig 3.1 for the definition of parameters for the path. In the real coordinate system the path is governed by the following equations:

(1) $R \cdot n(R) \sin \theta (R) = R_o n_o \sin \theta_o$ (Spherical Snell's law). $\theta(R)$ is the zenith angle at a variable point of the path, and θ_o is the zenith angle with which the path leaves the surface of the earth.

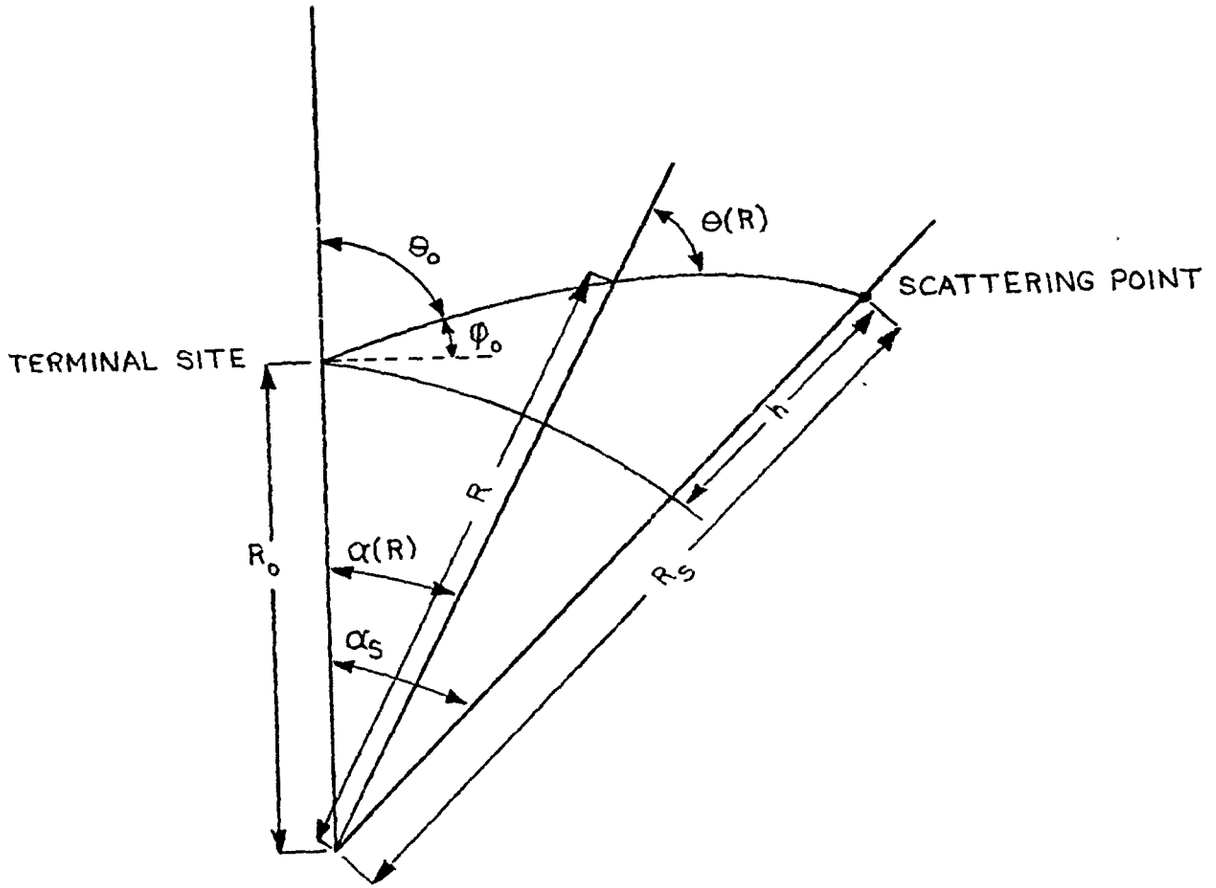

Fig. 3.1 Path Geometry of Tropospheric Scatter

(2) $R\, d\alpha = \tan\, \theta(R)\, dR$

$d\alpha$ is an infinitesimal change in angular distance along the path.

These two equations determine the path completely. In terms of the *-coordinates these equations become

(1^*) $\quad R^* \sin\, \theta(R^*) = R_{eff} \sin\, \theta(R_{eff})$

(2^*) $\quad R^*\, d\alpha^* = \tan\, \theta(R^*)\, dR^*.$

This is just the equations governing electromagnetic wave propagation in a homogeneous medium. Hence the rays are transformed in straight lines in this coordinate system. It is verified below that distances on the surface are unchanged by the transformation, so it follows that the velocity of propagation in the *-coordinates is equal to the surface velocity in the original coordinate system.

This completes the proof of the theorem.

The above result is applied to the troposcatter problem by considering separately the path from a terminal (transmitter or receiver) to a given point in the common volume. This path is transformed as above in the great-circle plane containing the terminal and the scattering point. The height of the scattering point in the *-coordinates is

$$h^* = R_{eff}\left[\left(1 + \frac{h}{R_o}\right)^{1-\gamma} - 1\right]$$

$$\simeq R_{eff}\left[(1-\gamma)\, h/R_o - \gamma(1-\gamma)\,(h/R_o)^2/2\right]$$

$$= h(1-\gamma h/2R_o).$$

It is seen that the height is changed only very little. As an example take h = 50,000 ft., and $\gamma = 0.25$ (standard atmosphere) then

$$h^* = 49{,}985 \text{ ft.}$$

The small difference between h and h^* can usually be ignored, but correction term will be used in the results to be presented later. The case of small h verifies that infinitesimal distances at the surface are unchanged by the transformation.

In the *-coordinates it is now easy to find the transmission delay, the take-off angle, and the angle with horizontal at the scattering point. These parameters are the same in the original coordinates. The angle at the scattering point is particularly important due to the drastic scattering angle dependence of the turbulent scatter cross section.

In the following we derive formulas for the dimensions of the scattering volume and the delay spread. The purpose of these sections is to document some of the formulas used in the prediction model. Sections 3.1.2 and 3.1.3 can therefore be skipped at a first reading.

3.1.2 Height and Size of the Common Volume

The extent of the common volume in the azimuth direction will be considered last. For the time being we can constrain the analysis to the great-circle through the two terminals. The coordinates are transformed in this plane such that the rays are straight lines. The transmitter and receiver beams are characterized by the take-off angles of the upper and lower rays in the beam. The notation used here and in Fig. 3.2 is

φ_{tu} = take-off angle at transmitter of upper ray.
$\varphi_{t\ell}$ = take-off angle at transmitter of lower ray.
φ_{ru} = take-off angle at receiver of upper ray.
$\varphi_{r\ell}$ = take-off angle at receiver of lower ray.

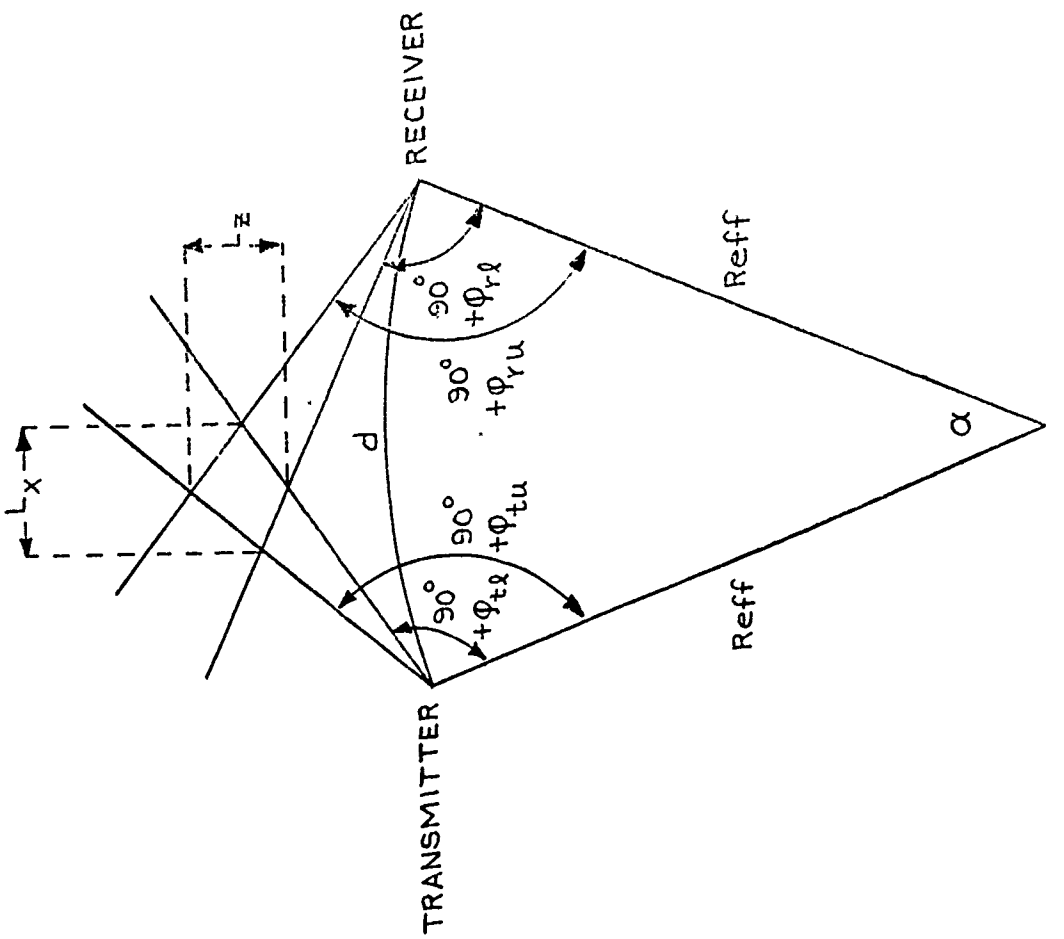

Fig. 3.2 Dimensions of the Common Volume

The beamwidths are

$$\beta_t = \varphi_{tu} - \varphi_{t\ell}$$

$$\beta_r = \varphi_{ru} - \varphi_{r\ell}$$

the take-off angles of the center of the beam are

$$\gamma_t = (\varphi_{tu} + \varphi_{t\ell})/2$$

$$\gamma_r = (\varphi_{ru} + \varphi_{r\ell})/2.$$

The altitude h of the lowest point of the common volume is found to be determined by

$$2h' - h'_r - h'_t + h'^2 - h'_r h'_t =$$

$$= \left[\frac{h_t/R_{eff}\cos\varphi_{t\ell} - h_r/R_{eff}\cos\varphi_{r\ell} + 2\sin\frac{\varphi_{t\ell}+\varphi_{r\ell}}{2} \cdot \sin\frac{\varphi_{r\ell}-\varphi_{t\ell}}{2}}{\sin(\alpha + \varphi_{t\ell} + \varphi_{r\ell})} \right]^2$$

$$+ (1+h'_r)(1+h'_t)\left(\sin\frac{\alpha}{2}\sin\left(\frac{\alpha}{2}+\varphi_{r\ell}+\varphi_{t\ell}\right) - \sin^2\frac{\varphi_{t\ell}-\varphi_{r\ell}}{2}\right) \Big/$$

$$\cos^2\frac{1}{2}\left(\alpha + \varphi_{t\ell} + \varphi_{r\ell}\right)$$

where $h'_r = h_r/R_{eff}$, $h'_t = h_t/R_{eff}$ and $h' = h/R_{eff}$.

This can be approximated by

$$h \sim \frac{h_r + h_t}{2} + \frac{1}{2R_{eff}}\left[\frac{h_t - h_r + R_{eff}(\varphi_{r\ell}^2 - \varphi_{t\ell}^2)/2}{\alpha + \varphi_{t\ell} + \varphi_{r\ell}}\right]^2$$

$$+ \frac{R_{eff}}{2}\left[\frac{\alpha}{2}\left(\frac{\alpha}{2} + \varphi_{r\ell} + \varphi_{t\ell}\right) - \left(\frac{\varphi_{t\ell} - \varphi_{r\ell}}{2}\right)^2\right] .$$

In particular, if the heights of the receiver and transmitter are zero,

$$h \sim \frac{R_{eff}}{2} \left\{ \left(\frac{\left(\varphi_{r\ell}^2 - \varphi_{t\ell}^2 \right)}{2(\alpha + \varphi_{t\ell} + \varphi_{r\ell})} \right)^2 + \frac{\alpha}{2} \left(\frac{\alpha}{2} + \varphi_{r\ell} + \varphi_{t\ell} \right) - \frac{\left(\varphi_{t\ell} - \varphi_{r\ell} \right)^2}{2} \right\} .$$

In the simple case where $\varphi_{t\ell} = \varphi_{r\ell} = \varphi$, and $h_t = h_r \sim 0$, we have

$$h \simeq \frac{R_{eff}}{2} \frac{\sin\alpha/2 \cdot \sin(\alpha/2 + 2\varphi)}{\cos^2\left((\alpha + 2\varphi)/2 \right)} \sim \frac{\alpha^2 R_{eff}}{8} \left(1 + \frac{4\varphi}{\alpha} \right).$$

The altitude of other points in the common volume are easily found by a simple substitution. In particular, the vertical thickness of this volume is approximately, assuming equal height terminals,

$$L_z = d \frac{\left(\gamma_t + \alpha/2 \right)^2 \beta_r + \left(\gamma_r + \alpha/2 \right)^2 \beta_t - \beta_t \beta_r \left(\beta_t + \beta_r \right)/4}{\left(\gamma_t + \gamma_r + \alpha \right)^2 - \left(\beta_t + \beta_r \right)^2/4} .$$

For a symmetric link, where $\gamma_t = \gamma_r$ (equal take-off angle) and $\beta_t = \beta_r = \beta$ we get simply

$$L_z \sim d \cdot \frac{\beta}{2} .$$

A similar calculation of the length of the common volume gives

$$L_x \sim d \cdot \frac{\left(\gamma_t + \alpha/2 \right) \beta_r + \left(\gamma_r + \alpha/2 \right) \beta_t}{\left(\gamma_t + \gamma_r + \alpha \right)^2 - \left(\beta_t - \beta_r \right)^2/4} .$$

The width of the volume is found to be approximately

$$L_y \sim d \cdot \frac{\beta_r \beta_t}{\beta_r + \beta_t} .$$

For a symmetric link,

$$L_y = L_z = \beta\, d/2$$

$$L_x = \beta d/(\gamma_t + \gamma_r + \alpha).$$

3.1.3 Delay Spread

The precise delay spread will be determined by a numerical integration over the common volume. However, an evaluation of the maximum delay spread within the volume can be made easily, given the nominal antenna beam widths, β.

The relative delay, as a function of height z above the lowest point of the common volume is found to be

$$\tau \sim \frac{2}{C_o}\left[\frac{zd}{2R_{eff}} + \frac{z^2}{d}\right],$$

where C_o is the surface velocity of propagation. In particular, if $z = L_z$ and the link is symmetric, we get

$$\tau \sim \frac{1}{C_o}\left[\frac{\beta d^2}{2R_{eff}} + \frac{\beta^2 d}{2}\right].$$

This represents the maximum delay spread for a symmetric link. Fig.3.3 shows the relative delay τ as a function z, and Fig.3.4 shows the maximum delay spread as a function of the path length d and the beamwidth β of a symmetric link.

3.1.4 Scattering Cross Section

The power scattered from a small cell of volume dV depends on the scattering angle and the spectrum slope parameter n. The following formula for the power received from the volume cell dV is used:

$$P_r \propto P_t\, G_t(dV)\, G_r(dV)\, \frac{dV}{\phi^n(dV)} \cdot \frac{1}{R_t^2} \cdot \frac{1}{R_\gamma^2} \cdot \frac{1}{h(dV)}$$

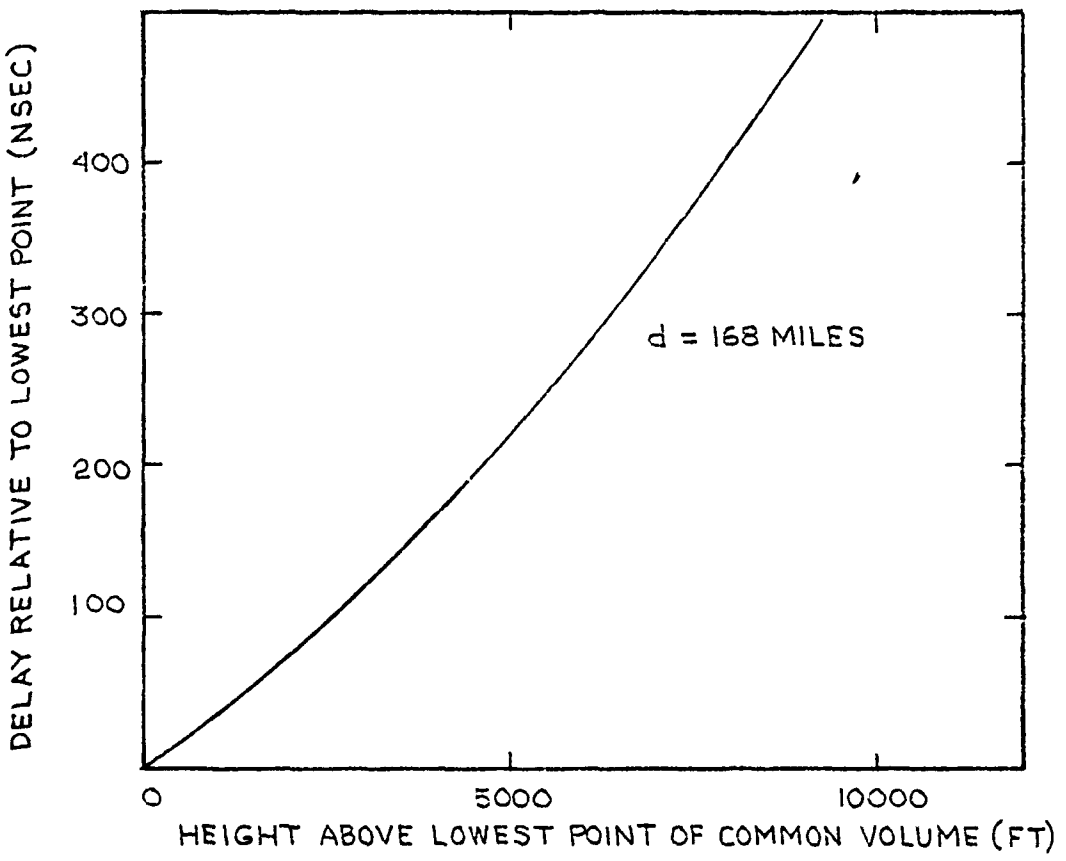

Fig. 3.3 Delay Profile, Standard Atmospheric

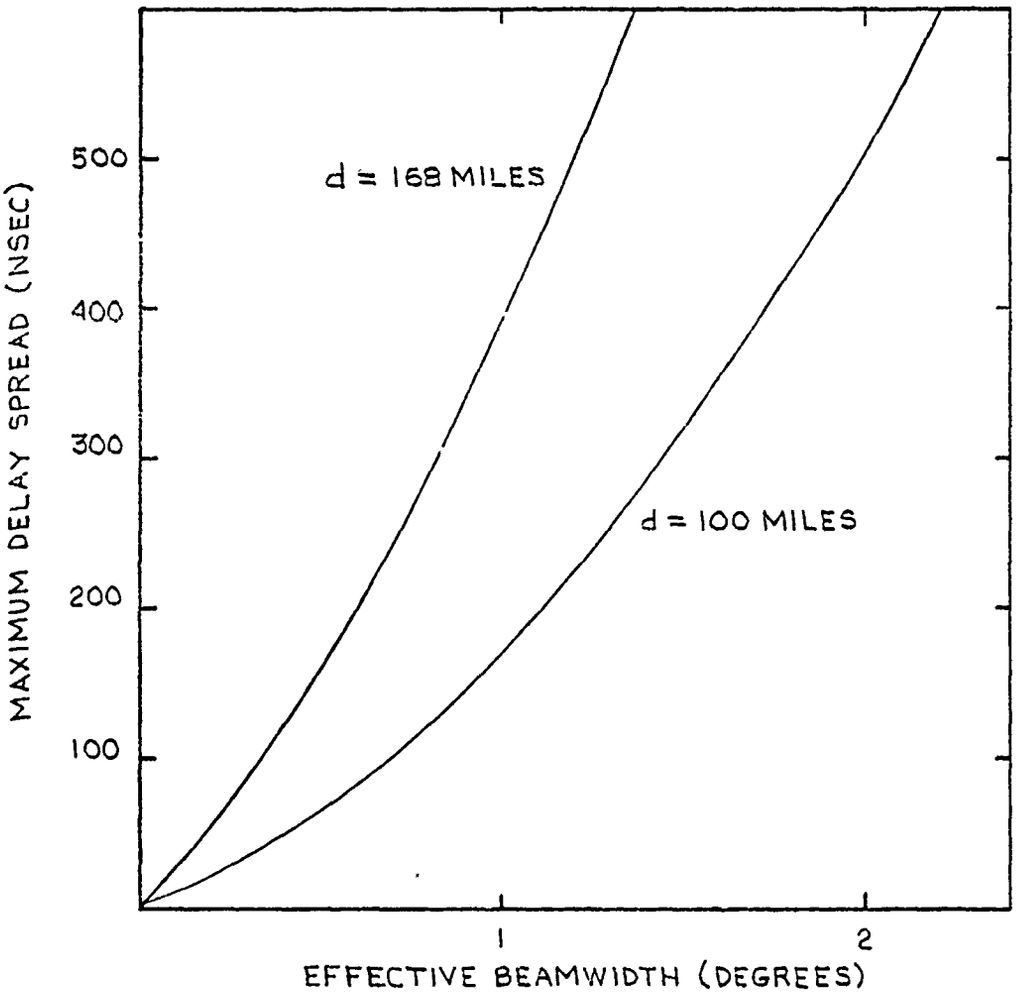

Fig.3.4 Maximum Delay Spread, Standard Atmosphere

The assumptions for the uncorrelated scattering model and the derivation of the received power equation were presented in Section 2.1. The parameters G_t and G_r are the gains to dV from the transmitting and receiving antennas, respectively, θ is the scattering angle, and R_r, R_t are the distances to the receiver and transmitter, respectively. The inverse dependence of height h accounts for the thinning out of the atmosphere with height. This dependence is customarily used in predicting troposcatter performances.

3.1.5 The Antenna Pattern

It is well-known that the gain pattern of a circular, uniformly illuminated aperture is

$$G(\varphi) = 2J_1(\zeta)/\zeta$$

where

$$\zeta = 2\pi R \sin \varphi/\lambda$$

and

$2R$ = Diameter of the dish

λ = wavelength,

$J_1()$ = Bessel function of order 1.

The 3 dB beam width of this pattern is

$$B_{-3dB} = 58^{\circ} \cdot \frac{\lambda}{D} .$$

In practice, a parabolic dish will not be uniformly illuminated due to the gain pattern of the feedhorn. Practical antenna's have a 3 dB beamwidth given by

$$B_{3dB} \simeq 70^{o} \frac{\lambda}{D}.$$

Rather than to evaluate the gain pattern of a dish with a specific nonuniform illumination, we have chosen to use the modified pattern

$$G(\varphi) = 2J_1(\zeta)/\zeta$$

where

$$\zeta = 1.67\ \pi R \sin \varphi/\lambda.$$

If the actual antenna gain need to be calculated, we can use the expression for the power gain

$$\text{GAIN} = \left(\frac{\pi D}{1.2\lambda}\right) D >> \lambda.$$

The factor 1.2 is included to account for imperfect illumination.

3.1.6 The Computer Programs

The computer programs that have been developed under this contract to find the delay spread on a troposcatter link uses a three dimensional integration over the common volume. At each scattering point the off boresight angles of each antenna are calculated using exact formulas, and the gain evaluated as described in Section 3.1.5. The scattering angle in the common volume is also found exactly, and used to determine the scattered power (Section 3.1.5). The model also yields the aperture-to-medium coupling loss by calculating the received power for the desired antennas with the power received with practically omni-directional antennas. The result of these calculations will be described in Section 3.3. The application to the angle-diversity mode, and the associated computer program is described below.

3.1.7 Prediction of Angle Diversity Path Parameters

In the preceding sections a model for troposcatter prediction was described. This model can also be applied to the angle diversity problem. The computer program used to evaluate the model in Section 3 has been modified to account for two receiving beams. This program calculates the power received by each beam in a given delay cell, as well as the correlation between the signals received in the same delay cell. This information makes it possible to evaluate the performance for a receiver using a tapped delay line, such as MDTS. The angle diversity program is still in the development stage, and extensive computational results will be presented in a later report. Here we describe some of the major concerns that have to be addressed, as well as some preliminary numerical results.

The two receiving antennas can be considered to be colocated, so the same power is scattered towards each of them. Let $g_1(\theta)$ and $g_2(\theta)$ be the voltage gain patterns of the two receiver beams. Similarly, the off boresight angles associated with a small cell dV in the common volume are denoted $\theta_1(dV)$ and $\theta_2(dV)$. If the power scattered to the receiver from the volume cell dV is $P_{sc}(dV)$, the total power received on the first (primary) beam $g_1(\cdot)$ is

$$P_1 = \int_{\substack{\text{common} \\ \text{volume}}} P_{sc}(dV) \, |g_1(\theta_1(dV))|^2 \, dV$$

On the second (angle diversity) beam $g_2(\cdot)$ the received power is

$$P_2 = \int_{\substack{\text{common} \\ \text{volume}}} P_{sc}(dV) |g_2(\theta_2(dV))|^2 dV \, .$$

The correlation between the signal received on the two beams is

$$P_{12} = \int_{\substack{\text{common} \\ \text{volume}}} P_{sc}(dv)\ g_1(\theta_1(dv))\ g_2^*(\theta_2(dv))\ dv.$$

This is in general a complex number, and it is important to realize that knowledge of the phases of the gain patterns is required to evaluate this integral accurately.

In the results we have obtained so far real gain functions of the form described in Section 3.1.5 have been assumed. An assessment of the error increased by making this approximation will be made at a later time.

It should also be pointed out that the sidelobes can make a considerable contribution to the correlation. This is in contrast to the single beam calculations in Section 3.1.6, where the sidelobes were justifiably ignored. This fact is illustrated in Fig. 3.5, where the upper and lower beams are overlapping at the 3 dB point. The amplitude of the "cross beam" voltage gain ($|g_1(\theta)g_2^*(\theta)|^{\frac{1}{2}}$) is shown together with the two primary beams. It should be clear from this figure that the sidelobes of this "product beam" are much more prominent than those of the two primary beams. Hence it is more important to include the sidelobes in the cross correlation calculation than in the determination of the power received on each beam.

Due to the high complexity of the computer program, only a few cases have been evaluated at this time. In particular, for the 4.5 GHz path in Table 3.2 and the two beams overlapping at the 3 dB point we have the results in Table 3.1 below. From these two cases it is seen that upper beam loses power relative to the lower beam at the higher elevation angle. However, it must be recognized that the

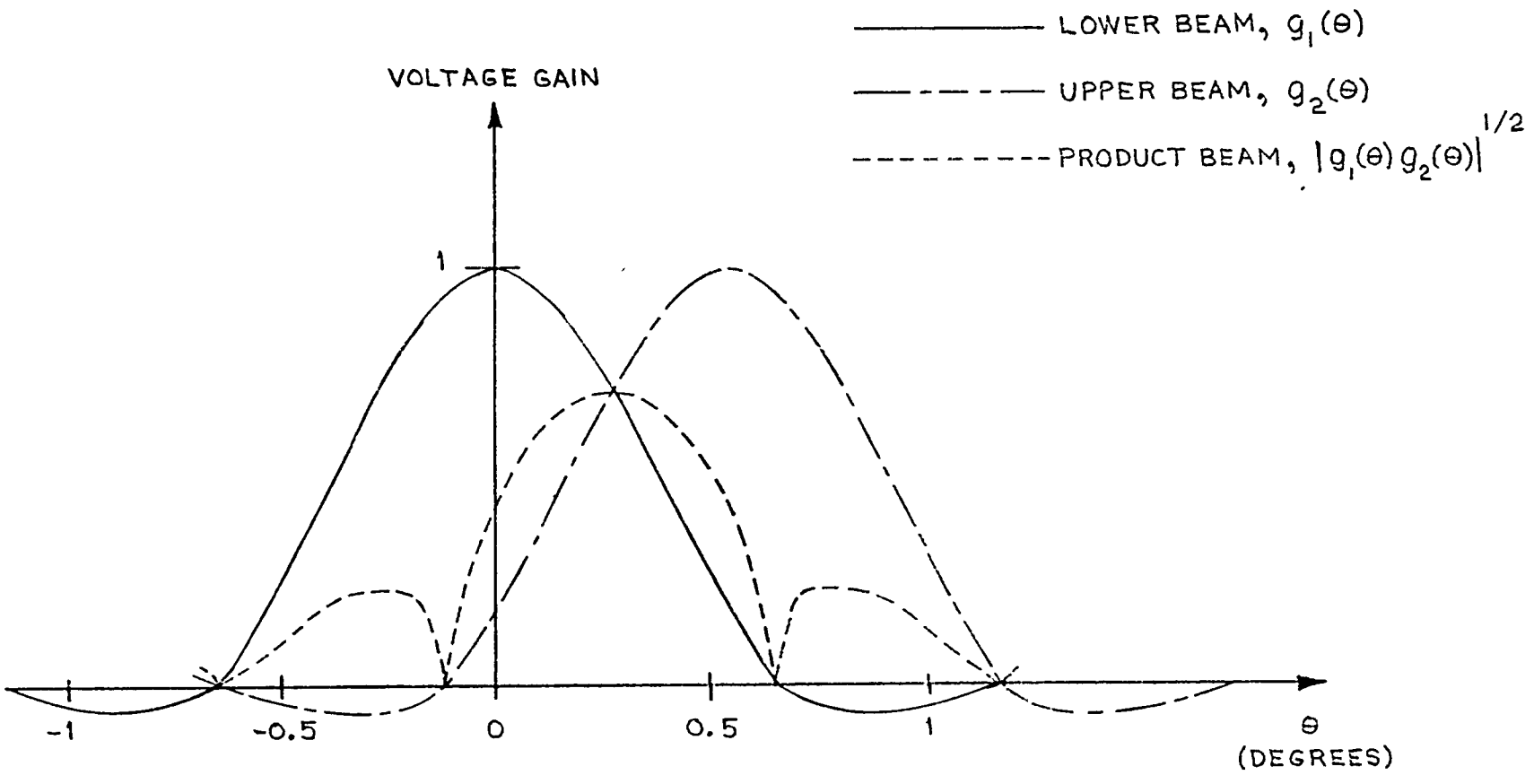

Fig. 3.5 Gain Patterns for a 28' Dual Feed Antenna

Table 3.1

Two Examples of Dual Feed Correlation

Path Data: 4.5 GHz Path in Table 3.2

Elevation of Transmitting and Lower Receiving Beam	0^{o}	$.27^{o}$
Effective Earth Radius factor K	1.3	1.1
Spectrum Slope Parameter n	3	2
Power Received on Upper Beam, Relative to lower beam	-0.5 dB	-2.6 dB
Correlation between Signals Received on the Lower and Upper Beams	0.58	0.33
2σ-delay Spread, Lower Beam	46 nsec	93 nsec
2σ-delay spread, Upper Beam	67 nsec	118 nsec

power in the lower beam is higher by 2-3 dB at the higher elevation angle (see Fig. 3.6). Hence it appears that elevating the beam by a quarter to a half beamwidth both increases the power and decreases the correlation. A more extensive example study of the angle diversity problem will be performed later.

3.2 Multipath Computations

The prediction model outlined in Section 3.1 has been tested with typical data for which empirical results have been obtained. Table 3.2 shows the path configuration and the two frequencies analyzed, together with multipath spreads measured during the MDTS test program at the RADC Verona-youngstown Link [3.1]. Several

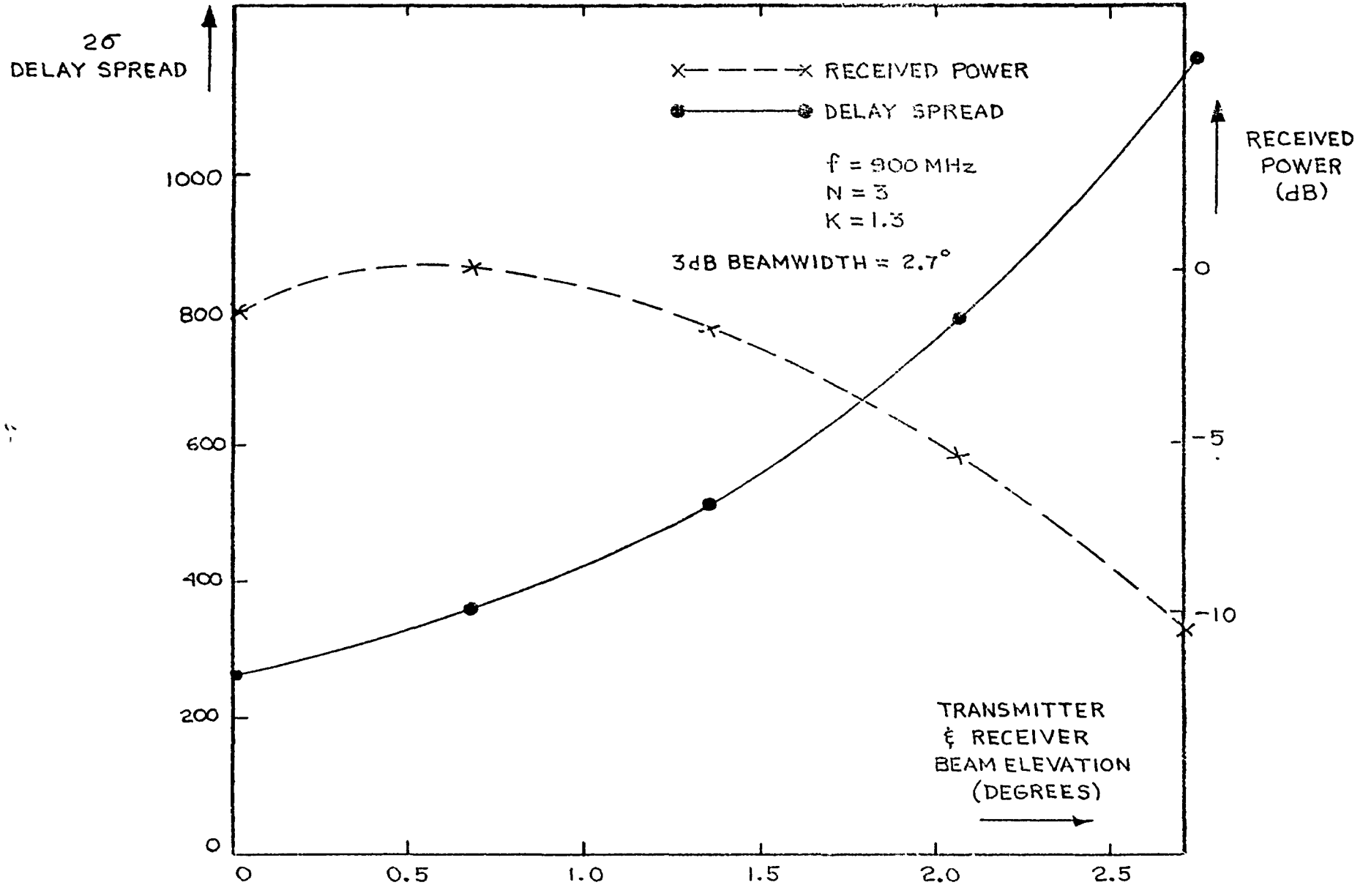

Fig. 3.6 Effect of Take Off Angles at 900 MHz (Path 1 in Table 3.1)

TABLE 3.2

EMPIRICAL MULTIPATH DATA USED IN EVALUATION OF THE TROPOSCATTER MODEL

	Path 1	* Path 2
Distance	168.3 st.mi.	168.3 st.mi
Antenna	28 ft	28 ft
Frequency	900 MHz	4.5 GHz
2σ-Delay Spread [nsec], median	290	118
max.	504	142
min.	139	66

* Corrected for correlation and noise effects as described in Section 3.2.2

parameters are unknown for the measured paths, such as the precise take-off angles and the atmospheric parameters. The troposcatter prediction model has therefore been applied for several of those parameters. The take-off angles have been varied to maximize the received power, and the take-off angles resulting in less than a 3 dB power loss have been found when possible. In this way the delay spread and coupling losses can be found for both optimally adjusted antennas, and for slightly misadjusted antenna pointing. The effective earth radius and the refractive index spectrum slope have been varied between the 10 and 90 percentiles found in most observations. These numerical results can then reliably predict the variability in troposcatter propagation.

3.2.1 Theoretical Results

Figure 3.6 illustrates the dependence on take-off angle for the 900 MHz path in Table 3.2.For full understanding of these curves it should be added that the 3 dB beamwidth of the antennas are approximately 2.7°. With a 0° beam elevation half of the beam is blocked by the earth bulge, so the received power is increased somewhat when the beams are slightly elevated . However as the beams are pointed higher the scattering angle is increased and this eventually causes a decrease in the received power. The curve for the received power is quite flat but the maximum is seen to be at approximately a quarter of the 3 dB beamwidth. The received power is reduced 3 dB with respect to its maximum value at a 1.7° beam-elevation. The most important result of Fig. 3.6 is the strong dependence of delay spread with the elevation. The delay spread varies from 260 nsec to 610 nsec as the elevation of both transmitter and receiver varies from 0° to 1.7°.

Figure 3.7 shows the same two curves for the 4.5 GHz path. The maximum of the received power is even flatter in this case, not falling 3 dB below the peak value until almost a full beamwidth elevation (0.54° 3 dB beamwidth). The delay spread varies from 44 nsec to 110 nsec when the received power varies over a 3 dB range.

Figure 3.8 shows how the delay spread depends on the effective earth radius factor K and the spectrum slope of the refractive index at 4.5 GHz. At this frequency the beam is so narrow that only a slight dependence on the spectrum slope is observed. The dependence on the K-factor can be explained as follows: For increasing K the scattering angle decreases and hence also the delay spread. Clearly the delay spread also decreases with increasing spectrum slope, since this implies a decreasing effective common volume. Figure 3.9 shows the same results at 900 MHz. As can be expected, a much stronger dependence on the spectrum slope is found, due to the wider beamwidth.

Figures 3.10 and 3.11 show the shape of some typical multipath profiles. The characteristic sharp build-up of power at small delay and slow fall-off at long delays is clearly observed on both of these figures.

In the next section the troposcatter model will be compared with some experimental data.

3.2.2 Comparison with Empirical Results

Troposcatter multipath tests were performed by Sylvania/SIGNATRON during Jan.-March 1976. The results of these tests will be used to validate the model, but first we will describe how these, and similar measurements, have been obtained. It is extremely important to understand the shortcomings of the measurement technique since

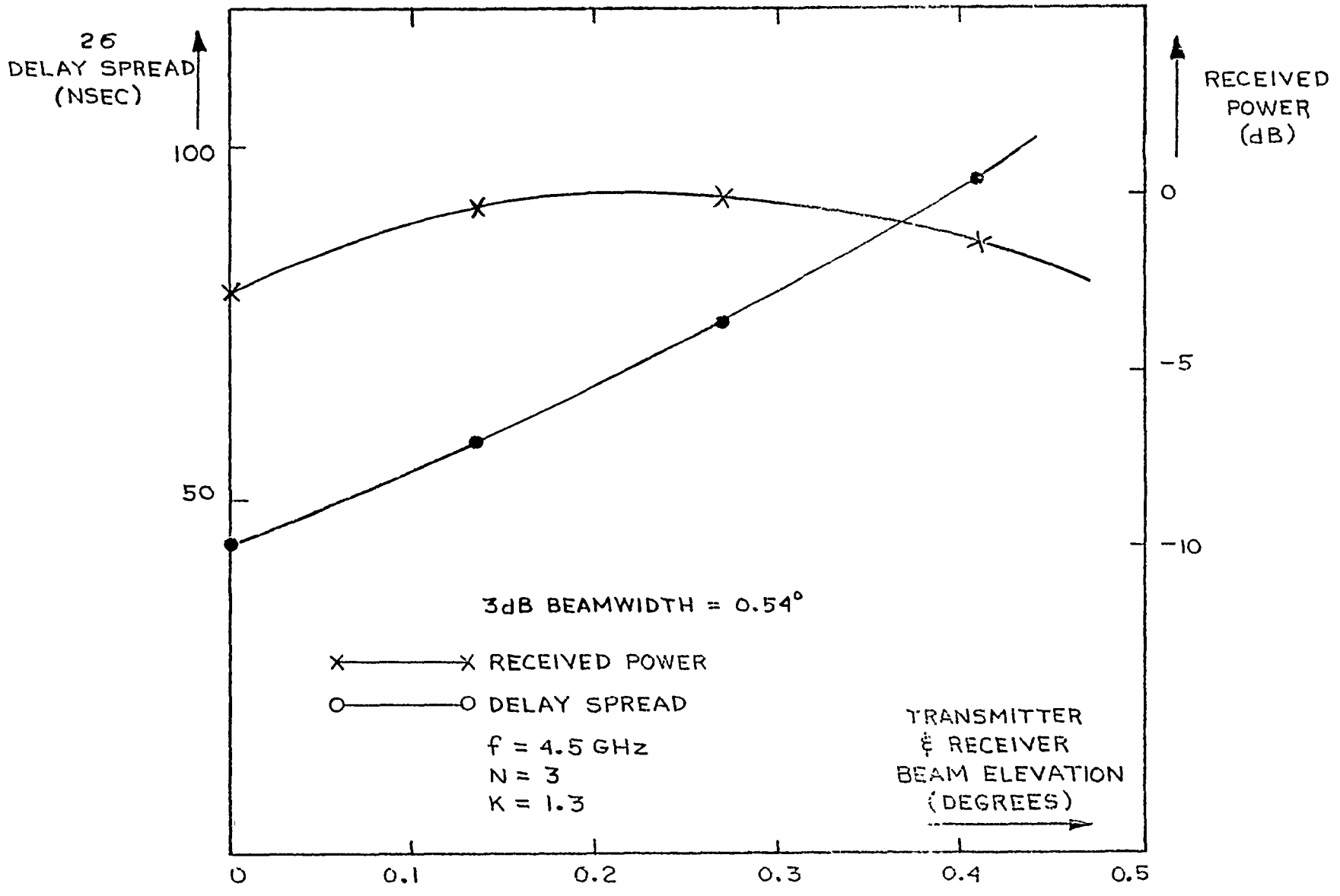

Fig. 3.7 Effect of Take Off Angles at 4.5 GHz (Path 2 in Table 3.1)

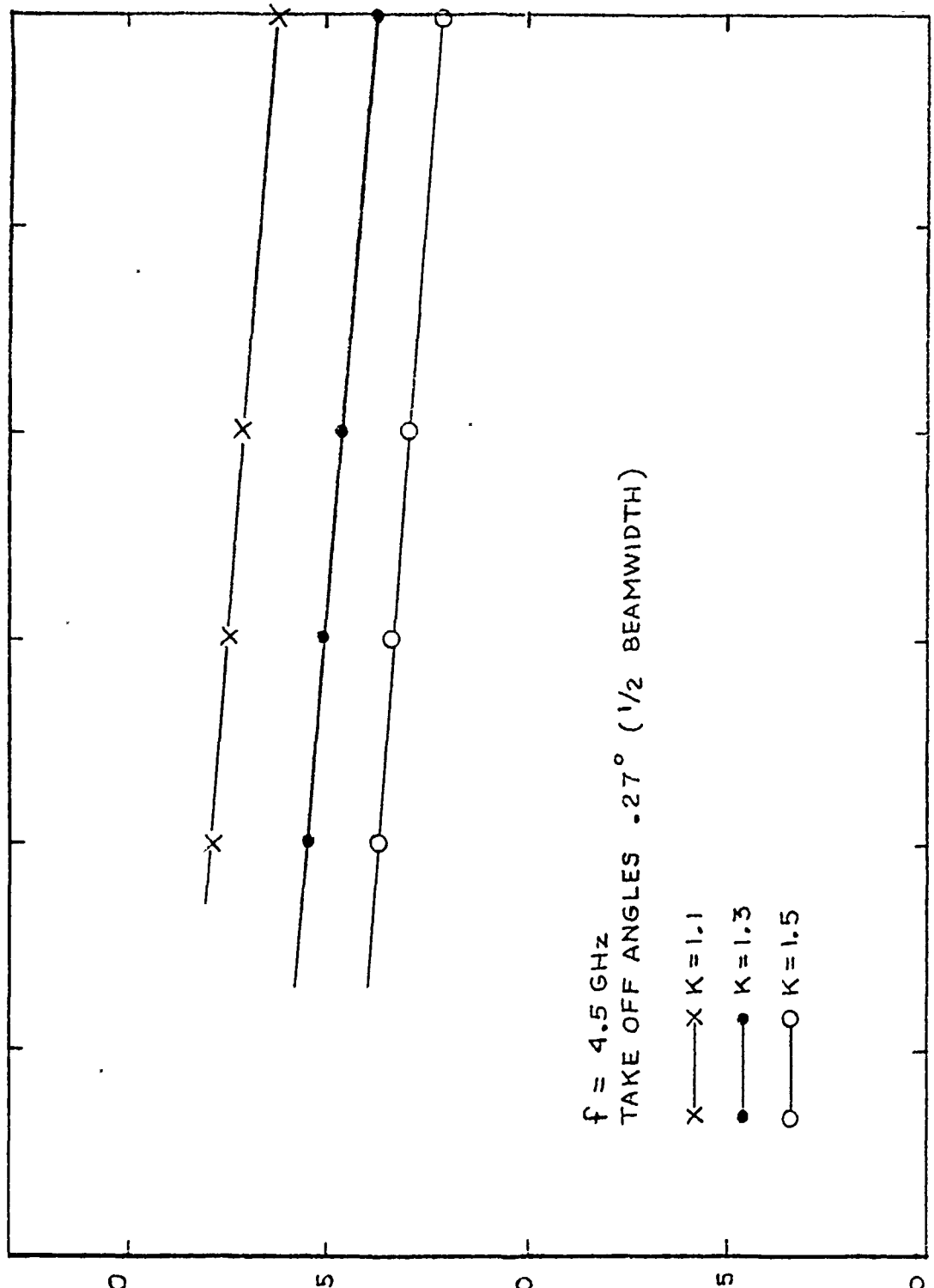

Fig. 3.8 Delay Spread as Function of Atmospheric Parameters at 4.5 GHz

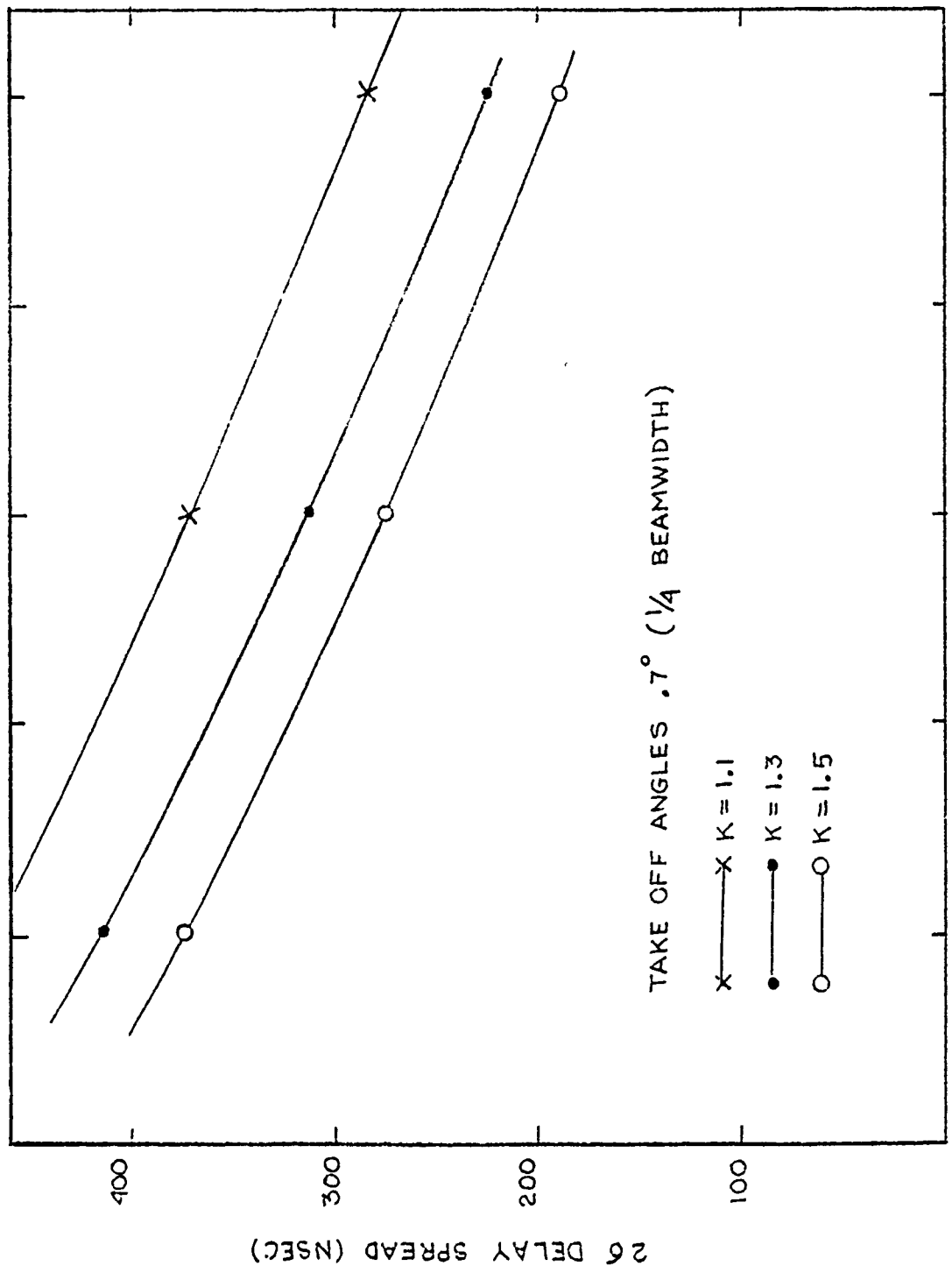

Fig. 3.9 Delay Spread as Function of Atmospheric Parameters at 900 MHz

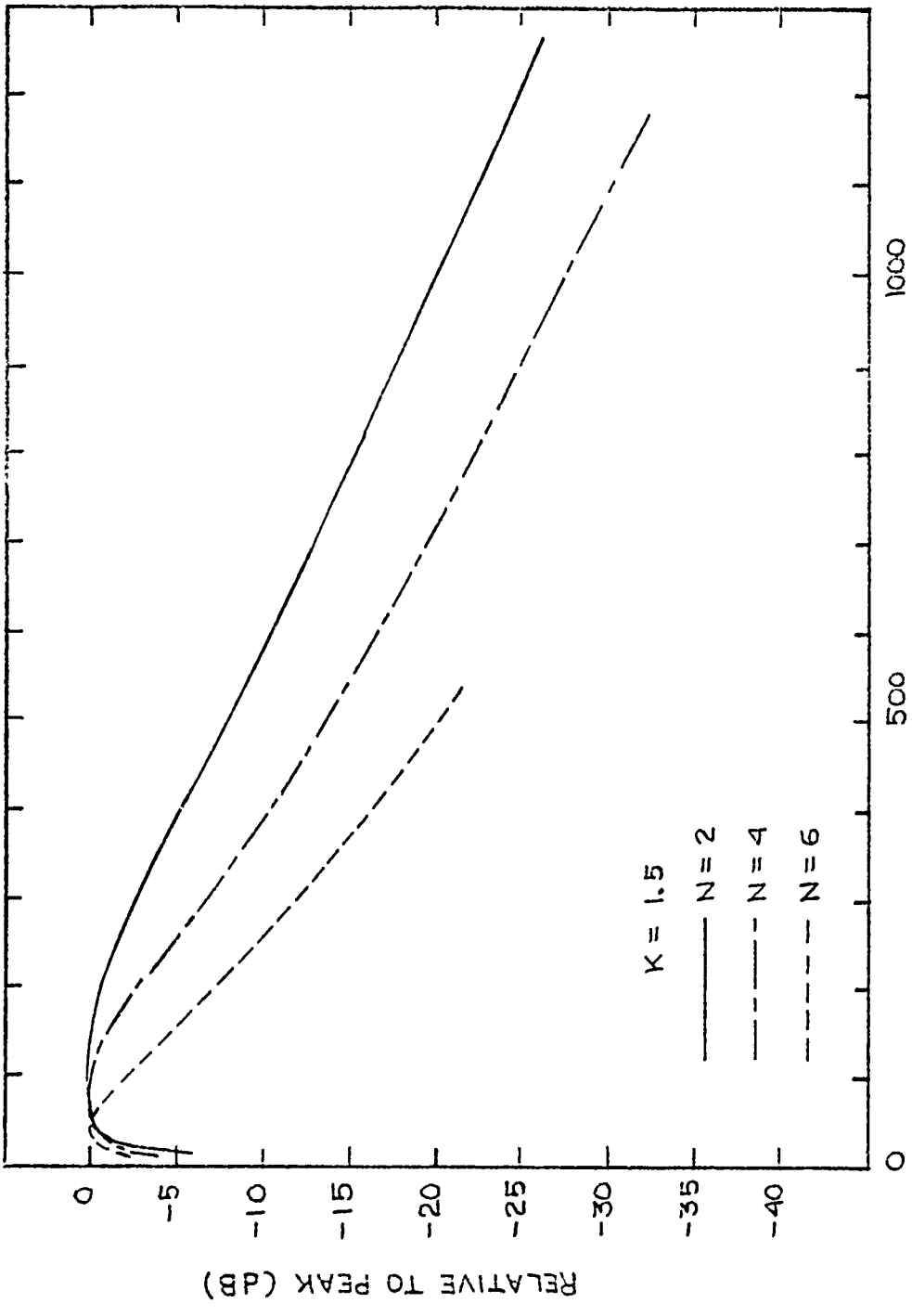

Fig. 3.10 Typical Multipath Profiles at 900 MHz

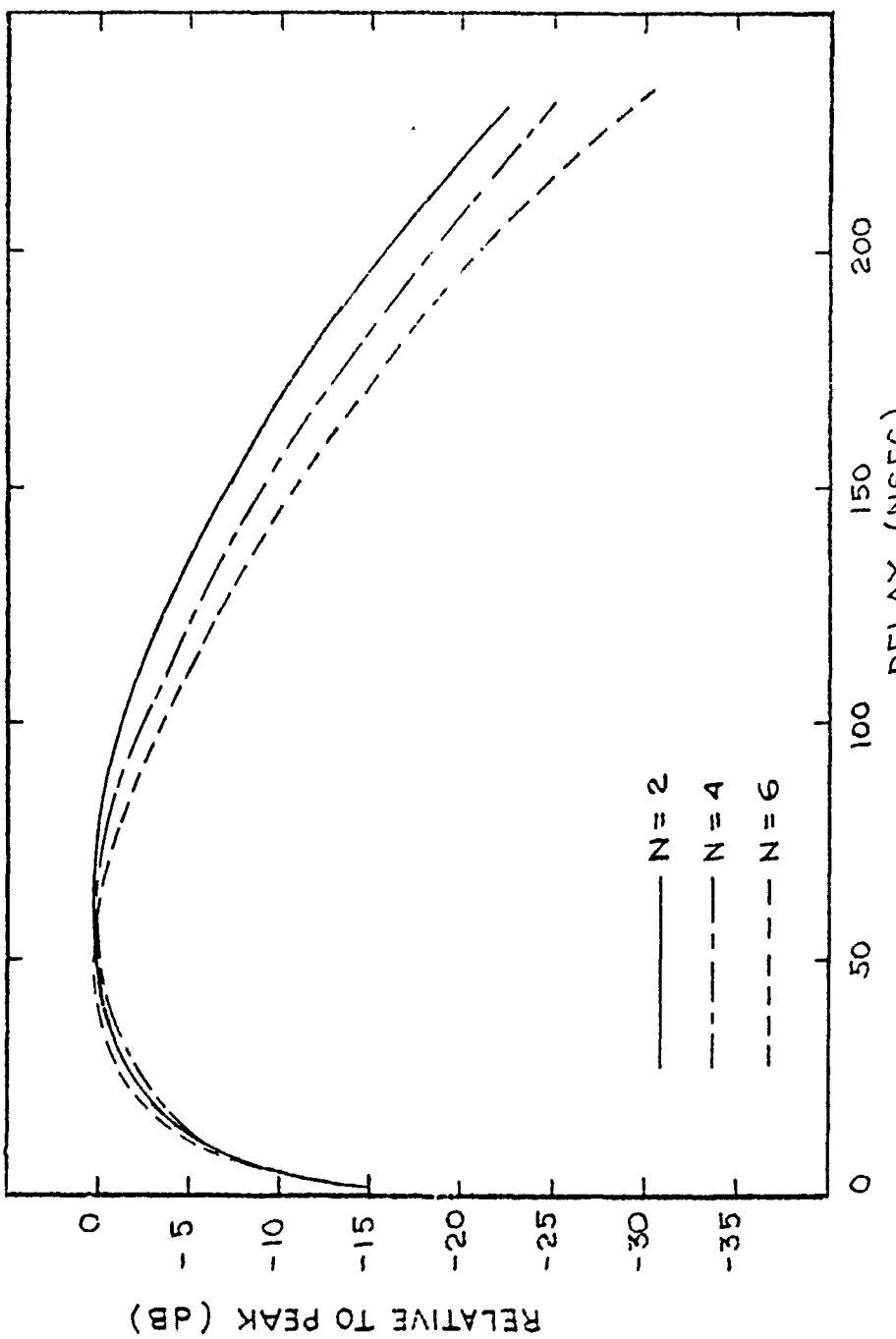

Fig. 3.11 Typical Multipath Profiles at 4.5 GHz

they are the major cause for the discrepancies between theoretical and empirical results found in previous studies.

The probing technique is illustrated in Fig. 3.12. Let the probing waveform (typically a PN-sequence) be p(t) and let the transmitted waveform be $p_t(t)$,

$$p_t(t) = \int_c^\infty h(\tau)\ p(t-\tau)d\tau,$$

where $h(\tau)$ is the impulse response of the transmitter filter. If the time varying channel impulse response is denoted $g(t,\tau)$ the received signal is

$$r(t) = \int_o^\infty g(t,\tau)\ p_t(t-\tau)d\tau \quad +n(t).$$

n(t) is additive white Gaussian noise. The theoretically optimal receiver is a filter matched to $p_t(t)$. In practice the received signal is correlated with delayed version of p(t). For our purpose we can consider the receiver to be a filter matched to p(t). The output, z(t), of this filter is

$$z(t) = \int r(\nu)p(T-t+\nu)d\nu$$

$$= \int d\nu \int d\tau\ g(\nu,\tau)\ p_t(\nu-\tau)p(T-t+\nu)$$

T is the signal duration. Squaring and averaging this yields (ignoring noise

$$\overline{z^2(t)} = \int d\nu_1 \int d\nu_2 \int d\tau Q(\nu_1-\nu_2,\tau)p_t(\nu_1-\tau)p(T-t+\nu_1)p_t(\nu_2-t)p(T-t+\nu_2).$$

In this expression $Q(\nu,\tau)$ is the tap gain correlation function defined by

$$E\left(g^*(t,\tau_1)g(t+\nu,\tau_2)\right) = Q(\nu,\tau_1)\delta(\tau_1-\tau_2).$$

It is assumed that the channel is WSSUS (Wide-Sense Stationary Uncorrelated Scatter). In practically all troposcatter situations the fading is so slow that we can make the "frozen" channel approximation

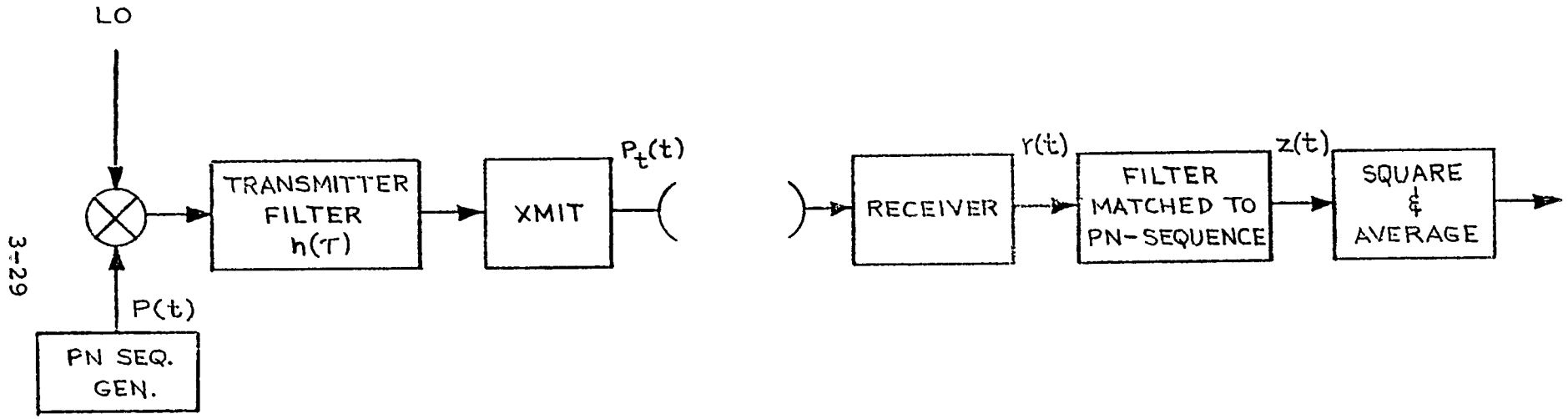

Fig.3.12 Prober Schematic

$$Q(\nu,\tau) \sim Q(0,\tau) \triangleq Q(\tau).$$

This gives

$$\overline{z^2(t)} = \int_0^\infty Q(\tau)\,|\rho(T-t+\tau)|^2 d\tau,$$

where $\rho(\tau)$ is the signal correlation

$$\rho(\tau) = \int p_t(\nu)\; p(\nu+\tau)\, d\nu.$$

If $|\rho(\tau)|^2$ were a Dirac delta function we would get

$$\overline{z^2(t)} = Q\;(t - T).$$

Probing signals are designed to approximate such a delta function, so we take as the estimate of $Q(\tau)$,

$$\hat{Q}\;(\tau) \triangleq \overline{z^2(t+T)}.$$

Usually the delay spread is characterized by the rms spread of $Q(\tau)$, defined by

$$\sigma_Q^2 \triangleq \int \tau^2 Q(\tau)\,d\tau / \int Q(\tau)\,d\tau - \left[\int \tau Q(\tau)\,d\tau / \int Q(\tau)\,d\tau\right]^2.$$

With this definition the measured delay spread is

$$\sigma^2_{\hat{Q}} = \sigma^2_Q + \sigma^2_{|\rho|^2}.$$

The second terms represents the error due to the fact that $|\rho|^2$ is not a delta function. This also includes the effect of the transmitter filter.

In the most common situation a PN sequence is transmitted, and $\rho(\tau)$ can be assumed to be

$$\rho(\tau) = \begin{cases} 1 - |\tau/T_o| & |\tau| < T_o \\ 0 & |\tau| > T_o \end{cases}$$

T_o is the period of the pulses. If the filter can be ignored and an essentially continuous sampling is assumed we have

$$\sigma^2_{|\rho|^2} = T_o^2/10.$$

For the measurements used in this report we have

$$T_o = 100 \text{ nsec.}$$

It follows that the minimum 2σ multipath spread is

$$2 \cdot \sigma_{|Q|^2} = \frac{2}{\sqrt{10}} T_o = 63 \text{ nsec}$$

In practice the transmitter filter can often cause long tails on $\rho(\tau)$, and hence substantially increase the multipath spread inherent in the measurement system. As a simple example, Table 3.3 shows the effect of a single-pole filter.

Table 3.3

2σ Delay Spread of Ideal Channel with a Single Pole Filter

$T_o \cdot B_{3dB}$	$2\sigma_{\|Q\|^2}$/nsec
∞	63
1	72
.5	92
.3	125

The effect of the additive noise is to add a constant to the estimated delay power spectrum $\hat{Q}(\tau)$. This means in principle infinite delay spread. This startling fact is somewhat alleviated by realizing that only a finite number of samples of $\hat{Q}(\tau)$ are used in practice, but it clearly underscores the importance of eliminating the noise. Also it must be pointed out that the RAKE adds a noise dither signal at the A/D input which produces a -15 dB input SNR.* The resulting noise of the output of the integrator is

* The output SNR is -15 dB + 10 log T_I/T_B where T_I = integration time, T_s = symbol length.

the main contributor to the above mentioned additive noise. In many of the measurements the RAKE tap value due to this noise alone contribute significantly to the measured spread. Since only 10 taps were used,the error is largest when the actual delay spread is relatively small (say 200 nsec or less). For this reason it is mainly the 4.5 GHz channel that is affected, while the measurements at 900 MHz are reasonably accurate (although the tail end often has been cut off). The results of the measurements were summarized in Table 3.1, where the effects of noise and measurement bias have been corrected for.

The fact that the prober only samples $\hat{Q}(\tau)$ at the rate of the transmitted PN-sequence means that the assumption of essentially continuous sampling is only approximately satisfied at long delay spreads. At smaller delay spreads variation in the sampling times can cause a large variability in the estimated spread. Suppose $\hat{Q}(\tau)$ is sampled at the instants $\tau_i = iT_o$. The estimated rms spread is calculated by

$$\hat{Q} \triangleq \hat{Q}(iT_o)$$

$$\sigma^2_{\hat{Q}} = T_o^2 \left(\Sigma\, i^2 \hat{Q}_i \; \Sigma\, \hat{Q}_i - \left(\Sigma\, i\hat{Q}_i \right)^2 \right) / \left(\Sigma\, \hat{Q}_i \right)^2$$

In general this does not relate simply to σ^2_Q, so let us consider a few simple examples.

Example 1:

$$Q(\tau) = \delta(\tau - \tau_o), \quad o < \tau_o < T_o$$

In this extreme case we clearly have

$$\sigma^2_Q = 0.$$

However, $\hat{Q}_i$ is

$$\hat{Q}_i = \int_0^\infty Q(\tau)\,|Q(iT_o + \tau)|^2\,d\tau$$

$$= |Q(iT_o + \tau_o)|^2$$

$$= \begin{cases} 0 & i < 0 \\ (1-\tau_o/T_o)^2 & i = 0 \\ (\tau_o/T_o)^2 & i = 1 \\ 0 & i > 1 \end{cases}$$

Hence the estimated delay spread is determined by

$$\sigma^2_{\hat{Q}} = T_o^2 \frac{Q_o Q_1}{(Q_o+Q_1)^2} .$$

If $\tau_o = 0$ or T_o we get the correct result, $\sigma^2_{\hat{Q}} = 0$. However if $\tau_o = T_o/2$ we get

$$\sigma^2_{\hat{Q}} = T_o^2/4.$$

Hence, if T_o = 100 nsec there can be an error in the 2σ - delay spread by the same amount, 100 nsec. This is larger than the 63 nsec for continuous sampling, but, in contrast, it is also possible to get the exact result.

It can be concluded from this example that the sparse sampling of $\hat{Q}(\tau)$ can be the source of much of the variation in the observed delay spreads when most of the received power falls in

a delay interval less than the tap spacing T_o. We will consider one more example to substantiate this.

Example 2:

$$Q(\tau) = \begin{cases} 0 & \tau < \tau_o \\ 1 & \tau_o \le \tau < \tau_o + T_o \\ 0 & \tau_o + T_o \le \tau \end{cases}$$

The corresponding delay spread is $\sigma^2 = T_o^2/12$, or $2\sigma = T_o/\sqrt{3}$. For simplicity we consider only the cases $\tau_o = 0$ and $T_o/2$. If $\tau_o = 0$ we have

$$\hat{Q}_i = \begin{cases} 0 & i < 0,\ i > 1 \\ T_o/3 & i = 0,\ 1 \end{cases}$$

Hence

$$\sigma^2_{\hat{Q}}\left[\tau_o = 0\right] = T_o^2/4$$

The 2σ spread is therefore too large, by a factor of $\sqrt{3}$, when $\tau_o = 0$.

If $\tau_o = T_o/2$ we have

$$\hat{Q}_i = \begin{cases} 0 & i < 0,\ i > 2 \\ T_o/24 & i = 0,\ 2 \\ 7T_o/12 & i = 1 \end{cases}$$

This gives an estimated variance of

$$\sigma^2_{\hat{a}} \left[\tau_o = T_o/2\right] = T_o^2/8 \ .$$

The 2σ spread is now too large by a factor of $\sqrt{2}$. It is interesting to note that if the above estimates are corrected as for continuous sampling we get

$$\sigma^2_{\hat{a}} \left[\tau_o = 0;\ \text{corrected}\right] = 3T_o^2/20 = \frac{T_o^2}{12} \cdot \frac{9}{5}$$

and

$$\sigma^2_{\hat{a}} \left[\tau_o = T_o/2;\ \text{corrected}\right] = T_o^2/40 = \frac{T_o^2}{12} \cdot \frac{3}{10} \ .$$

The average of these delay variances is almost equal to the correct value.

From these two examples we conclude that the correction derived for continuous sampling can be used for both long and short delay spreads, but that it must be interpreted as an average over sampling times at short delay spreads, with considerably variation possible around this value. In general, delay spread shorter than T_o (100 nsec) cannot be expected to be accurate.

With the above discussed measurement errors in mind we can now compare the empirical and theoretical results. The results of the measurements were tabulated in Table 3.2. At 900 MHz the median delay spread is 290 nsec, if the error due to noise and sampling are ignored. This is a reasonable approximation at this frequency but an uncertainty of up to $\pm$ 50 nsec should be allowed for. This measured delay spread can be compared with the theoretical result of 260 nsec with antenna pointed at the horizon and K= 1.3, N = 3 (Fig.3.6). If the antennas are pointed to maximize the power the delay spread is seen to be approximately 340 nsec with the

same atmospheric parameters. From Fig. 3.9 it is seen that 290 nsec spread is achieved with 0.7° take off angles, K = 1.3, and N ≃ 14/3.

The correspondence between theoretical and empirical results at 900 MHz is well within uncertainties due to unknown atmospheric parameters, pointing angles, noise, and time synchronization.

At 4.5 GHz the delay spread is so small that it is necessary to subtract an estimate of the noise from $Q(\tau)$, and to compensate for errors in the correlation process. As justified above, the correction corresponding to continuous sampling has been used. The results (corrected) were symmarized in Table 3.1, showing a median delay spread of 118 nsec. In contrast, the median without correction is approximately 145 nsec. The theoretical value when the beams are pointed at the horizon is only 44 nsec. (Fig. 3.6) but with the same received power the beams could be pointed 0.47° above the horizon, corresponding to a delay spread of 108 nsec. It is in fact likely that one or both of the antennas are pointed slightly upwards to avoid local obstructions. The measured delay spread can easily be explained this way, but it is perhaps more likely that the delay spreads estimated from the measurements are still too large. The large uncertainties associated with timing errors, receiver noise and dither, pointing angles, and atmospheric noise explains easily the small differences (50-100 nsec) between the empirical and theoretical data.

3.2.3 Summary, Multipath Computations

The theoretical model developed in Section 3.1 gives a reasonable agreement with measured results. As can be expected the differences are most pronounced at the high frequency (narrow beam) where the results are much more sensitive to given parameter

variations. The agreement is well within the uncertainties, and much better than reported in previous studies [3.2].

3.3 Coupling Loss Computations

The aperture-to-medium coupling loss on a troposcatter link is defined as the loss incurred by not using the total available scatter potential. In other words, omnidirectional antennas have no coupling loss, while the gain of two narrow beam antennas is offset by the coupling. It will be shown that from elementary considerations the total gain increases asymptotically for very narrow beams by 3 dB each time the beamwidths are halved. This corresponds to a 9 dB aperture-to-medium additional coupling loss incurred when the beamwidths are halved.

The troposcatter prediction model developed herein can be used to predict the coupling loss. While the validity of the model for delay spread calculations was verified in Section 3.2, we compare here the predicted values of the aperture-to-medium coupling loss with several empirical results.

3.3.1 Predicted Aperture-to-Medium Coupling Loss

The coupling loss is calculated simply by computing the power received with a wide, essentially omnidirectional beam and the desired narrow beamwidths. The ratio of the received powers (eliminating the antenna gains) is the coupling loss.

In Fig. 3.13 the computed coupling loss is shown for the 4.5 GHz link in Table 3.1. As the two atmospheric parameter N,K,varies, the coupling loss varies between 10 and 16 dB. This can be compared with some known results. The nomogram (by Collins Radio) in Figs. 13-22 in Panter [3.3] yields the estimate 11.5 dB. The curves (by Hartman and Wilkerson, 1959) in Figs. 12-15 also in Panter tells us that a 10 dB coupling loss can be expected.

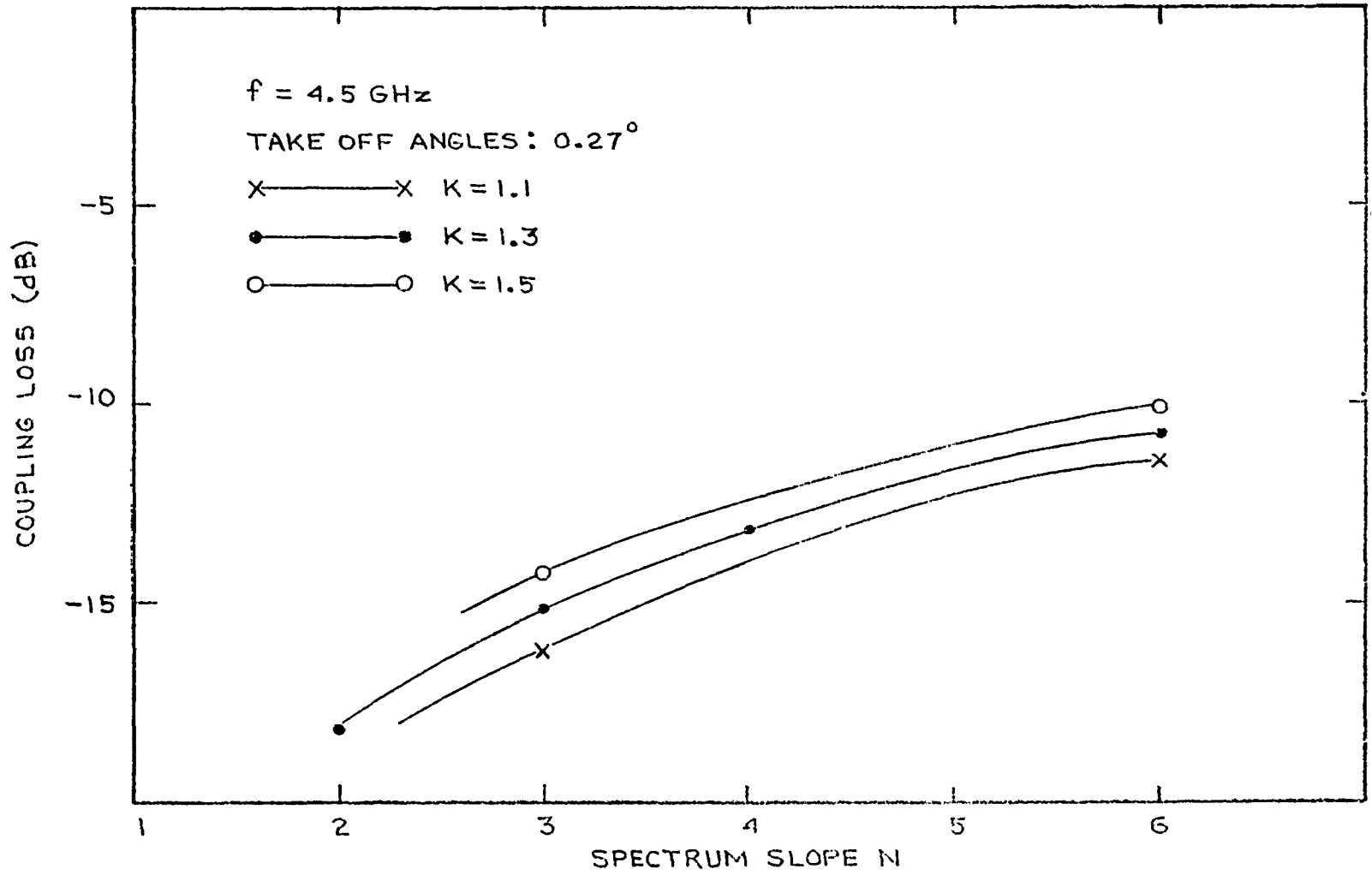

Fig.3.13 Aperture-to-Medium Coupling Loss as a Function of Spectrum Slope N and Earth Radius Factor K

These numbers are all in the low end of the range of the coupling loss calculated from our model. However, it must be realized that all these nomograms and curves are constructed from empirical data, where the antennas may well be pointed higher than the 0^{o} elevation angle assumed in our calculations. This uncertainty in the reported measurements places the actual coupling loss for the link configuration use in Fig.3.13 somewhere in the range of 10-15 dB, in better agreement with the predicted results.

The results in Fig.3.13 are for the 4.5 GHz link. Figure 3.14 shows the aperture-to-medium coupling loss as a function of frequency. The calculations have been performed for two relatively extreme sets of atmospheric parameters. In combination with Fig. 3.13 it is possible to find the coupling loss by extrapolation for almost my situation. Also shown in Fig.3.14 are some of the known results referenced in connection with Fig. 3.13.

It should be emphasized that these predicted values of coupling loss represent median quantities. The long term variability of coupling loss can be computed from Figs.3.13 and 3.14 given probability distribution information on the effective earth radius factor K and the refractive index spectrum slope N. The knowledge of antenna take-off angles and atmospheric parameter variations is essential if the effects of aperture-to-medium coupling loss are to be adequately accounted for.

3.3.2 Specific Considerations

Coupling loss effects have special significance for transmission systems where radio carrier frequency changes are anticipated because the increased loss at higher frequencies may preclude operation with adequate system margin. We examine here some of the salient features associated with a frequency change (doubling of the frequency is used as an example), provide a simplistic but

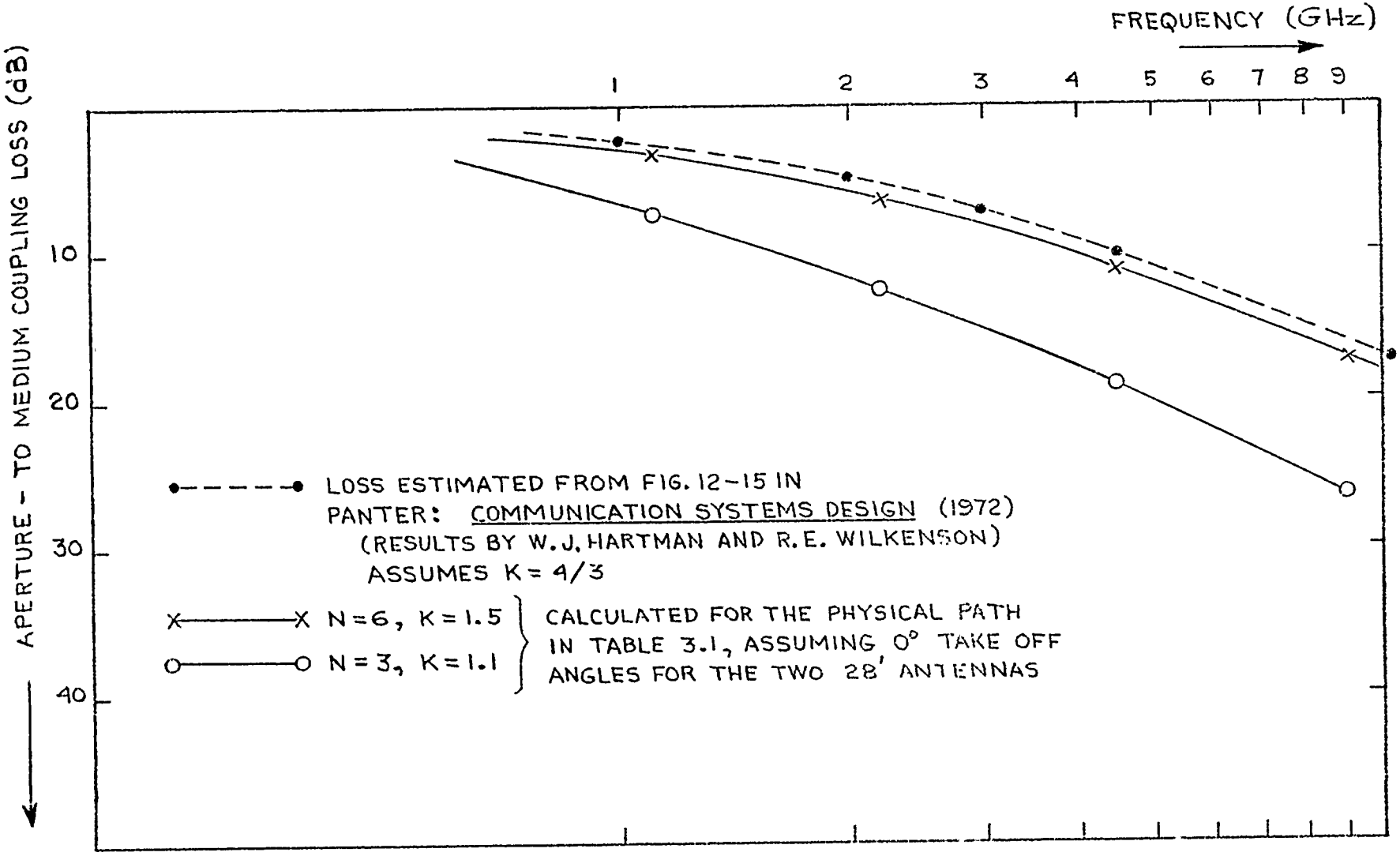

Fig.3.14 Coupling Loss as a Function of Frequency for 168 mi Path vs 28' Antennas

asymptotically accurate interpretation of coupling loss, and finally we discuss the relative advantages of multiple feedhorns (angle diversity) vs. multiple antennas (space diversity) as a means of alleviating the coupling loss problem.

If the operating frequency of an existing tropo link is doubled there are three factors affecting received power:

(a) Free-space antenna gain at each terminal increases by 6 dB for a total increase of 12 dB.

(b) The tropo path loss between isotropic radiators increases by 9 dB. (See, for example, P.F.Panter, Communication Systems Design,pp.384-397, McGraw-Hill,1972.) Of this 9 dB, 6 dB is the normal free-space isotropic aperture area loss, and 3 dB is the scatter anomaly.

(c) The aperture-to-medium coupling-loss increases.

There is thus a 3 dB gain excluding the change in coupling-loss.

Using the nomographs in Panter (op.cit.) the change in coupling loss can be evaluated for a few simple cases, listed in the following table.

TABLE 3.4

Increase in Coupling loss from
Doubling the operating frequency

	14 foot dish 1.0° at 4.4GHz 2.0° at 2.2GHz	28 foot dish 0.5° at 4.4GHz 1.0° at 2.2GHz
Path length 100 nmi Scatter angle 1.25°	1 dB at 2.2GHz 3 dB at 4.4GHz Change = 2 dB Net gain: 1 dB	3 dB at 2.2GHz 10 dB at 4.4 GHz Change = 7 dB Net Loss: -4 dB
Path length 200 nmi Scatter angle 2.5°	2 dB at 2.2GHz 7 dB at 4.4GHz Change = 5 dB Net Loss:-2 dB	7 dB at 2.2GHz 16 dB at 4.4GHz Change = 9 dB Net Loss = 6 dB

The mechanism of coupling loss can be understood somewhat better by looking at the shape of the useful scattering region. This region is bounded below by the tangent planes to the 4/3 earth at transmitter and receiver, which determine the lower limits of common visibility. It is (roughly speaking) bounded above by a curved surface where the scattering angle is, say, twice the minimum value. This curved surface is generated by passing a circle of a certain specific radius through the transmitter and receiver and rotating it while holding those two points fixed. The resultant scattering region looks something like that shown in Figure 3.15 in plan and elevation. It should be noted that the scattering efficiency is greatest on the shortest path through the point marked A on the figure, and falls off several dB toward the edges.

From the figure, we see that as the dimensions of the transmitted beam get very narrow, the actual scattering volume defined by the transmitter becomes just proportional to the product of the azimuth and elevation beamwidths. Thus if we halve the two beamwidths, we quadruple the incident power density but quarter the illuminated volume thus scattering the same total power out of the beam. Now if the receiver has the same size antenna, there is essentially no loss of power due to its azimuth beamwidth, which is seeing the same width of scattering region that the transmitter illuminates. However, if the elevation beamwidth of the receiver is halved, only half as much length of the illuminated region is seen. The consequence is that a total increase of free space gain of 12 dB results in only a 3 dB increase in received power, so the coupling loss asymptotically increases by 9 dB for every 6 dB increase in dish gain. Another way of viewing this is to recognize that the common scattering volume is proportional to the cube of its linear dimension, or inversely proportional to the cube of dish

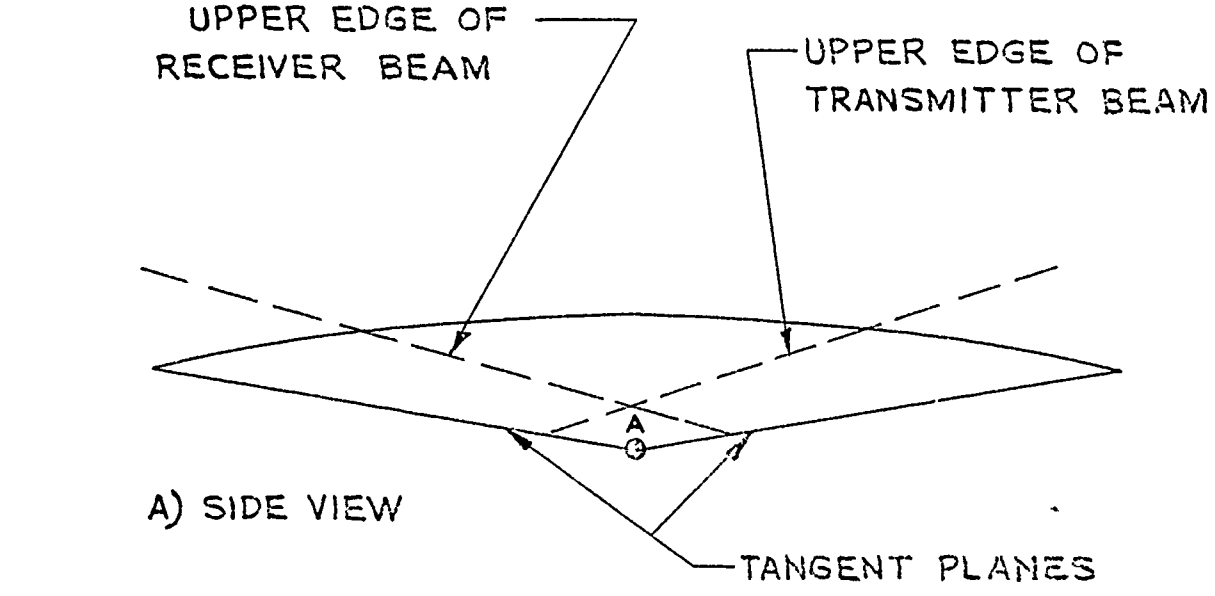

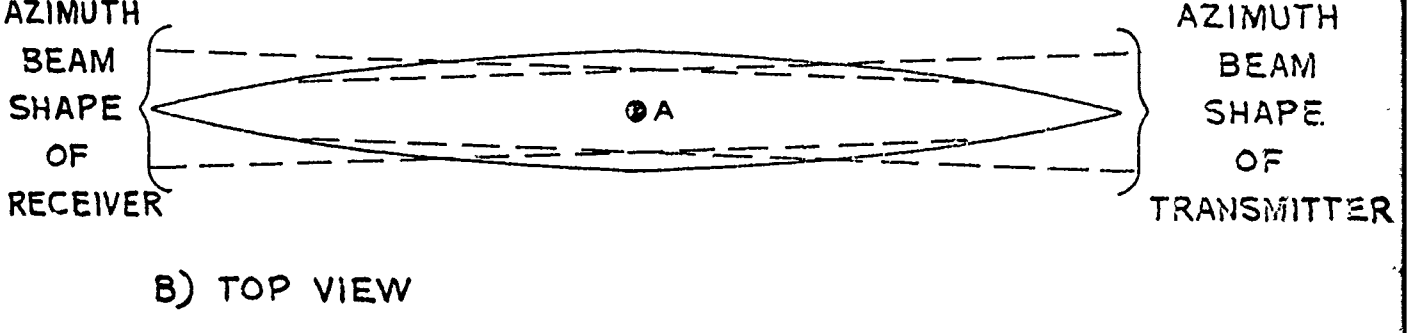

Fig.3.15 Sideview and Top View of Scattering Region

diameter in wavelengths, so that since total gain is proportional to fourth power of dish diameter, the net gain is only increasing linearly with the dish diameter in wavelengths. With this way of looking at the loss phenomenon, we can view the total dB coupling loss as consisting of three components.

(a) 1/3 of the dB loss from the vertical beamwidth of the transmitter

(b) 1/3 of the dB loss from the vertical beamwidth of the receiver

(c) 1/3 of the dB loss from the narrower of the transmitter and receiver azimuth beamwidths.

The preceding argument shows that roughly 1/3 of the dB coupling loss can be regained by using dual vertical angle diversity at the receiver. This would result in the loss values of the following table.

Table 3.5

Median Loss Incurred from Doubling the Operating Frequency and Using Vertical Angle Diversity

	14 foot dish	28 foot dish
100 nmi	Gain: 2 dB	Loss 2 dB
200 nmi	Loss: 0 dB	Loss 3 dB

The median loss is computed for an idealized vertical angle diversity system with equal but uncorrelated energy in the elevated beam. For such a system there would also be a diversity gain advantage. This diversity gain advantage is reflected in Fig. 3.15 where ideal CPSK at fourth and eight order diversity is compared. At 10^{-5} bit error probability there is a total improvement of approximately 5 dB, 3 dB of which is the median loss improvement and 2 dB is the diversity gain advantage. Note that no additional power

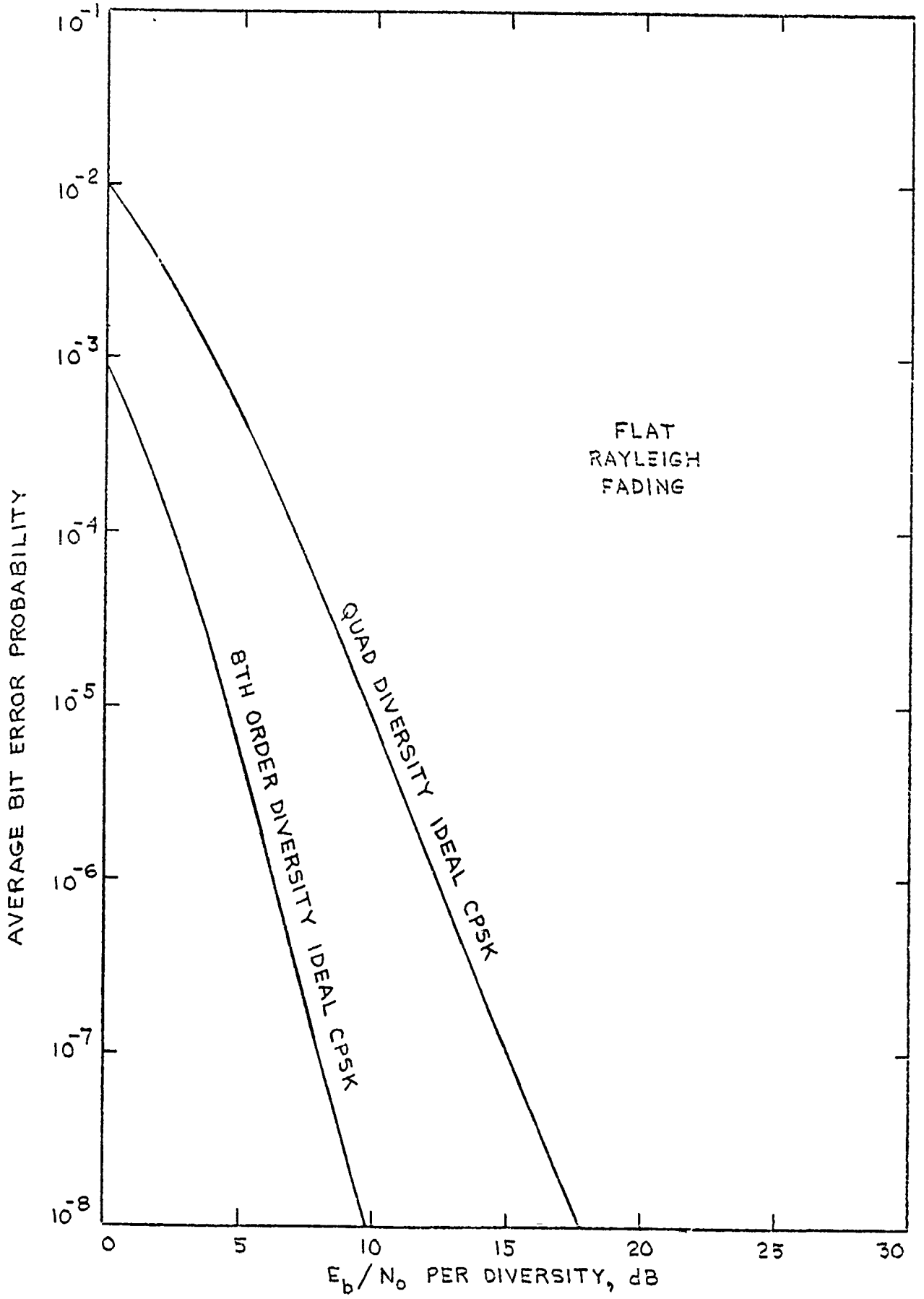

Fig. 3.15 Flat Fading Channel Performance

must be transmitted in an angle diversity system in order to realize this 5 dB improvement at 10^{-5} BER. The improvement results from an interception of additional transmitter beam energy not used by the quad diversity system. Of course, realistic systems will not realize perfect decorrelation and exactly equal energy in the elevated beam to which also must be included the effects of multipath (implicit diversity) and implementation losses. Thus a comprehensive performance evaluation must be undertaken in order to assess the full impact of frequency changes on existing systems.

In any case, for any <u>fixed</u> order of diversity and receiver complexity at the new frequency, there is probably <u>no</u> technique which is significantly more efficient than vertical angle diversity! Consider, for example, the case of a 140 nmi path using 20 foot dishes at 4.4 GHz. These values yield 1.75° scattering angle and 0.7° antenna beamwidth which in turn results in an 8 dB coupling loss. With vertical angle diversity, this could be reduced to a median effective loss of 5 dB, after diversity combining. We might consider as an alternative approach dual space diversity using 2 dishes with 14 foot diameters in place of every 20 foot dish; the total aperture area is then the same as the angle diversity setup. The coupling loss with this setup is reduced to 4½ dB. However, the total antenna gain is decreased by 6 dB yielding a total effective loss per antenna of 10½ dB which only reduces to 7½ dB after diversity combining. Thus the vertical angle diversity is 2½ dB better than the equivalent complexity and aperture space diversity setup.

3.4 Reference to Section 3.

[3.1] L.E.Ehrman,P.Monsen,"MDTS Field Test Report,"SIGNATRON Technical Report No. A163, June 1976.

[3.2] Sherwood,A, and L.Suyemoto, Multipath Measurements Over Troposcatter Paths, Mitre Corporation, Report MTP-170, April 1976.

[3.3] Panter, P.F.,Communication Systems Design: Line-of-Sight and Troposcatter Systems, McGraw-Hill Book Co., New York, 1972.

SECTION 4

ADAPTIVE ANTENNA CONTROL TECHNIQUES

The Defense Communication System utilizes transhorizon radio communication links as an important component of its strategic communication network. The propagation mode for these transhorizon link is either forward scatter or diffraction. The performance of both of these modes is subject to variations in angle of arrival due to changes in the effective earth radius, ducting phenomena, or shifts in the effective common antenna volume. We summarize here three major approaches for the compensation of this effect. One of the approaches, angle diversity, not only has the potential to compensate for angle of arrival variation but can utilize the angle of arrival decorrelation to provide a performance improvement due to increased diversity. This section concludes with a brief review of previous angle of arrival experimental programs.

4.1 Mechanical Steering

The most obvious method of correcting for long term variations in the angle of arrival of the received signal is to move either the antenna or the feedhorn structure. Control of the mechanical movement can be effected by adaptation algorithms which maximize median received power or some monotonically related function such as signal-to-noise ratio. Two types of control are possible, single ended (open loop) or double ended (closed loop). For single ended control, each antenna pointing angle is adjusted independently to maximize its median received power. Adjustments must be infrequent, on the order of minutes in order to allow time for measurement of median power. The reciprocal nature of the transmit/receive paths in a typical transhorizon radio link make single ended operation without feedback control possible. When reciprocity does not

hold, for example a single transmit horn and multiple receive horms, closed loop control can be effected by using feedback information transmitted over an order wire channel. The control must consider the duplex nature of the transhorizon radio system. One approach is to adjust the antenna pointing angle one at a time and always in a direction which jointly maximizes the received signal power at both ends. In most applications only adjustments in the vertical plane are required as earth bulging or ducting phenomenon produces greater variation along the vertical axis.

Because of the difficulty of moving large parabolic antennas, an attractive alternative for mechanical steering is the movement of the feedhorn which illuminates the parabolic surface. As can be seen from Fig. 4.1* the loss associated with an off-axis feed is very small for large pointing angle variations.

A major advantage of mechanical steering is the capability to point the antenna at any feasible signal arrival direction with little or no beam degradation from boresight conditions. Electronic steering to be discussed next is limited by power levels and physical considerations which under certain conditions preclude antenna pointing at some angles without beam degradation.

4.2 Electronic Steering

Electronic beam steering of a high gain aperture such as a parabolic antenna can be accomplished by gain and phase adjustments

---

* Data from Microwave Antennas and Techniques, M.I.T. Lab. Series No. 12, edited by S. Silver, McGraw Hill Book Company, 1949.

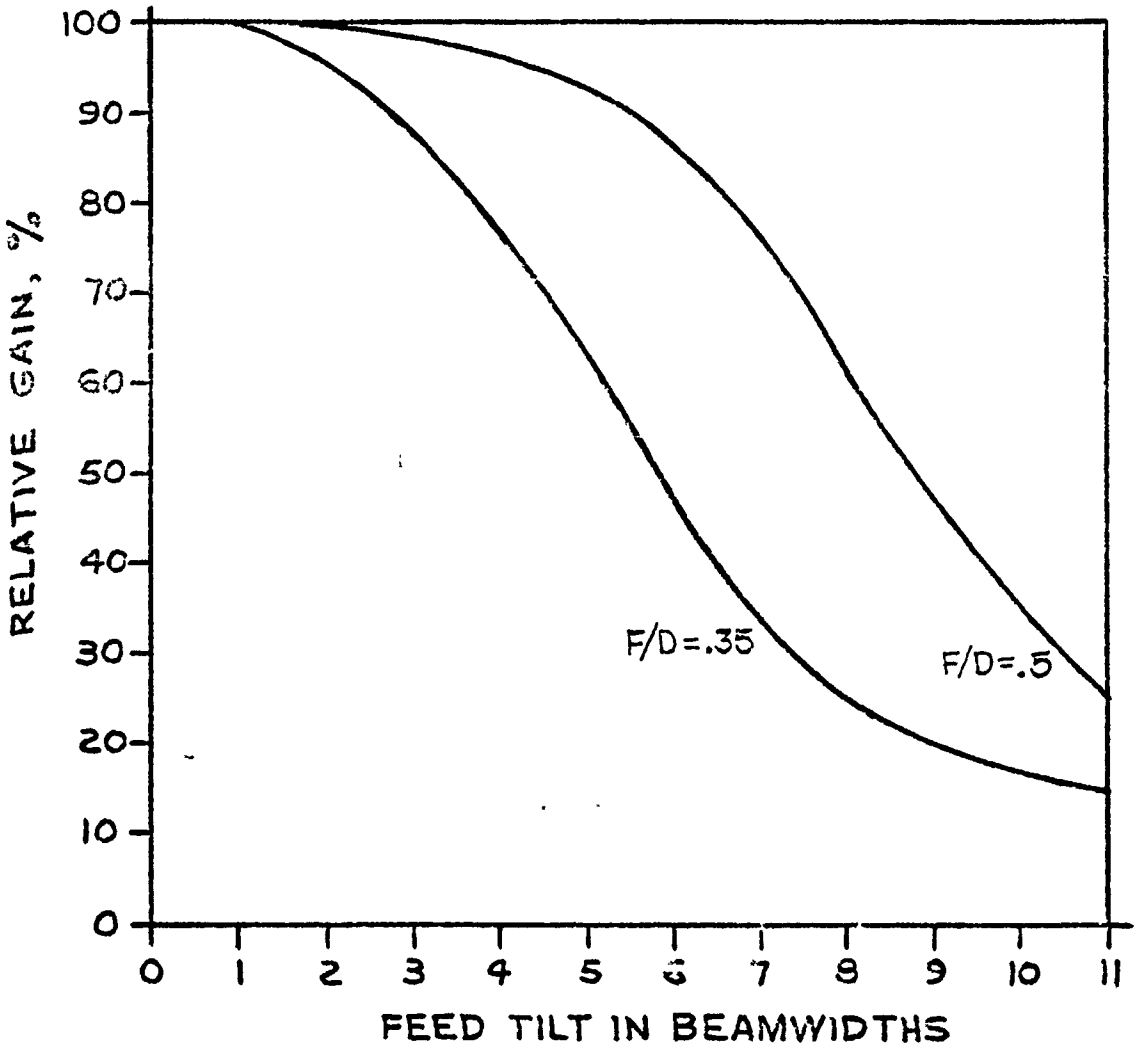

Fig. 4.1 Antenna Gain Degradation

of multiple excitations which are used to illuminate the aperture. As an example consider two feedhorns arranged in a vertical stack as in Fig. 4.2. Consider the top feedhorn to be directed at the parabola center to produce a beam in the boresight direction. The lower horn generates an elevated beam raised α degrees above the boresight direction. If H is the horn size and F is the focal length of the antenna system, the angle α is given by

$$\alpha = (\text{BEAM FACTOR}) \tan^{-1} (H/F). \qquad (4.1)$$

The beam factor accounts for non uniform illumination of the aperture and spill-over beyond the aperture. Parabolic antennas for transhorizon radio systems have beam factors on the order of 0.8. Amplitude and phase adjustments of the feedhorn signals form an antenna beam at any angle between 0 and α from boresight.

If the beam separation angle α is too large in an electronic steering application a significant reduction in antenna gain can result at angles near $\alpha/2$. The gain in dB as a function of angle β from boresight of a parabolic antenna can be approximated

$$G_p = 20 \text{ LOG } [2J_1 (3.2\beta/\Omega) / (3.2\beta/\Omega)] \doteq -3 (2\beta/\Omega)^2 \text{ dB} \qquad (4.2)$$

where Ω is the half-power beamwidth. Say we wish to aim the antenna at the intermediate point, $\alpha/2$. This is accomplished by applying equal amplitude and phase weights to the two feedhorn signals. If single horn excitation at boresight corresponds to unity voltage, then after splitting the power equally between feedhorns, each beam at $\alpha/2$ contributes $0.707 \times 10^{-3(\alpha/\Omega)^2/20}$ volts. The antenna gain relative to single horn excitation as a function of α is

$$G_r = 3 - 3(\alpha/\Omega)^2 \text{ dB} \qquad (4.3)$$

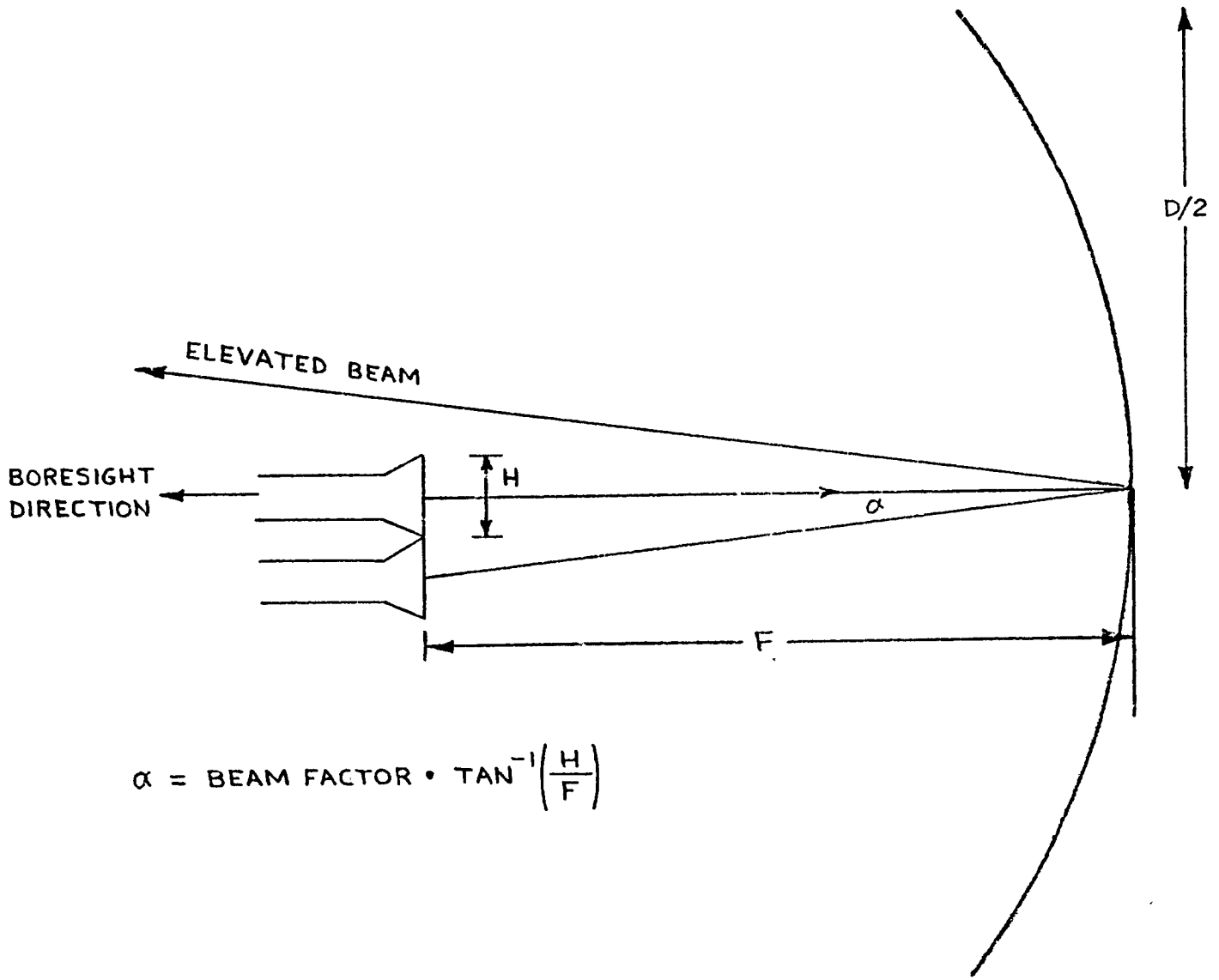

Fig. 4.2 Multiple Feedhorn Excitation of a Parabolic Antenna

If the feedhorns can be constructed such that the 3 dB beamwidths overlap, no loss in antenna gain results from pointing the antenna midway between the beams. Physical limitation, however, restrict the minimum value of α and may result in some loss at the midway pointing angle. For example a horn not designed for an electronic steering application has a typical size equal to twice the product of focal length (F) and wavelength divided by reflector diameter (D). Allowing for flange clearance, a practical engineering choice would be

$$H = 2.3\ (F/D)\lambda. \tag{4.4}$$

Larger horn sizes result in higher sidelobe levels due to phase changes at the parabola extremeties and smaller horn sizes result in some reduced antenna efficiency due to energy spillover at the parabola edges. Using (4.1) we can calculate the angle between beams for a multiple feedhorn application with this horn size.

$$\alpha = 0.8 \tan^{-1} \frac{2.3(F/D)\lambda}{F} \doteq 0.8\ (2.3)\lambda/D.$$

Since the antenna beamwidth in degrees is approximately $60\lambda/D$, we have

$$\alpha \doteq \frac{0.8(2.3)57.3}{60}\ \Omega = 1.76\ \Omega\ . \tag{4.5}$$

However for electronic steering this represents a relative gain of

$$G_r = 3 - 3\ (1.76)^2 = -\ 6.3\ \text{dB} \tag{4.6}$$

which is excessive for any practical transhorizon radio system. We conclude from this simple analysis of multiple feedhorn excitation that more sophisticated methods of deriving displaced beams are required if electronic beam steering is to be a viable approach.

Some of the alternatives for reducing the beam displacement for electronic steering include

- sacrifice of antenna efficiency in exchange for reduced horn size,
- use of multimode excitation within a single horn to produce displaced beams,
- use of a dielectric lens in conjunction with vertically stacked feedhorns.

The reduction in horn size necessary to move the beam close enough such that only a 1 dB degradation in the combined beam at the midway pointing angle can be calculated from (4.1) and (4.3). For 1 dB loss we must have

$$G_r = -1 = 3 - 3(\alpha/\Omega)^2$$

or

$$\alpha/\Omega = \sqrt{3}/2 \ . \tag{4.7}$$

Then from (4.1)

$$\frac{H}{F} \doteq \frac{\alpha}{0.8} = \frac{\sqrt{3}}{1.6}\,\Omega = \frac{\sqrt{3}(60)}{1.6(57.3)}\,\frac{\lambda}{D}$$

$$H \doteq 1.13(F/D)\,\lambda, \tag{4.8}$$

which is a 49% reduction in horn size from the engineering design example described.

An engineering design of a reduced feedhorn aperture is under development by R. F. Systems, Inc., subcontractor to SIGNATRON. The preliminary results of the design show that the loss in efficiency due to beam spillover balances well with improved edge intensity such that a significant decrease in horn size is possible without concomitant decrease in antenna efficiency. With a square horn size of 0.58 λ and a beam factor of 0.9, calculations show only a 0.05 dB loss at boresight. Since most troposcatter systems have

an F/D ratio of approximately 0.5, this horn size will facilitate electronic steering with less than a 1 dB degradation. The beam separation angle for a horn size of 0.58 λ and a F/D of 0.5 would be

$$\alpha = 0.9 \tan^{-1} \frac{0.58\lambda}{0.5D} \doteq \frac{0.8(0.58)57.3}{(0.5)(60)} \quad \Omega$$

$$\alpha \doteq \Omega,$$

i.e., the half power points of the adjacent beams would intersect. Because the feedhorn design developed by RF Systems successfully overlaps the beams at the 3 dB power points with very small efficiency loss (~0.05 dB), this approach is an obvious choice for either electronic steering or angle diversity. The other methods for small beam separation are discussed in subsequent paragraphs for completeness.

Monopulse radars use a vertically polarized TE_{10} and TE_{20} mode in a single horn to provide azimuthal angle of arrival measurements. Figure 4.3 illustrates how horizontally polarized TE modes could be used to produce two independent displaced vertical beams. The addition of a TE_{10} and TE_{20} in phase produces a vertical squint in one direction and the addition of a TE_{10} and TE_{20} out of phase produces a vertical squint in the other direction. A single feedhorn at the parabola focus can support both electromagnetic modes. The major limitation of this approach is the requirement for trans-horizon systems to operate with dual polarized horns. In a quadruple diversity forward scatter system, the typical transmit and receive configuration is as shown in Fig. 4.4. Note that the feedhorn must receive both vertical and horizontally polarized waves. The use of dual polarized feedhorns allows for more convenient signal separation and is standard practice. Thus although the horizontally polarized wave can be used in a multimode horn to produce two vertically displaced antenna beams, the vertically polarized wave for a similar configuration would result in beams displaced in azimuth. Since the significant angle of arrival fluctuations are

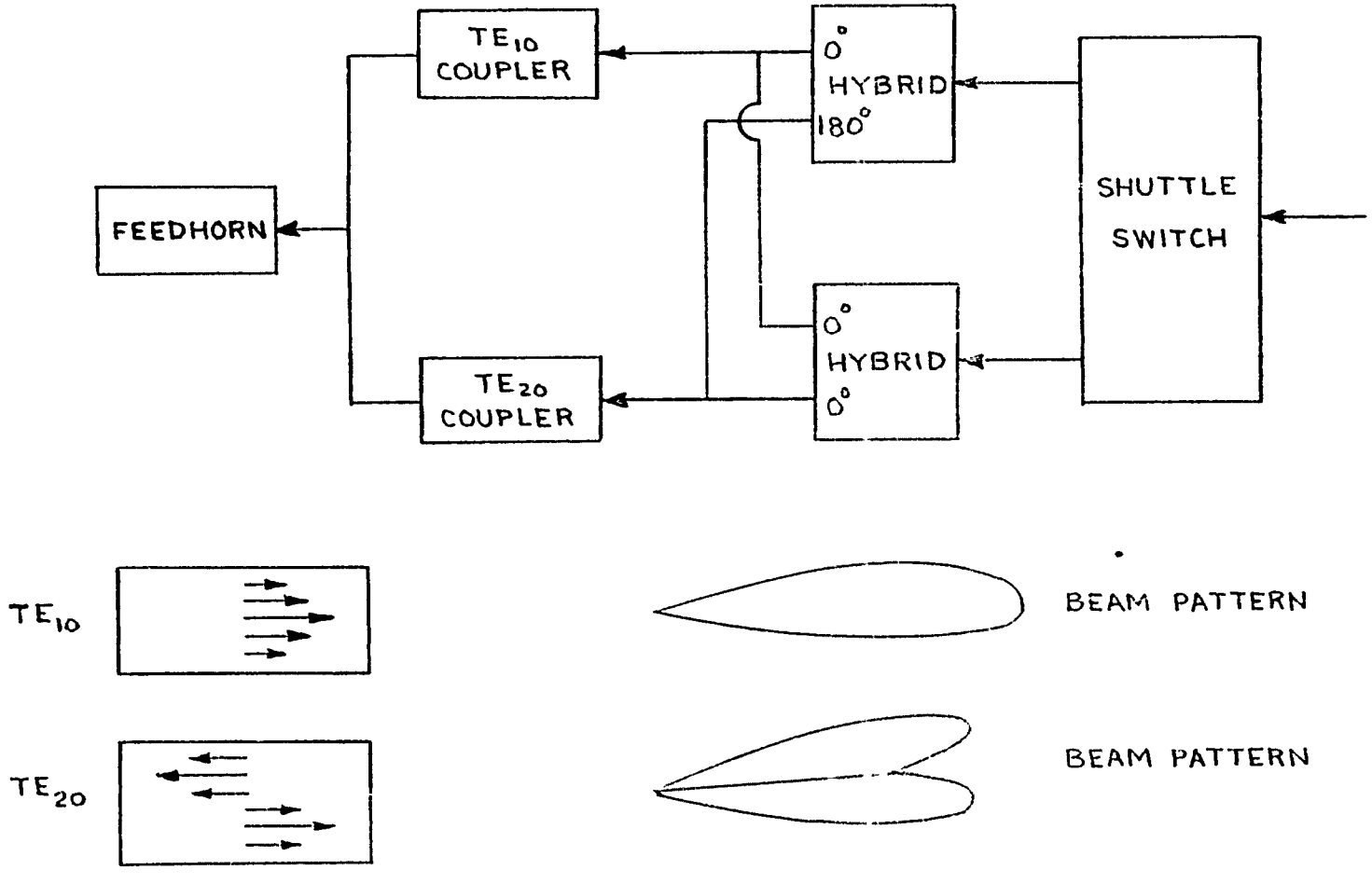

Fig. 4.3 Beam Control Using Two Horizontally Polarized Modes

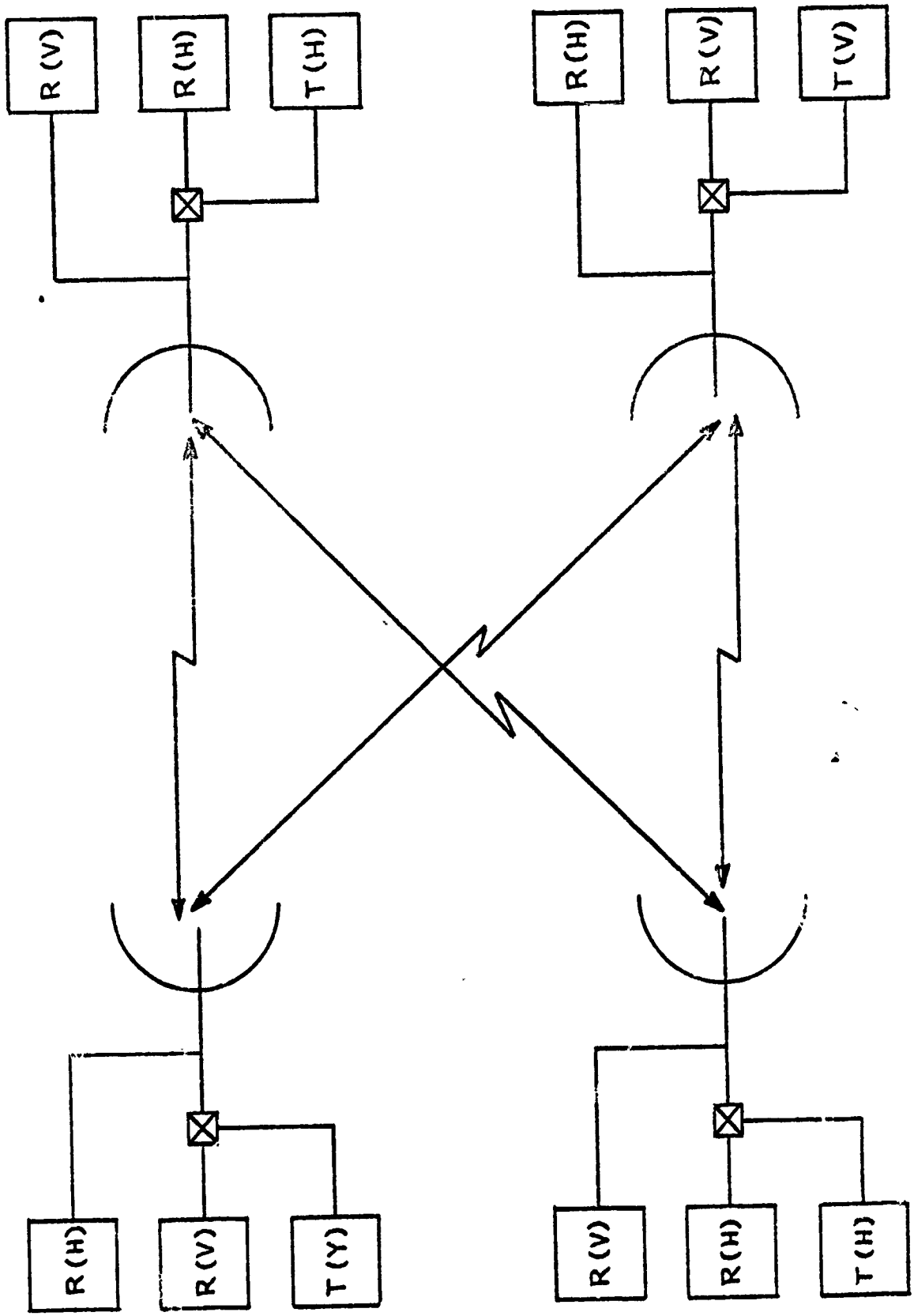

Fig. 4.4 Typical Troposcatter Link Configuration

in the vertical plane, there remains the question of how to produce vertical displacement with vertically polarized waves. Study of other modes used in single horn monopulse radars, e.g., TE_{11} and TM_{11}, has been completed with only negative results. The inability of this technique to produce vertically displaced beams for <u>both</u> polarization is a major limitation.

A dielectric lens can be used either in an end-fire feedhorn configuration [4.5] or as a wave bending surface to produce beams closer together for a fixed feedhorn separation. The major difficulty of this approach is the operation with large power at the lower frequencies required for troposcatter transmission.

The use of physically close feedhorns to produce beams overlapping at approximately the half power beamwidth is the most attractive of these approaches for reducing beam separation. A further consideration in the electronic steering of the beam given adequately close beams is the requirement for beam steering of the transmit power. Some of the alternatives include the use of either ferrite phase shifters or shuttle switches to produce amplitude and phase differences between beams to "point" the antenna. Ferrite phase shifters are subject to arcing at 10 kW power levels and would require an extensive waveguide pressurization system. The shuttle switch which diverts a fraction f of the power to one feedhorn and 1-f to the other feedhorn is limited in state of the art applications to about 2 kW. We conclude that although it may be possible to place the beams within one beamwidth of each other (a desirable quality for angle diversity also), electronic steering of up to 10 Kw of power appears to have higher risk and cost than mechanical steering by feedhorn movement.

4.3 Angle Diversity

In the last subsection we established that vertically stacked feedhorns located at the focus of a parabolic antenna produce antenna beams whose centerlines are separated by at least one beamwidth. For forward scatter systems one would intuitively expect the energy received at each feedhorn to be largely decorrelated with energy from other feedhorns since the respective common volumes are almost disjoint. Experimental and theoretical studies have confirmed that the correlation between vertical angle of arrival signals is small enough to realize significant diversity advantage. If the correlation coefficient is below 0.6, most of the diversity is realized. The combining of received angle of arrival signals as separate diversity signals is termed angle diversity (AD). In forward scatter systems, AD has the distinct advantage over steering techniques in that the diversity gain in dB usually far exceeds the improvement realized by optimally pointing the antenna. In an AD system, the short term fading effects are mitigated by the diversity combining action.

The correlation coefficient between beams is inversely related to the width of the angular power spectrum as seen by the antenna because of the Fourier transform relationship between the spatial correlation function of the received signal at the antenna and its angular spectrum. For narrow beam antennas, the angular spectrum in the azimuthal direction is limited by the beamwidth of both antennas whereas the angular spectrum in the vertical direction is limited by the beamwidth of the receiving antenna and the scattering angle dependence. Since the scattering angle dependence falls off more slowly than the beamwidth in most

practical applications, the vertical angular spectrum is broader than the azimuthal angular spectrum. Thus, the correlation coefficient between vertical beams is smaller than for azimuthal beams given the same displacement. The smaller correlation coefficient for vertical angle diversity beams makes it a superior choice over horizontal angle diversity.

The angle of arrival diversity can be realized by either multiple transmit beams, receive beams, or both. Multiple transmit beams have the distinct disadvantage of requiring either additional costly power amplifiers or a splitting of power into multiple feedhorns. The 3 dB loss in median signal due to transmitter power splitting does not result if only one transmit beam aimed approximately at the horizon is used and multiple receive beams are used to intercept it. The low correlation of vertically displaced beams and the power advantage of multiple receiver beams make receiver/vertical angle diversity the most attractive angle of arrival diversity configuration.

Long term variations in median signal strength as a function of angle of arrival are compensated for in a steering system. However, an AD system also provides protection against long term diffraction conditions because of the presence of additional angle of arrival signals. This protection results in a long term decorrelation advantage of AD over space or frequency diversity system. Because these diversity systems use the same common volume, they

are subject to long term fading resulting from conditions effecting that common volume. Angle diversity, on the other hand, employs virtually separate common volumes which in the long term have decorrelated statistics. For example, earth bulge effects which may seriously degrade space or frequency diversity systems would have much less effect on an angle diversity system. A mechanically steered system in a troposcatter system may provide a small dB advantage by accurately tracking the long term optimum pointing angle. An AD system, because of the beam separation, may not have the resolution to track small long term variations but protects against degradation due to larger changes in angle of arrival.

Thus in a forward scatter system, AD provides protection against short term fading effects and compensates for long term gross variations in angle of arrival. Note that in a transhorizon diffraction radio system since there is no scattering and thus no multipath fading, it is necessary only to track the optimum pointing angle (no diversity is necessary). If the antenna beam centerlines can be separated by 1 beamwidth, the angle diversity system on a diffraction path becomes a highly effective electronic steered system. As indicated in Section 4.2 however, practical alternatives to accomplish this end are limited due to the difficulty of electronic steering of large transmit powers.

4.3.1 Angle Diversity Applications

Because of the diversity advantage of an AD system on a forward scatter link, the remainder of our comments on angle diversity will be directed toward forward scatter operation. The geometry for a vertical angle diversity system is shown in Fig. 4.5. Define

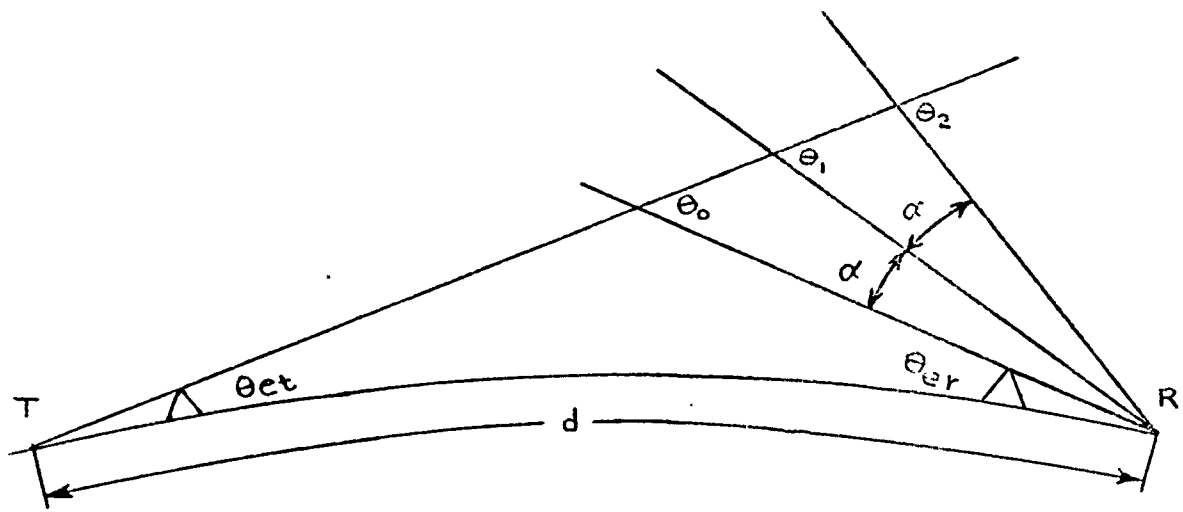

$$\theta_o = \frac{d}{a} + \theta_{et} + \theta_{er}$$

$$\theta_1 = \theta_o + \alpha$$

$$\theta_2 = \theta_o + 2\alpha$$

a = EARTH RADIUS

Fig. 4.5 Angle Diversity Geometry

θ_{et} = transmitter take-off angle

θ_{er} = receiver take-off angle

α = beam separation

d = path length

a = earth radius

θ_i = scattering angle for ith beam, i = 0,1,2.

From the geometry we find

$$\theta_i = \frac{d}{a} + \theta_{et} + \theta_{er} + i\alpha.$$

Because of the increased scattering angle associated with elevated beams, the received power for these beams will be reduced and the multipath delay spread will be increased. The effect of the reduced power is to limit the usefulness of the angle diversity branch to protection against fades deeper than the relative power for that branch. The increased multipath will produce more intermodulation distortion in analog systems and will require equalization in high speed digital systems. Horizontally displaced feedhorns also increase the scattering angle resulting in increased loss. The effect is more promounced on longer paths than on shorter paths. For shorter paths however, the correlation coefficient is large enough to limit the diversity capability.

In order to assess the links for potential application of angle diversity we consider a simplified performance analysis. The improvement due to angle diversity can be estimated* by considering

---

* These simplified calculations are presented here to briefly outline the general capability of angle diversity systems. In Section 3, the analysis is presented for the more detailed and exact performance computations which will follow in a later phase of the contract.

the average error probability for DPSK on a fading channel with Mth order diversity, viz.,

$$\bar{P} = \frac{1}{2}\left(1 + \bar{E}_b/N_o\right)^{-M} \tag{4.9}$$

The quantity $\bar{E}_b/N_o$ is the average received energy per bit divided by the noise power in 1 Hz. Equation (4.9) is a good approximation to performance of practical systems when the implicit diversity effect due to multipath is not large. If an angle diversity system had D feedhorns with independent relative received powers, $1, r_1, r_2, \ldots r_D$, the average error probability is

$$\bar{P}_D = \frac{1}{2}\prod_{i=1}^{D}\left(1 + r_i\bar{E}_b/N_o\right)^{-M}. \tag{4.10}$$

The relative powers of the angle diversity branches must be computed using an angle diversity model whose theoretical development is detailed in Sections 2 and 3. In order to parametrically evaluate the effects of reduced signal power on the angle diversity branches, we conservatively estimate the relative powers by using an exponential dependence on scattering angle. This estimate has been shown in experimental studies to be conservative because it ignores the contribution of both the lower sidelobe and the lower half beam width of the elevated beam.

The scattering angle dependence is taken as

$$\ell(\theta) = \sin^{11/3}\theta \tag{4.11}$$

For the first elevated beam, the dB loss is conservatively estimated as

$$L_1 = 10 \log \frac{\sin^{11/3}(\theta_o + \alpha)}{\sin^{11/3}(\theta_o)} \doteq 36.66 \log\left(\frac{\theta_o + \alpha}{\theta_o}\right) \tag{4.12}$$

We have determined the minimum practical beam separation to be one beamwidth. Thus

$$L_1 = 36.66 \log(1 + \Omega/\theta) \tag{4.13}$$

which is plotted in Fig. 4.6. The RADC link has a beam width to scattering angle ratio of

$$\frac{0.58^\circ}{1.82^\circ} = 0.319.$$

which gives a relative loss of 4.4 dB.

In detailed AD calculations for the RADC path, we have computed a smaller relative power loss but the received signals from the two feedhorns are not independent as assumed in the simple formulation presented here. The rather conservative estimate of relative loss suggested by (4.11) is balanced somewhat by the assumption of zero correlation between received signals. Thus the simple parametric calculation to determine the general parameters of troposcatter circuits amenable to AD techniques is probably quite accurate.

As a general rule if the elevated beam has a relative power greater than one-tenth it will be useful contributor to a quadruple diversity system. Weaker relative powers are useful in a dual diversity configuration where the fades are deeper. For a quadruple diversity system the error rate is reduced by $(1+0.1\ \overline{E}_b/N_o)^{-4}$ for a one-tenth relative power AD branch per explicit diversity branch If $\overline{P} = 10^{-5}$ without AD, the improvement with AD from (4.9) and (4.10) is a factor of 33 better. At 2.5 dB/decade this corresponds to an improvement of approximately 3.8 dB. From Fig. 4.6 for L_1 = 10 dB one finds that the 10 dB contour corresponds to

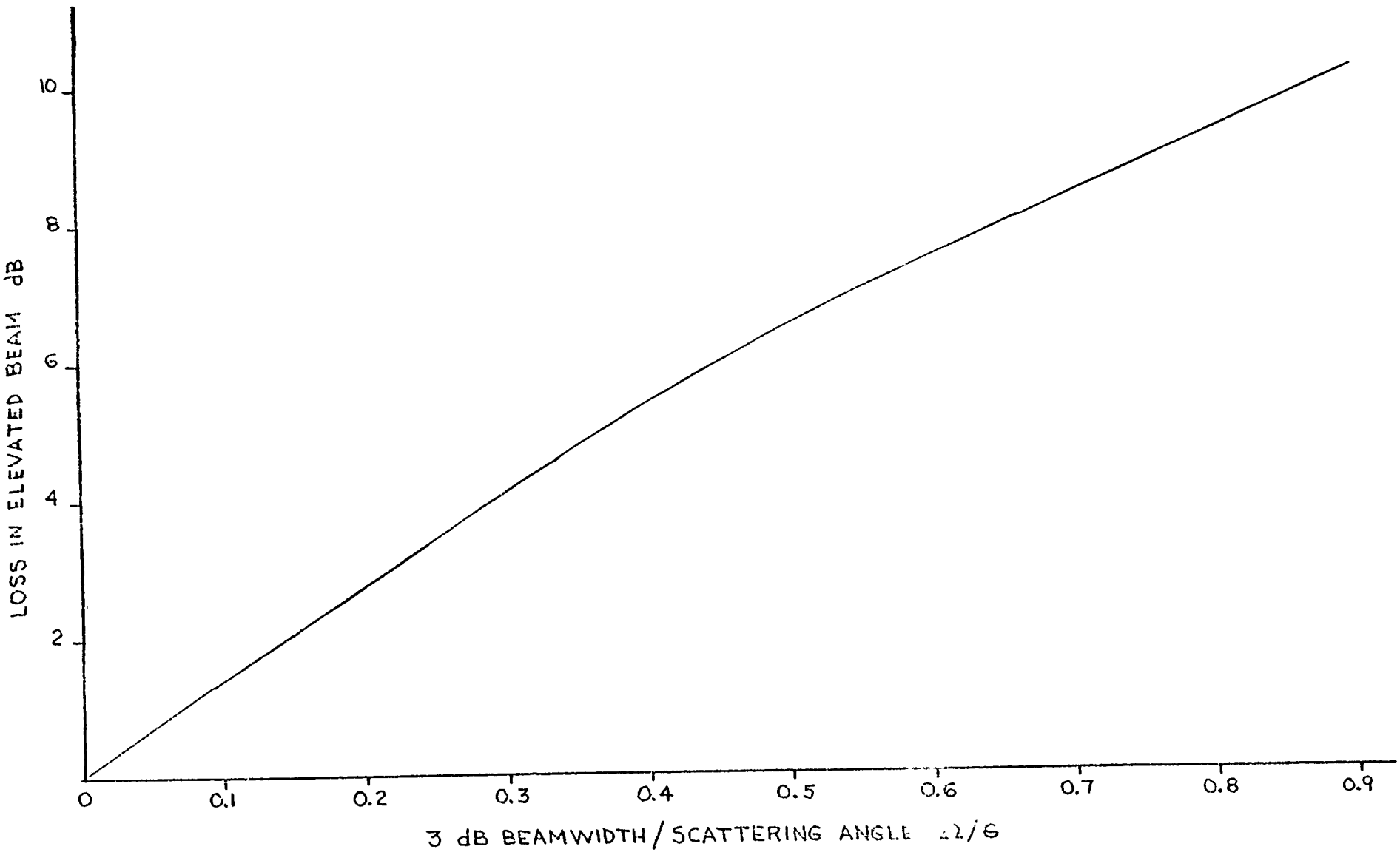

Fig. 4.6 Angle Diversity Relative Power Loss

$$\Omega/\theta = 0.875, \text{ 10 dB controur,} \tag{4.14}$$

i.e., AD is useful when Ω/θ is less than 0.875.

The expressions for beamwidth and scattering angle are

$$\Omega = \frac{60\lambda}{57.3D} \tag{4.15}$$

$$\theta = d/a. \tag{4.16}$$

From these relationships, the 10 dB contour as a function of frequency and path length can be computed and they are plotted in Fig. 4.7. For AD systems with length/frequency parameters above the contour a significant performance improvement will result. Note that most DCS forward scatter systems lie above these contours.

4.3.2 Summary of Previous Adaptive Antenna Control Experiments

In the field of tranhorizon radio communication, empirical results from radio experiments have continued to provide major contributions to the growth of the art. The approach to an adaptive antenna control system should be developed in light of the wealth of past angle of arrival radio experiments. In this subsection we review some of the more significant of these experiments and summarize the major findings to date concerning this communications mode.

In an early study, Crawford, Hogg, and Kummer [4.1] performed a comprehensive experimental study of transhorizon tropospheric propagation. The experiments included antenna pointing studies and an investigation of angle diversity. They established that, on the average, the maximum signal level is received when the antennas are aimed along the great circle between transmitter and

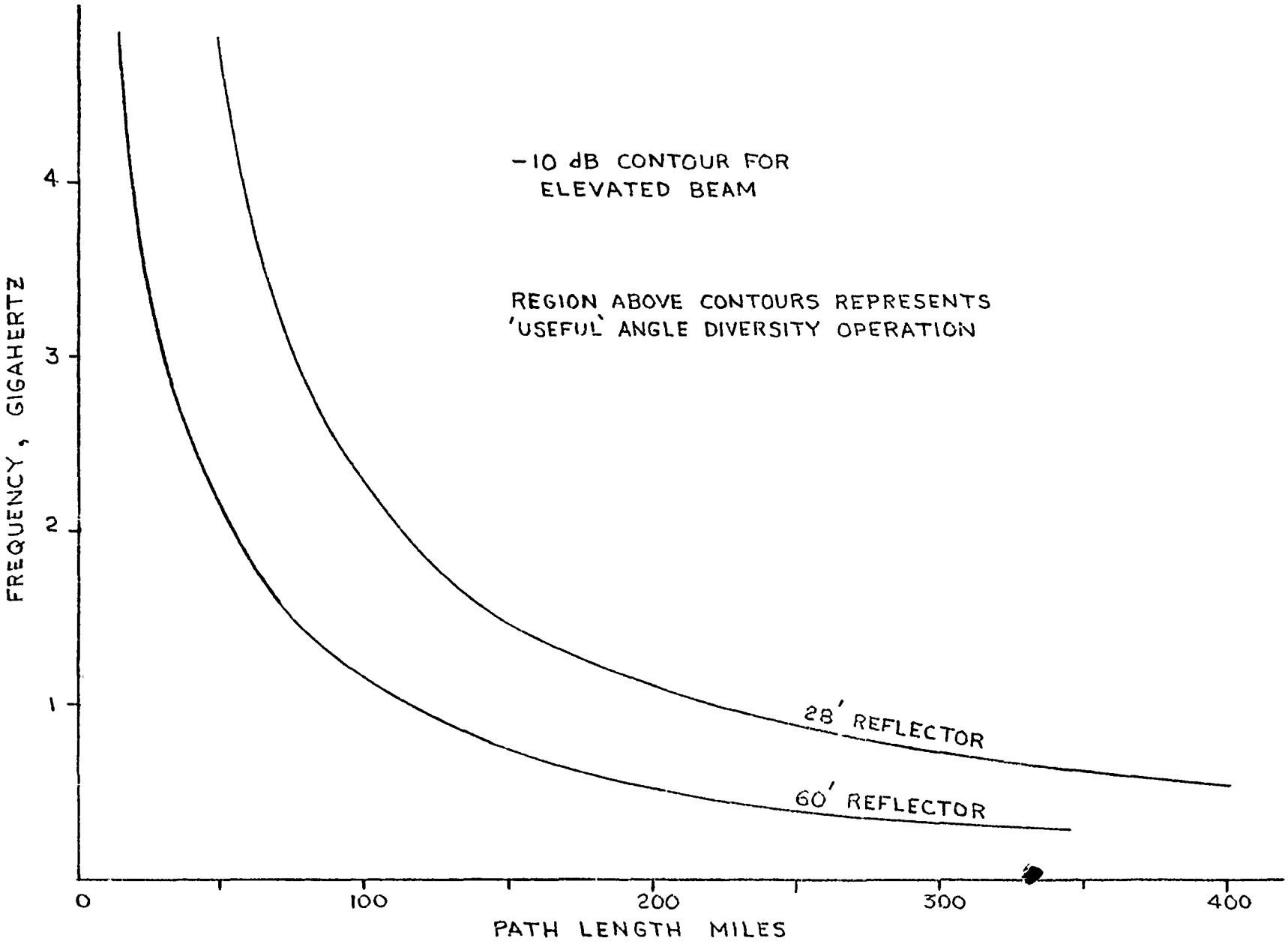

Fig. 4.7 Angle Diversity Contours

receiver location, with each being aimed just above the horizon. However, they found that local atmospheric refraction can exert considerable influence on the signals received on narrow beam antennas. In their angle diversity experiments they found that vertically displaced feeds provided essentially uncorrelated channels at both 460 and 4110 MHz. Their results with horizontally displaced feeds revealed a fade rate dependency. The theoretical diversity improvement was obtained in almost all cases at 4 GHz except when the fade rate was extremely slow, indicating the presence of very large horizontal layers. At 460 MHz the theoretical diversity improvement was not realized in many cases. When the rms Doppler spread was below approximately 0.5 Hz (which it will frequently be at this frequency of operation), large correlation between the horizontally displaced signals significantly degraded this type of diversity. In another study of azimuthal angle diversity, Chisholm, Rainville, Roche, and Root [4.2] measured correlation coefficients of 0.7 with 0.8 beamwidth separation and 0.5 with 1.2 beamwidth separation on a 2 GHz, 188 mile link. Significant diversity advantage is realized even with this high degree of correlation. The correlation coefficient dependency on fade rate and resulting loss in diversity gain was not investigated experimentally. Vogelman, Ryerson, and Bickelhaupt [4.3] measured negligible correlation between vertically displaced beams with separation of approximately 3 beamwidths. This large separation leads to excessive power loss in the elevated beams, however, due to an increase in the scatter angle. The theoretical relationship between correlation coefficient and angular separation in beamwidth has been derived [4.3,4.4] and is shown in Fig. 4.8. Since considerable correlation (< 0.6) will not significantly degrade the realizable diversity gain, it is advantageous to place the beams closer together to reduce the power loss in elevated beams.

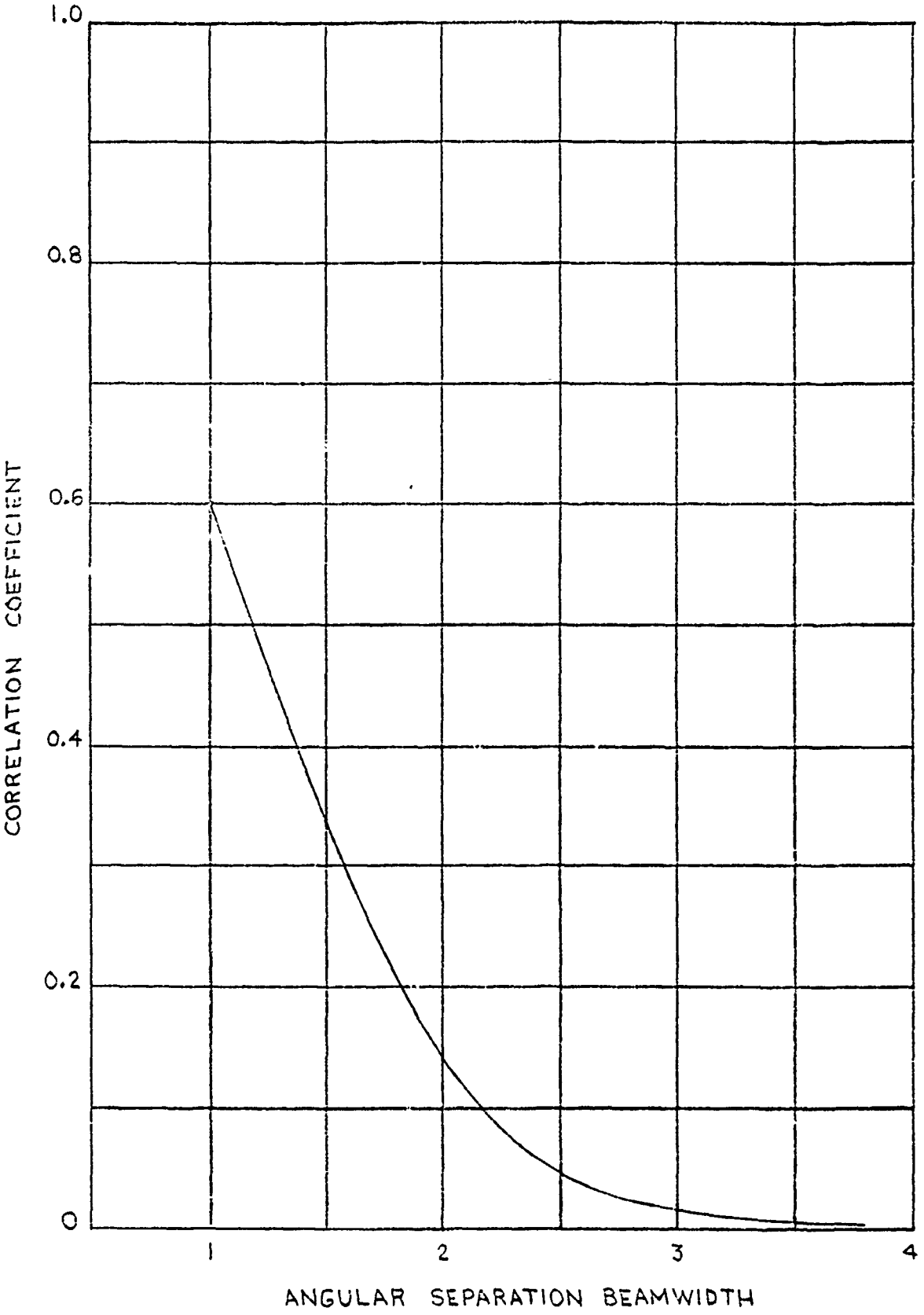

Fig. 4.8 Correlation Coefficient vs. Angular Separation in Beamwidths

Angle diversity tests at 8 GHz have been reported on by Surenian [4.5]. A significant feature of this work was the use of dielectric material at the feedhorn opening to produce and end-fire array. This approach provided decorrelated vertical and azimuthal beams with only a small median difference in signal strength beams. There is question, however, whether this approach would be successful at lower troposcatter frequencies because of

(1) increased dielectric loss and associated problems of high power transmission, and

(2) the effects of slow fading conditions which increase the correlation coefficient between horizontally displaced beams.

An angle diversity system was implemented for test purposes on the DCS troposcatter link between Greenland and Iceland. This link is characterized by 800 MHz FDM/FM operation, 120-foot parabolic reflectors, and a path length of 440 miles. The test results have been reported by Travis [4.6]. They found considerable correlation and relatively weak signal strengths in the horizontally displaced beams but very low correlation and relative median signal strengths of -5, 0, -2, and -8 dB in the four center vertically displaced horns. The tests included the use of an equal gain predetection combiner [4.7] of the type to be described in Section 5. Because of excessive multipath conditions it was necessary to modify the combiner by measuring intermodulation noise and switching out diversity channels where the combined thermal plus intermodulation noise was 6 to 10 dB higher than the noise in the best channel.

These system tests led to the development by Bell Laboratories of an angle diversity test system from Monrovia, Maryland to

Crawford Hill, New Jersey. The results of this program have been reported by Monsen [4.8], Bailey [4.9], Merrill [4.10], and Brady and Lima [4.11].

Some of the more significant findings of the program include:

- a beam swinging experiment established that the antenna pointing angle should be reduced roughly 1/2 beamwidth for each additional vertical feedhorn (simplex link).
- A triple angle diversity system was shown to have approximately the same outage probability vs. received signal level as a conventional dual diversity system.
- Angle diversity exhibits a long term correlation advantage due to the long term independence of the separate common volumes.
- The multipath delay spread increased by a factor of 1.6 for the first elevated beam and by a factor of 2.7 for the second elevated beam.
- Double humped multipath profiles were measured frequently, particularly on the elevated beams.
- The Merrill model for prediction of angle diversity relative signal strength was very accurate for the second skybeam but somewhat optimistic for the third.
- AD performance improvement close to the theoretical was shown in 0.5 and 1.0 Mb/s PSK data tests.

Adaptive antenna control with application to knife-edge diffraction links has been investigated in tests on a DCS link in southern Europe. Multiple feedhorns were used to determine if outage conditions in the main beam occurred independently from outages in elevated beams. During the test period no instances of

stronger elevated beams were noted [4.12]. In later tests [4.13] order wire control of both transmitter and receiver antennas was used to optimize performance. Typical daily variations in diffraction conditions resulted in improvements on the order of 1 or 2 dB due to optimized antenna pointing. During storm conditions, however, more extreme refractive index changes led to larger improvements under adaptive antenna control.

4.4 References

[4.1] A.B.Crawford, D.D.Hogg, and W.H.Kummer, "Studies in Tropospheric Propagation Beyond the Horizon," Bell Syst. Tech. J., Vol. 38, pp.1067-1178.

[4.2] J.H.Chisholm, L.P.Rainville, J.R.Roche, and H.G.Root, "Angular Diversity Reception at 2290MC over a 188-mile Path," IRE Trans.Commun. Syst., Vol. CS-7, pp.195-201, Sept. 1959.

[4.3] J.H.Vogelman, J.L.Ryerson, and M.H.Bickelhaupt, "Tropospheric Scatter System Using Angle Diversity," Proc. IRE, Vol. 47, pp.688-696, May 1959.

[4.4] R.Bolgiano,N.H.Bryand, and W.E.Gordon, "Diversity Reception in Scale Communication with Emphasis on Angle Diversity," Res. Rep. EE 359, Sc. Elec.Eng. Cornell Univ., Ithaca, N.Y., Jan. 30, 1958.

[4.5] D.Surenian, "Experimental Results of Angle Diversity System Tests," IEEE Trans. Commun. Technol., Vol. COM-13, pp. 208-219, June 1965.

[4.6] G.W.Travis, "Angle Diversity Tests," in Proc. Nat. Electron. Conf., Vol. 24, pp.518-523, 1968.

[4.7] J.W.Boyhan, "A New Forward Acting Predetection Combiner," IEEE Trans. on Comm. Tech., Vol. COM-15, October 1967, pp.689-694.

[4.8] P.Monsen,"Performance of an Experimental Angle Diversity Troposcatter System," IEEE Trans. on Comm., Vol. COM-20, No.2, April 1972, pp.242-247.

[4.9] C.C.Bailey,"Multipath Characteristics of Angle Diversity Troposcatter Channels," in Conf. Rec. 1971 IEEE Int.Conf. Communications, Montreal, Que., Canada, Sess. 26, pp.7-12.

[4.10] H.S.Merrill,Jr.,"An Impulse Response Model for Troposcatter Channels," in Conf. Rec. 1971 IEEE Int.Conf. Communications, Montreal, Que., Canada, Sess.26, pp.13-18.

[4.11] D.M.Brady and P.J.Lima, "Experimental PSK Error Rate Studies on an Angle Diversity Troposcatter System," in Conf. Rec., 1971 IEEE Int.Conf. Communications,Montreal, Que., Canada, Sess. 26, pp.19-24.

SECTION 5
SYSTEM CONSIDERATIONS

The different adaptive antenna control approaches must be considered with respect to the type and character of transhorizon radio systems within the Defense Communications System. This section examines the impact of AAC applications in the DCS environment and proposes significant areas to be studied and resolved during the contract phase. We also address the effect of time delay differences in either steering or angle diversity systems. The section concludes with a presentation on feasible combiner structures for both analog and digital systems.

5.1 AAC Application for Diffraction and Troposcatter Paths

Transhorizon radio links within the DCS utilize either forward scatter or knife-edge diffraction. Although there are significantly more scatter circuits within the DCS, the use of AAC techniques is to be considered for both modes in order not to limit network availability due to outages on diffraction systems. In the forward scatter mode, diversity must be provided to compensate for the short term (0.1 to 5 Hz fade rates) multipath fading. Outages on these circuits are produced by these short term fading conditions in combination with depressed median signal conditions. The depressed median conditions are most common in winter months and are largely due to substandard refractive gradients which increase the scattering angle and thus the path loss. Outage conditions can be mitigated, therefore, most efficiently by adding additional diversity. If this additional diversity is in the form of angle of arrival diversity, the adaptive combining used in this approach results in a broad optimum for the antenna pointing angle at the receiver.

At the transmitter, depressed median conditions due to substandard refractive index gradients are best alleviated by pointing the antenna on or slightly below the horizon. Thus the requirement for adaptive antenna pointing in a receive angle diversity troposcatter system does not exist. Some of the theoretical considerations supporting this argument are detailed in Section 6 and in Section 7 empirical data from a Bell Laboratories angle diversity test is summarized to establish the existence of the broad optimum in antenna pointing angle.

For diffraction links the reverse situation is encountered. Propagation via the diffraction mode results in reception of a steady nonfading signal which at worst may have a small fading component which will result in Rician fading. If the fading component is absent, no diversity at all is required and if it is present, switched diversity such as that used in land based LOS systems or dual diversity should provide adequate protection. Outage conditions on diffraction links are produced primarily not by short term fading effects as in troposcatter,but by long term changes in the refractive index gradient which produce antenna beam blockage by the earth's surface. This effect is best compensated for by adjustments in the transmit and receive antenna pointing angles. A steered system as opposed to an angle diversity approach is therefore appropriate for the diffraction links within the DCS.

Because of the difficulty of electronically steering large transmitter powers ($\sim$ 10 Kw), mechanical steering of the antenna pointing angle is most attractive. RF Systems, Inc., is developing a design of a weatherized moveable feedhorn structure for a typical DCS antenna configuration. This approach is simple, low cost, and can be easily implemented within a closed loop adaptive system for optimizing the antenna pointing angle.

For troposcatter systems, the angle diversity approach will be reduced to practice and evaluated on the RADC test circuit. Within the study phase of the contract, the troposcatter systems within the DCS will be classified into groups having approximately equal angle diversity characteristics. Performance predictions for dual and quadruple diversity operation with and without additional angle diversity will be developed to assess the performance improvement realizable within the DCS. The RADC tests will provide an important empirical comparison to validate the prediction approach.

5.2 Time Delay Effects

In both steering and angle diversity systems, the larger channel time delay associated with larger antenna pointing angles must be accommodated. The geometry for calculating the increase in mean channel time delay for an increase in pointing angle δ is shown in Fig. 5.1. The chord of length $X\delta$ forms an approximate 90° angle with the line segment X such that

$$\alpha \doteq 90-\theta$$
$$\beta \doteq \theta.$$

Thus

$$Z = \frac{X\delta}{\sin\theta} \doteq \frac{X\delta}{\theta} \qquad (5.1)$$

$$X \cdot Y \doteq Z \cos\theta \doteq Z\ (1-\theta^2/2). \qquad (5.2)$$

The path length differential is

$$Z+Y-X = Z-Z(1-\theta^2/2) = Z\theta^2/2$$
$$\doteq x\delta\theta/2 \doteq d\delta\theta/4 = d^2\delta/4a, \quad a = \text{effective earth radius.} \qquad (5.3)$$

For a 4/3 earth radius the differential delay in nanoseconds is

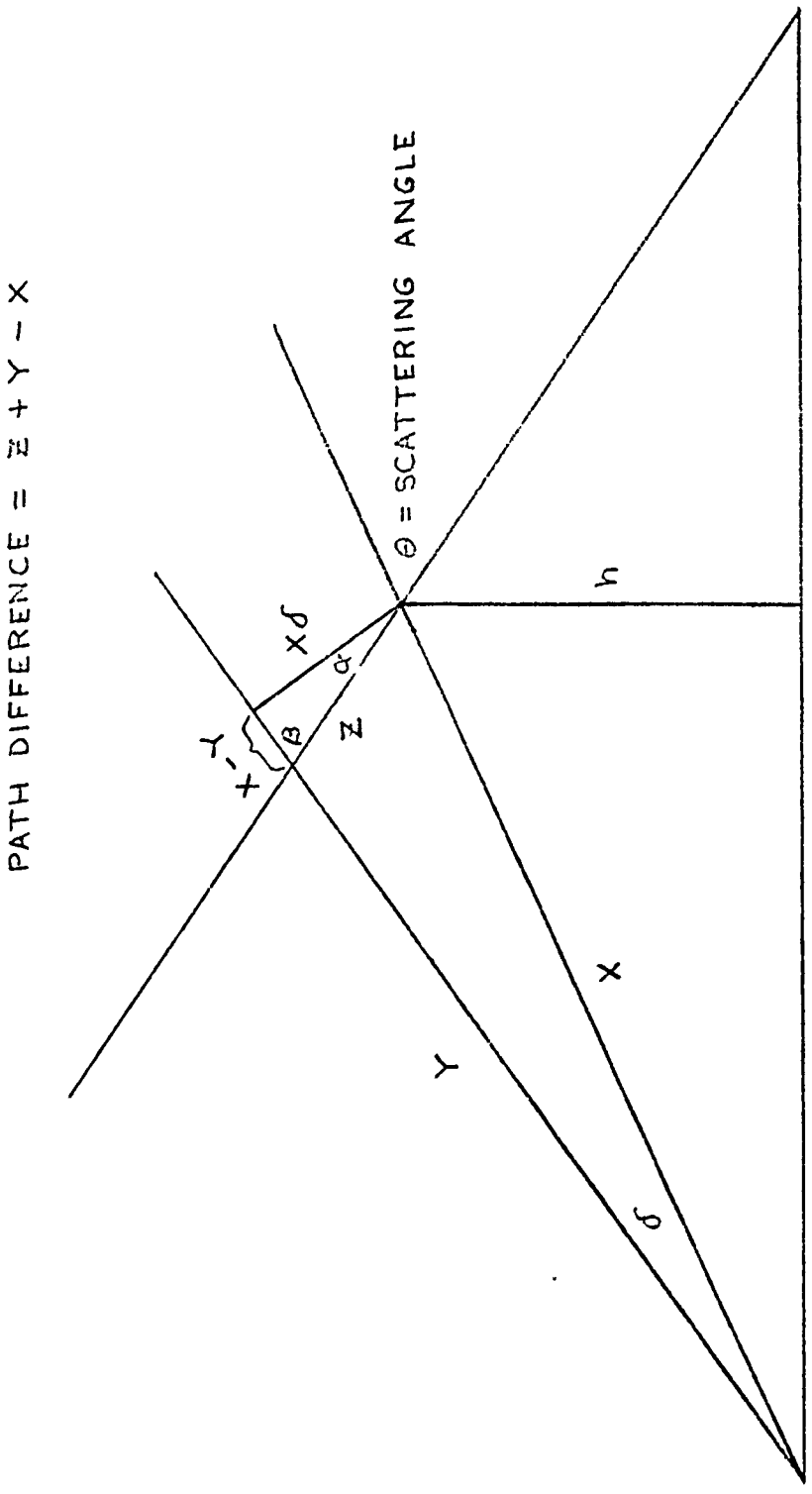

Fig. 5.1 Geometry for Calculation of Differential Delay

$$\text{Differential Delay} = \frac{d^2_{mi}\,\delta_{deg}(5280)}{4(5278)(57.3)} = 0.0044\; d^2_{mi}\,\delta_{deg}. \qquad (5.4)$$

Thus a 1° change in the antenna pointing angle on a 200 mile path will produce approximately 176 nanoseconds of additional delay. The Megabit Digital Troposcatter Subsystem (MDTS) is designed to operate at 1.5,3.1,6.3,9.4, and 12.6 Mb/s. At the highest data rates, the symbol length is 160 nanoseconds and thus steering adjustments in the antenna pointing angle must be made small compared to the symbol length to avoid loss of bit synchronization. Since the steering adjustments compensate for a long term effect, the adjustments can be made with steps which correspond to a differential time delay of a small fraction of a symbol interval. For angle diversity both analog and digital systems will require delay padding of the shortest angle of arrival path in order to compensate for the differential delay. Since the mean path delay for troposcatter and diffraction systems does not vary appreciably with time, an initial delay pad insertion for each feedhorn would eliminate differential delay effects from both an electronically steered system or an angle diversity system.

In angle diversity systems, one must consider the method of diversity combining. Analog and digital systems will be treated separately.

5.3 Diversity Combining/Analog Systems

The combining of independent FDM/FM signals can be accomplished by a well known phase stripping technique [5.1]. The basic concept is illustrated in Fig. 5.2. Using complex notation, the ith diversity signal has some RF phase angle θ_i. After multiplying the diversity signal by a reference signal and removing the modulation by averaging, the received phase angle θ_i can be stripped off by another

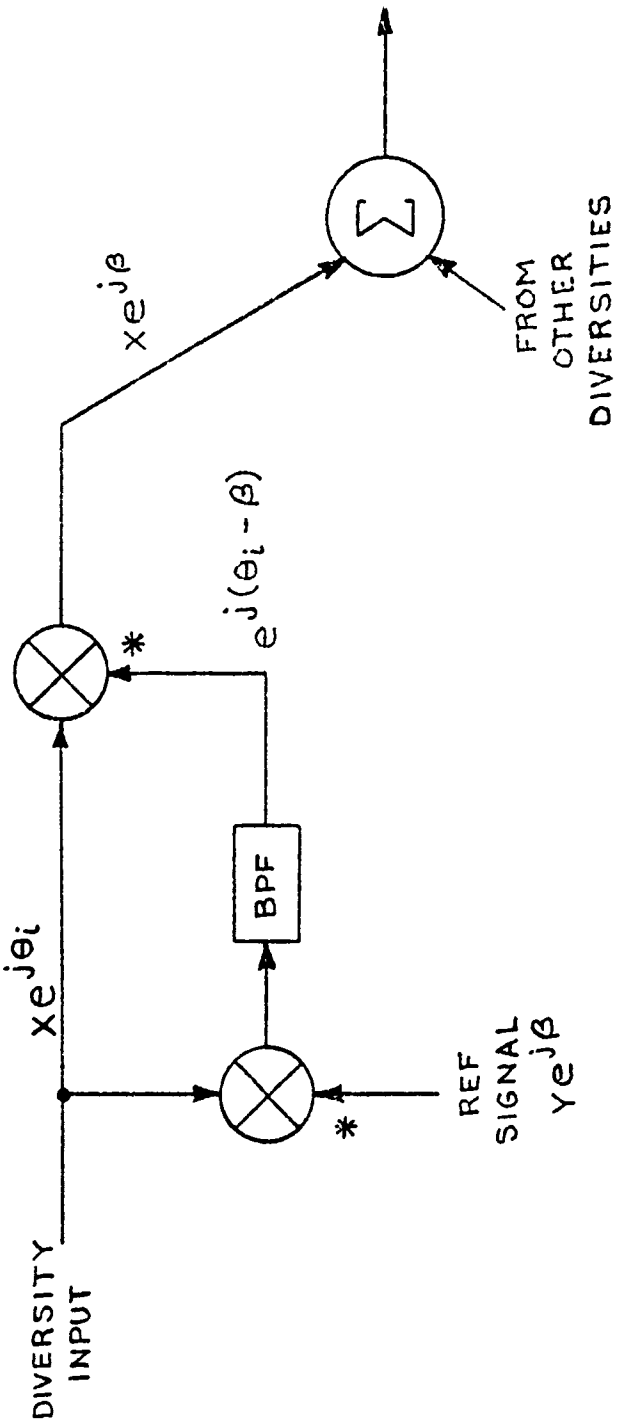

Fig. 5.2 General Analog Diversity Combining Technique

multiplication operation. The early combiners [5.2] used a local oscillator to generate the reference signal and mixers for the multiplication operations. For this combiner the transmitted signal must contain a carrier component for proper operation. The use of mixers instead of multipliers reduces the combiner from maximal ratio to equal gain for which there is not a large performance difference. More recent combiners use a gain controlled version of the combiner output as the reference signal to produce what is termed a regenerative predetection combiner. This type of combiner is stable and does not require a carrier component. The principle of operation can be understood from solution of an eigenvalue problem. For the regenerative predetection combiner, the output can be considered the dot product of diversity multipliers w_i with diversity inputs $xe^{j\theta_i}$

$$y = \sum_{i=1}^{m} w_i^* \, xe^{j\theta_i} = \underline{w}'\underline{x} \tag{5.5}$$

where $xe^{j\theta_i}$ is the ith component of the vector $\underline{x}$.

The reference is Gy and from Fig. 5.2, the weight vector $\underline{w}$ must satisfy the relationship

$$Gy^*\underline{x} = \underline{w}$$

$$\underline{x}\,\underline{x}'\,\underline{w} = \frac{1}{G}\,\underline{w} \tag{5.6}$$

which is an eigenvalue problem. The regenerative predetection combiner operates in an identical manner to the recursion method [5.3] for finding the largest eigenvalue and its eigenvector for the Hermetian matrix $\underline{x}\,\underline{x}'$. It is easy to see that the largest eigenvalue is 1/G and its eigenvector is proportional to $\underline{x}$. Thus in the steady state, the diversity multiplier weight vector is proportional to $\underline{x}$ which both strips off the RF phase and maximal ratio combines the signals i.e., each diversity input $xe^{j\theta_i}$ is multiplied by the complex conjugate of the weight $w_i = xe^{j\theta_i}$. In

the absence of multipath conditions the regenerative predetection combiner is optimu. Although channel multipath in analog systems introduces intermodulation distortion, in well designed analog systems the bandwidth is kept small to avoid these distortion effects. This also insures that the combiner will not fail due to multipath effects. Under extreme multipath conditions, intermodulation distortion and combiner degradation will severely limit analog system performance.

5.4 Diversity Combining/Digital Systems

In digital systems the bandwidth is usually large enough that multipath effects are an important consideration in receiver design. In fact, the multipath can be used to improve performance by using the decorrelation between multipath components to realize an implicit diversity gain. The MDTS modem uses a decision feedback equalizer [5.4] to eliminate intersymbol interference due to multipath and to coherently recombine the multipath components. Diversity combining of channels is accomplished by use of a three tap transversal filter for each diversity signal. In general any diversity combining technique for high speed digital systems must in some manner cope with the presence of significant multipath. The use of a regenerative predetection combiner without special attention to the multipath effect is not possible. The possible approaches for combining of the angle diversity signals include the same approaches for reception of high speed digital data over troposcatter channels. The most successful of these techniques are the equalizer concept used in MDTS and a transmitter time gating approach [5.5] with matched filter detection over the received symbol length. The time gating technique is somewhat simpler to realize because only one signal multiplication per diversity branch is required. The equalizer technique requires two or more (MDTS uses three) signal multiplications per diversity branch. However, the time gating technique requires a time gated transmit signal and its multipath protection

is by necessity limited to less than one symbol interval. Furthermore the time gate at the transmitter increases the system bandwidth by the reciprocal of the duty cycle. The three tap forward filter equalizer used in MDTS can handle multipath delays greater than one symbol interval and this feature is probably an overriding consideration in angle diversity because the elevated beams will have significantly more multipath than the lower beams.

Another advantage of the equalizer structure is its striking similarity to the regenerative perdetection combiner in terms of hardware realization. The operations shown in Fig. 5.2 for the regenerative predetection combiner are identical to the operations required for weight generation and signal multiplication in the MDTS equalizer. The difference between the two systems is the multiplicity of taps for the equalizer and the type of reference signal used. For analog combining the reference is a gain controlled version of the combiner output. For digital combining the reference is a 4PSK error signal which is an instantaneous measure of the difference between the sampled quadrature components before decision making and the resulting decision. The generation of the error signal can be accomplished for any linear modulation modem (PAM,2PSK,QPSK, Staggered QPSK, MSK) by delivering at the modem output at least one quadrature sampled signal from which a comparator makes a decision. From this signal the error signal is formed by taking the sign of the difference of the input and output of a comparator with the same reference level as used in the modem. In many modems the error signal is already available in the form of a quality measure, e.g., pseudo-error techniques for BER estimation.

A combiner which could be used for both analog and digital system combining is shown in Fig. 5.3. For the analog system the reference is the combiner output and only one tap per diversity is

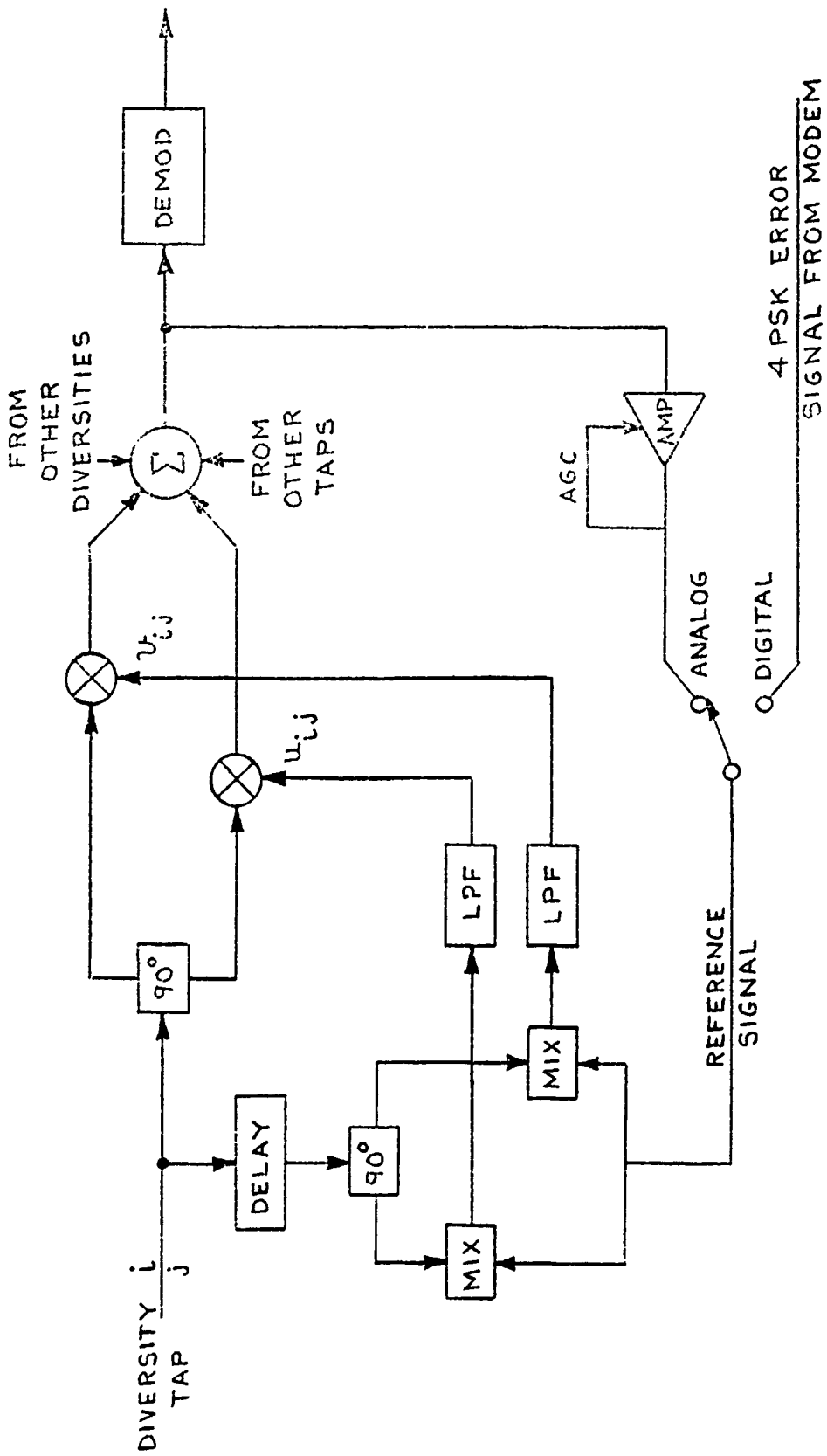

Fig. 5.3 Diversity Combiner for Analog or Digital Systems

used. In the steady state, the weights $w_{il} = u_{il} + jv_i$, $i = 1, 2,...M$, are the optimum weights for a maximal ratio combiner. For the digital system the 4PSK error signal is selected as the reference signal and multiple taps, $j = 1,2,...J$, in a transversal filter configuration are used. In a typical application the taps would be spaced at one-half the symbol interval and the number of taps required would span the multipath spread. For most DCS applications, 3 taps would probably be sufficient.

In the digital mode, the use of an error signal derived from the modem leads to optimum combining of the diversity signals because the sample and hold operations in the modem are included in the combiner optimization. In almost any transhorizon radio modem this error signal is either available in equivalent form or can be easily extracted. In the absence of this error signal, the angle and space diversity channels can be combined in pairs to reduce 8 digital diversity channels to four. The reference for this type of combining is the difference output of a hybrid. The sum output is the combiner output. This type of combining is based on the power inversion principle used to eliminate strong jammers. In a power inversion system the adaptation is used to cancel signals which are identical except for a linear filtering operation. A block diagram of this type combiner is shown in Fig. 5.4. The equalizers adapt to drive the reference signal to a minimum which means the sum output of the hybrid is a combined signal. A major disadvantage of this type combiner is that it attempts to align the phase at every point in time rather than only at the sampling time. Aligning the phase at every point in time is much more difficult and unless a large number of taps are used, the combining may be poor.

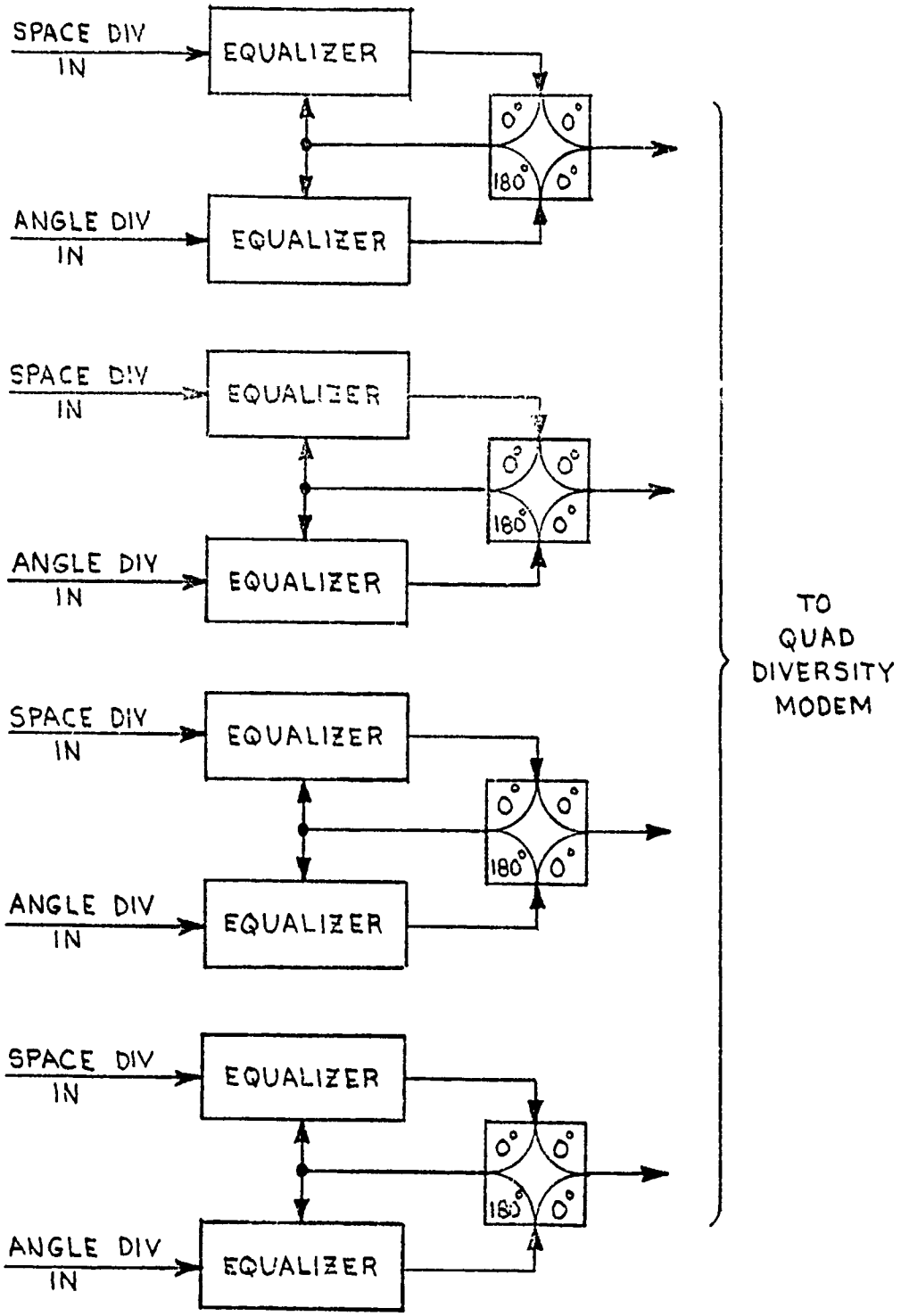

Fig. 5.4 Power Inversion Diversity Combining

In summary, an equalizer combiner can be used to combine DCS FDM/FM signals by operation in an analog mode and it can be used to combine high speed serial data in an optimum manner using a modem supplied error signal or if this signal cannot be obtained, suboptimum combining by power inversion can be used.

5.5 Description of Paths

The two types of communication link under consideration are sketched in Figures 5.5 and 5.6.

On the diffraction link, a physical obstruction (mountain ridge) is within the radio horizon of both the transmitter and receiver; the dominant propagation mode is diffraction from the highest points of this obstruction.

The optimum configuration of antennas for this link involves aiming the antennas so their directions of peak gain are lined up with the rays that terminate at the diffraction point. It will be noted that we have sketched these rays as curved trajectories. This, in fact, is a correct representation of the normal downward-bending of the radio path due to decrease in tropospheric refractive index as altitude increases.

The principal source of suboptimum performance can readily be visualized from the figure: when the refractive index gradient changes as a result of diurnal, seasonal or weather frontal conditions, the curvature of the ray from either antenna to the diffraction point will change, so that the takeoff angle of the ray relative to the local horizon will change. If the antenna boresighting is not changed in a corresponding manner, then the ray will leave the antenna at a direction other than that of maximum gain causing a decrease in received power.

The tropospheric scatter path sketched in Figure 5.6 is significantly different; the propagation mechanism consists of

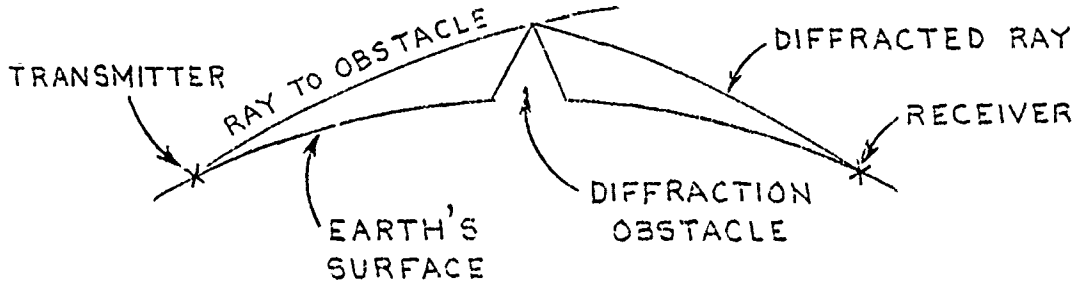

Fig. 5.5 Diffraction Geometry

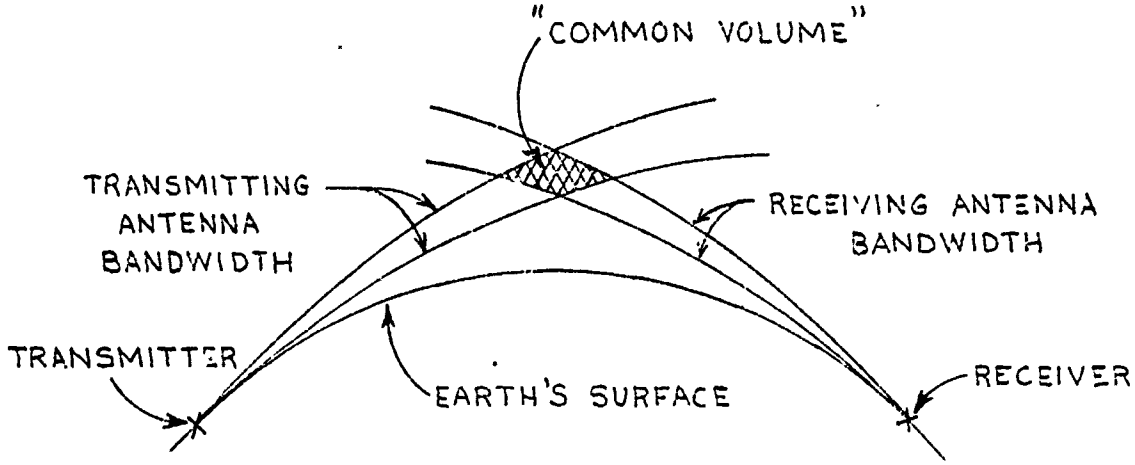

Fig. 5.6 Troposcatter Geometry

scattering from tropospheric inhomogeneities that are simultaneously visible by the transmitting and receiving antennas. Since the scattering mechanism is strongly angle-dependent, most of the scattered energy will arise from points that are at the minimum height permitting mutual visibility. The optimum aiming point for a single beam is correspondingly as close to the horizon as possible. Although refractive index variations can cause changes in performance of scatter circuits, there is no steering technique for single beam antennas that leads to any significant improvement over horizontal aiming. For example, if substandard refractive gradients exist, the propagating rays will more closely approximate straight lines so that the lowest scattering point is at a higher elevation, the scattering angle is greater,and the average path loss increases. However, the strongest signal component still arises from rays emanating at a horizon angle with zero tilt from the antennas.

With superrefractive or ducting conditions, on the other hand, there is a theoretical possibility that a horizontal ray will be bent downward so strongly that it will intersect the ground, and that the rays connecting transmitter and receiver will originate from slightly elevated angles of emission. However, even though these are not at the peak gain of the antenna pattern, the loss is more than compensated by the major increase in field strength accompanying the change from scatter to refractive propagation.

The availability of <u>dual</u> beams from the receiving antenna <u>does</u> permit a performance improvement for tropo paths even in the absence of refractive anomalies through the use of diversity reception techniques. Figure 5.7 illustrates the general principle

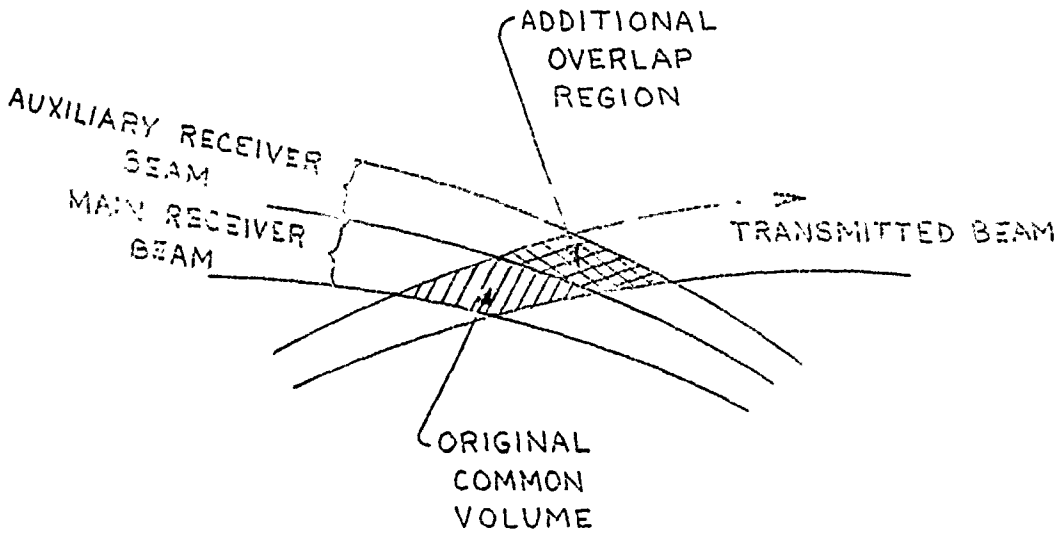

Figure 5.7 Geometry for Angle Diversity

involved. The second receiving antenna beam is elevated from the primary beam and also intersects the transmitted beam; the scatterers in the additional common volume produce a random collection of phasor contributions to the second beam output, yielding an approximately independent fading amplitude on the second beam. In principle, this permits effective doubling of the order of diversity when the appropriate diversity combining equipment is available. The four sources of degradation of this desirable extra diversity improvement are:

(1) Lower power level in upper beam due to greater scattering angle,

(2) Partial correlation of fading due to beam overlap,

(3) Possible degradation of lower beam by inclusion of feed for upper beam, and

(4) Increased multipath dispersion of upper beam.

There are several specific problems that warrant analytical solution for the diffraction and scatter paths.

For the diffraction path the principal problem of interest is the determination of the path elevation angle as a function of refractive index variations. This can be converted into a description of incremental path loss due to effective antenna aiming error for the conventional unsteered antenna, which in turn measures the potential gain from steered beam techniques.

For the tropopath the analytic problems involved are those of computing power level and correlation of the signals on the two beams, and determining the multipath dispersion of each and the correlation between individual multipath components. These and other system performance factors will be considered in the next section.

5.6 References

[5.1] Cutter, Kompfner, Tillotson,"Self Steering Array Repeater"(STAR), BSTJ, September 1963.

[5.2] J.W.Boyhan, "A New Forward Acting Predetection Combiner," IEEE Trans. on Comm. Tech., Vol. COM-15, October 1967, pp. 689-694.

[5.3] F.B. Hildebrand, Methods of Applied Mathematics, Prentice Hall, Englewood Cliffs, N.J., Section 1.2

[5.4] C.J.Grzenda, D.R.Kern, and P. Monsen, "Megabit Digital Troposcatter Subsystem," NTC Conference Record, New Orleans, December 1975, pp. 28-15 to 28-19.

[5.5] M.G.Unkauf, J.B.Gadhoury, "A Simple High Speed Modem for Dispersive Channels," EASCON Conference Record, October 1974, pp. 414.

SECTION 6

SYSTEM PERFORMANCE

The proposed adaptive antenna control system tracks the optimum pointing angle for diffraction link application and combines additional angle of arrival diversity signals in a space/angle or frequency/angle troposcatter application. The performance of this system is of course dependent on the link propagation mode, link geometry, and atmospheric conditions. Prediction of system performance as of function of link and atmospheric paramaters will utilize the propagation model developed in Sections 2 and 3 and a communication system model which defines the performance of the FDM/FM terminal for analog systems and high speed modem for digital systems. In the Bell Laboratories angle diversity test program [6.1], the prediction model was shown to agree well with the experimental results. The analytic base for prediction calculations has been extended from the Bell Laboratories work to include a performance evaluation of high speed data transmission over troposcatter channels. For this communications mode the performance calculation requires an assessment of both the angle diversity improvement and the implicit diversity improvement resulting from coherent combining of decorrelated multipath components.

6.1 Performance Improvement from Beam Steering

Steering of the antenna beam to track the optimum pointing angle will provide performance improvement over fixed beam antenna for transhorizon radio systems which use diffraction as the propagation mode. Experimental evidence is also presented here to show that a broad optimum for the antenna pointing angle exists on angle diversity troposcatter systems. Because of this broad optimum, tracking of the optimum is not deemed necessary for troposcatter.

For both types of communication paths, we are faced with analyses of curved paths over a curved earth, as indicated in Figure 6.1 (a). If we perform a bilinear fractional transformation of the plane including the transmitter, receiver and earth center, we can map the earth center into the point at infinity, the curved earth surface into a horizontal line, and the rays into upward-bending circles. This conformal map preserves the scattering angle at ray intersections, and preserves the angle of a ray with respect to the local horizontal, but simplifies the calculation of all of these angles because of the fixed Cartesian coordinates. Furthermore, in the new geometry the vertical coordinate gives local altitude directly.

The second analytical simplification is the highly accurate one of treating ray segments as parabolic segments rather than circular arcs. We therefore take:

x = horizontal displacement along path relative to midpoint,

h = altitude (same units as x),

and describe rays by a formula of the general type

$$h = A(x-x_o) + B(x-x_o)^2.$$

In this expression x_o is the ground terminal of the ray segment and A is the tangent of the angle the ray segment makes with the ground; for all practical purposes we can take A to be the angle itself, measured in radians.

The parabolic coefficient B is given by

$$B = \frac{1}{2R} + C\nabla N$$

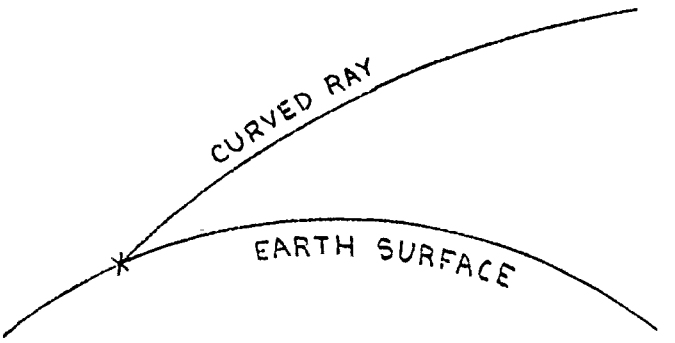

(a) ACTUAL GEOMETRY

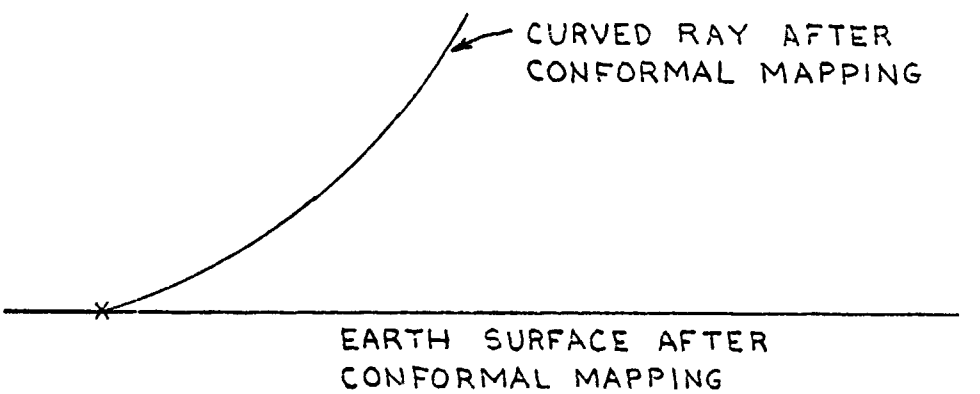

(b) CONFORMALLY-MAPPED GEOMETRY

Fig. 6.1 Conformal Geometry

where R is the actual earth's radius, C is a constant and ∇N is the gradient of the refractive index which is negative in the standard and superrefractive or ducting atmospheres, and positive in the strongly subrefractive atmosphere. It is a convenience for analysis in arbitrary units to rewrite B as

$$B = \frac{1}{2 R_{eff}}$$

where R_{eff} is an effective earth's radius that includes the refraction effects. It will be noted that in the ducting atmosphere we will have negative values of R_{eff}.

We can model a typical diffraction path as consisting of an obstacle of elevation H at x = 0, with transmitter and receiver at -D/2 and D/2 respectively, where D is the total path length. Since the local elevation of a horizontally-aimed ray is

$$h = B(x + D/2)^2,$$

the elevation of the ray at path midpoint is

$$h_o = B\, D^2/4.$$

Clearly, for the diffraction effect to result rather than troposcatter, it must hold that

$$H > B\, D^2/4.$$

Using the 4/3 earth as typical for the standard atmosphere, we have

$$R = 3444 \text{ nmi},$$

$$R_{eff} = 4592 \text{ nmi}$$

so that

$$B = 1.088 \times 10^{-4} (\text{nmi})^{-1}$$

and if

$$D = 100 \text{ nmi}$$

then

$$H > 0.2722 \text{ nmi} = 504 \text{ meters} = 1654 \text{ feet.}$$

For an arbitrary value of H and D, the ray to the obstacle from the transmitter is given by the equation

$$h = A(x + D/a) + B(x + D/2)^2,$$

so that at $x = 0$ we have

$$H = A\ D/2 + B\ D^2/4,$$

and consequently the ray takeoff angle A is given by

$$A = (2/D)\ (H - BD^2/4).$$

The condition for ducting is that the refractive gradient be

$$\Delta N \approx -157 \text{ N-units/km.}$$

The normal refractive index gradient is about 1/4 to 1/3 of the ducting value, corresponding to effective earth radius equal to 4/3 to 3/2 of actual earth radius. In most locations on the earth, gradients ranging from

$$\Delta N = +50$$

to

$$\Delta N = -150$$

are the only values that will be seen for any appreciable percentage of the time. The corresponding effective earth radius will range from about 3/4 actual radius up to approximately infinity while the corresponding B values will range from

$B = 0$ (superrefractive)

through $B = 1.1 \times 10^{-4} (\text{nmi})^{-1}$ standard

to $B = 1.9 \times 10^{-4} (\text{nmi})^{-1}$, subrefractive.

From the previous formula for takeoff angle we see that

$$A_{min} \approx 2H/D - 10^{-4}\ D \quad \text{when } B \approx 2 \times 10^{-4}$$

$$A_{max} \approx 2H/D \quad \text{when } B \approx 0$$

so that

$$A_{max} - A_{min} \approx 10^{-4} D$$

no matter what the obstacle height. Thus, the variation in take-off angle for a knife-edge diffraction link is porportional to link distance and independent of obstacle height.

A path length of 175 nautical miles could therefore have a spread of elevation angles of 1° or upward and downward fluctuations of $\frac{1}{2}^{\circ}$. Correspondingly fixed-steered antennas with 1° beam width at each terminal could experience a 3 dB loss at each terminal, while $\frac{1}{2}^{\circ}$ beam width antennas could experience a complete loss of signal. Thus for diffraction systems, steering can eliminate complete outage conditions due to changes in the refractive index gradient.

The potential performance improvement from optimum antenna pointing under varying refractive index conditions is small for the forward scatter mode. Considerable empirical data to support this result has been collected and evaluated in a beam steering experiment conducted during the Bell Laboratories angle diversity tests[6.1].

In these tests three vertical feedhorns were used to receive angle of arrival signals and antenna pointing at the receiver was accomplished by movement under manual control of the 60' parabolic reflector. The path length was 180 miles and a frequency of 2.1 GHz was used in the tests.

The beam swinging experiment consisted of 33 days of data collection spaced between September 24 and December 30, 1970. The data consisted of measuring the median received powers for each feedhorn as a function of antenna pointing angle. The antenna at the Crawford Hill receiver has a beamwidth of 0.6° and was varied in 0.2° steps between elevation angles of -0.6° to 0.8°. The elevation angle is defined as the angle between the beam center

of the main feedhorn and the horizontal. The horizon ray was depressed by 0.1^{o} so boresight on the horizon corresponded to -0.1^{o}. The data was reduced by calculating the outage probability for dual and triple angle diversity for each of the 33 experiments. For each of the experiments the optimum pointing angle was determined at each outage level. Deviation from the optimum by as much as a 1/2 beamwidth in either direction produced little change in the outage level. The following table* which is a computer printout of the reduced data for the October 20 experiment is typical of all the experiments in revealing the broad optimum for antenna pointing angle. Higher order diversity systems would sharpen the optimum by the Dth power of the outage probabilities determined. The optimum still remains broad, however, and one concludes that there is little performance improvement to be realized by adaptive steering of a vertical angle diversity system.

6.2 Performance Improvement for Angle Diversity

The performance improvement for angle diversity systems depends on the

(1) system and link configuration
(2) diversity configuration
(3) received power per diversity channel
(4) correlation between diversity signals and
(5) multipath structure.

We have outlined system trade-off considerations which suggest a vertical angle diversity augmentation to existing troposcatter systems. The elevated angle diversity beams can be derived from placing feedhorns below the main beam feedhorn. Since it is desirable to place the beams close together in the sky, a replacement

*Subtract 1^{o} from the reference elevation readings to obtain the elevation angle defined in the text.

MEDIAN SIGNAL STRENGTHS AND STANDARD DEVIATIONS

ELEVATION	HORN 1		HORN 2		HORN 3	
1.8	-85.00	2.2	-91.43	2.5	-110.00	2.5
1.6	-85.42	1.6	-88.57	2.4	-111.67	2.6
1.4	-84.44	1.2	-92.83	3.8	-105.00	4.5
1.2	-82.78	1.1	-94.57	1.2	-103.00	2.2
1.0	-85.42	1.1	-90.05	2.8	-103.13	2.3
0.8	-89.33	1.0	-89.24	1.0	-101.88	1.1
0.6	-94.11	1.1	-82.59	1.1	-96.00	3.7
0.4	-102.50	1.2	-83.33	1.0	-96.00	3.1
0.2	-101.00	1.2	-83.18	1.1	-95.33	1.1
0.0	-102.00	1.0	-84.70	0.9	-91.43	2.4

OUTAGE PROBABILITIES - DUAL DIVERSITY - HORNS 1 AND 2

OUTAGE LEVEL ELEVATION	-95.00	-100.00	-105.00	-110.00	-115.00
1.8	0.350-01	0.500-02	0.560-03	0.580-04	0.590-05
1.6	0.370-01	0.510-02	0.570-03	0.590-04	0.600-05
1.4	0.110-01	0.120-02	0.130-03	0.130-04	0.130-05
1.2	0.100-01	0.120-02	0.130-03	0.130-04	0.130-05
1.0	0.090-02	0.100-02	0.100-03	0.100-04	0.100-05
0.8	0.160-01	0.170-02	0.170-03	0.180-04	0.180-05
0.6	0.130-01	0.160-02	0.170-03	0.180-04	0.180-05
0.4	0.350-01	0.430-02	0.480-03	0.500-04	0.510-05
0.2	0.300-01	0.490-02	0.570-03	0.610-04	0.620-05
0.0	0.450-01	0.850-02	0.100-02	0.110-03	0.110-04
OPTIMUM ANGLE	1.0	1.0	1.0	1.0	1.0

OUTAGE PROBABILITIES - TRIPLE DIVERSITY - HORNS 1,2 AND 3

OUTAGE LEVEL ELEVATION	-95.00	-100.00	-105.00	-110.00	-115.00
1.8	0.330-01	0.390-02	0.260-03	0.110-04	0.410-06
1.6	0.350-01	0.420-02	0.320-03	0.160-04	0.600-06
1.4	0.840-02	0.570-03	0.250-04	0.890-06	0.290-07
1.2	0.800-02	0.560-03	0.250-04	0.890-06	0.290-07
1.0	0.620-02	0.350-03	0.140-04	0.480-06	0.150-07
0.8	0.910-02	0.470-03	0.180-04	0.610-06	0.200-07
0.6	0.340-02	0.140-03	0.490-05	0.160-06	0.520-08
0.4	0.990-02	0.500-03	0.240-04	0.820-06	0.260-07
0.2	0.720-02	0.380-03	0.140-04	0.490-06	0.160-07
0.0	0.520-02	0.270-03	0.100-04	0.350-06	0.110-07
OPTIMUM ANGLE	0.6	0.6	0.6	0.6	0.6

RATIO OF DUAL TO TRIPLE OUTAGE AT OPTIMUM ANGLES

OUTAGE LEVEL	-95.00	-100.00	-105.00	-110.00	-115.00
RATIO	0.361015	0.142427	0.048015	0.015534	0.004948

of the existing feedhorn structure with a new structure with smaller feedhorns for each beam has been suggested. In almost all link applications, no more than dual angle diversity will be recommended as an effective cost and performance system improvement.

Diversity configurations are identified by the number of different diversity types and in almost all applications the total diversity order is equal to the product of the number of diversity channels in each type. Thus a N_1 space (S), N_2 frequency (F), N_3 angle (A), and N_4 polarization (P) system would have a total of $N_1\ N_2\ N_3\ N_4$ diversity channels. Note that the effective diversity order may be smaller than this product. Some of the most typical diversity configurations are summarized in Table 6.1.

Table 6.1

Diversity Configurations

Diversity Type	Total Diversity Order	Number of Power Amplifiers	Additional Power Factor
2S	2	1	0 dB
2F	2	2	3
2A	2	1	0
2S/2F	4	2	3
2S/2A	4	1	0
2S/2F/2A	8	2	3
2S/2P/2A	8*	2	3

Note that the system with additional frequencies or polarization require an additional power amplifier to realize the same received diversity signal-to-noise ratio. Thus, the space and/or

*The effective diversity order for this system is approximately 6th order due to correlation of the cross paths [6.3].

angle diversity systems enjoy an initial 3 dB advantage for a fixed transmitted power. Since any reasonable performance comparison should be based on the same transmitted power for the compared systems, the relative dB advantages and performance curves will be normalized to a 0 dB power factor or equivalently a single power amplifier. One should recognize that multiple frequency systems require two power amplifiers (since the amplifiers are operated in saturation, signals cannot be combined prior to final amplification) and thus the 3 dB disadvantage of frequency diversity systems is reflected in additional cost rather than system performance margin.

The received power per diversity channel, the correlation statistics, and the multipath structure for the performance analysis will be determined using NBS prediction methods to obtain the main beam path loss distribution and the results of the prediction model described in Sections 2 and 3 for computation of coupling loss, relative received power, and the cross-channel multipath profile, $Q_{\ell m}(\xi)$. This profile is a complete description of the correlation and statistical properties of the multi-filter uncorrelated scatter channel. Before discussing in greater detail the computations required for performance assessment of digital systems, we consider first analog system performance.

For analog systems, diversity improvement is measured by the outage distribution, i.e., the probability that a given fade depth will be exceeded. The predetection combiner outlined in Section 5.3 provides maximal ratio combining for which the outage distribution can be calculated for unequal and correlated diversity branches by a transformation of the complex Gaussian received processes to a set of independent received processes. This is a standard calculation for correlation diversity systems [6.2] and the details are omitted. The outage distribution for analog transmission over the

C-band RADC test link configured for dual vertical angle diversity has been computed as an example. For a 168 mile path with 28 foot antennas at 4.46 GHz, the elevated beam has a relative loss of 1.7 dB and a power correlation coefficient of 0.52. Antenna sidelobes were not included in this first calculation but the computer program is being modified to incorporate their effect. The calculated outage distribution for this C-band troposcatter link is given in Fig.6.2.

The dual space/dual frequency curve assumes only one power amplifier at the transmitter which is all that is required for a dual space/dual angle system. The conventional quad diversity configuration uses two power amplifiers which also could be used in the dual/space dual angle configuration to improve performance by 3 dB. The dual space/dual frequency/dual angle also assumes one power amplifier and could be improved by 3 dB with the use of the second power amplifier present in a conventional configuration. The improvement of an eighth order system using angle diversity over a conventional quad system is seen to be 7 dB for an outage level of 0.001%.

It is generally desirable to use two power amplifiers in an operational situation in order to provide redundancy in case of amplifier failure. A dual space/dual angle configuration requires the use of two power amplifiers at the same frequency. One approach to accomplish the end is to add the power amplifier outputs in a summer and direct the sum port output to one antenna and the difference port output to the other antenna. To reduce the scalloping of the antenna pattern resulting from equal power/displaced antennas, a phase shifter at the exciter output of one transmitter can be used to minimize one of the splitter outputs.

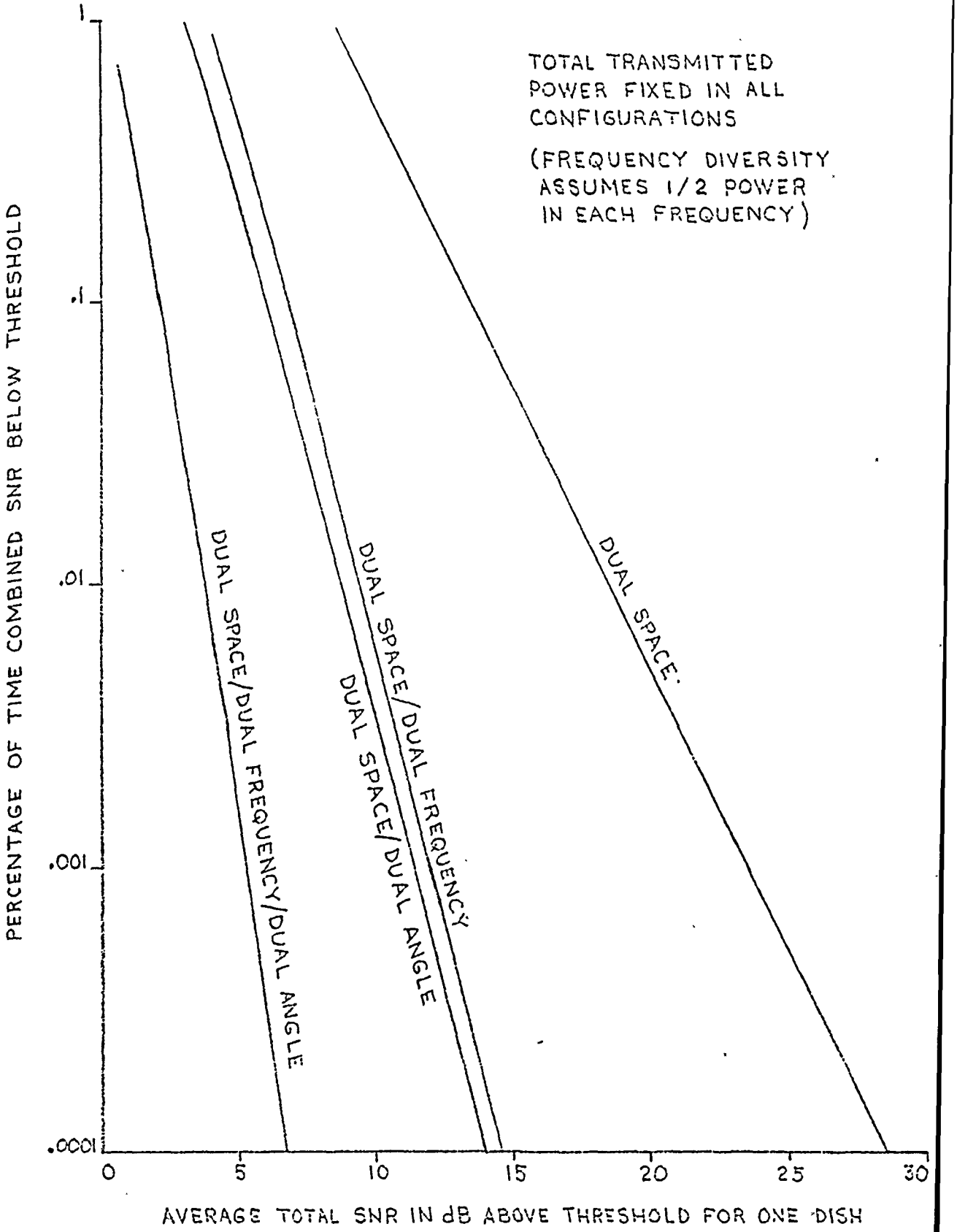

Fig. 6.2 Outage Distribution

For digital systems the improvement due to angle diversity must include the capability of modern modems, e.g., MDTS, DAR-4, to realize implicit diversity from multipath contributions. This is particularly important with angle diversity because the elevated beam contains more multipath. We outline here a performance prediction model for the MDTS modem which will be useful for predicting performance during the proposed digital data tests on the RADC link and for projecting the angle diversity performance on DCS links in general.

The performance prediction model is an analysis which computes the average BER as a function of the ratio of average bit energy to noise power in 1 Hz, i.e., E_B/N_o. The computation includes the MDTS modem degradations which significantly affect the average BER. These degradations account for approximately a 2 to 3 dB shift from the ideal CPSK error probability curve. The major contributors the degradations are (1) imperfect 90^o splitters in the transmitter and receiver, (2) non ideal matched filtering, (3) time tracker offset, (4) and adaptive equalizer misadjustment. The analysis considers the number N of forward equalizer taps per diversity channel as the rank of a linear vector space. For the complex Gaussian uncorrelated scattering troposcatter model, an orthogonal transformation exists in this vector space which converts the available implicit diversity and correlated angle diversity into independently fading diversity channels. Each of these diversity channels has the fraction λ_i, $i = 1,2,...N$ of the average E_B/N_o associated with it. The λ_i's are the eigenvalues for the transformation and they satisfy

$$\sum_{i=1}^{N} \lambda_i \leq 1, \quad 0 < \lambda_i, \quad i = 1,2,...N.$$

In a manner of speaking the analysis converts the implicit diversity and correlated angle diversity structure present in the function $Q_{\ell m}(\xi)$ to an angle diversity structure with each angle diversity path receiving independent power contributions λ_i, $i = 1,2,...N$ of the average received power.

The computation of the optimum equalizer weights after this transformation is tribial as the equalizer reduces to the maximal ratio combiner. Since the average BER performance for the latter is well known for PSK systems, the orthogonal transformation make calculation of the average BER as a function of implicit diversity possible. The orthogonal transformation considers only one bit and neglects intersymbol interference.

Because the intersymbol interference is neglected the performance calculated is a lower bound which ignores the loss in implicit diversity due to the need to remove intersymbol interference. This loss which is termed the intersymbol interference penalty is less than a dB for small to moderate multipath spreads,e.g.,ratios of twice the rms multipath spread (2σ) to baud length (T), which satisfy

$$2\sigma/T < 0.5.$$

For the larger ratios the intersymbol interference penalty is larger and the bound is not tight. A mathematical model to include the effects of intersymbol interference and thus obtain performance predictions for $2\sigma/T > 0.5$ has been developed. The model validity has been established by comparing the model results with MDTS simulator and empirical results. Currently a computer program modification of the model to include the effects of angle diversity correlation is being undertaken. The modification will utilize the numerical integration outputs of the analytic procedure described in Sections 2 and 3 for determining the cross-channel multipath profile $Q_{\ell m}(\xi)$.

In the next interim technical report, a description of the modem prediction technique for angle diversity channels will be given along with performance results for typical and actual troposcatter link configurations.

6.3 References

[6.1] P.Monsen, "Performance of an experimental angle diversity troposcatter system, IEEE Trans. on Comm., Vol COM-20, No.2, April 1972, pp.242-247.

[6.2] Schwartz, Bennett, Stein, Communication Systems and Techniques, McGraw-Hill, 1966, Chapter 10.

[6.3] E.F.Florman, "Comparison of space-polarization and space-frequency diversities," IEEE Transaction on Comm. Technology, Vol. COM-16, No. 2, April 1968.

APPENDIX A

SCATTERED FIELD SOLUTION

In this appendix the solution from Maxwell's equations of the scattered field at the receive antenna is obtained in terms of the incident field in the scattering volume and the refractive index fluctuations. The derivation is based on the original scattering field solution derived by Tatarski .*

Consider the tropospheric scatter geometry shown in Fig. A.1. For an incident field distribution $\underline{A}(\underline{r}')$ in the scattering volume we wish to determine the electric field at the observation point $\underline{r}$ from the origin O near the center of the scattering volume. Because of the distance between scattering volume and antennas we can take both the incident and scattered fields to be plane.

We assume that the magnetic permeability u is unity. The permittivity ϵ and the refractive index n are related by $\epsilon = n^2$. The refractive index is composed of a fixed mean value $\bar{n}$ near unity and a random component n_1.

$$n = \bar{n} + n_1$$

It is the presence of the random component which produces scattered energy back to the receiver on the earth's surface. Without loss of generality we can take the mean value of the refractive index to be unity and account for any deviations from this assumption by replacing the propagation constant

$$k = \frac{\omega}{c} = 2\pi/\lambda$$

---

*V.I.Tatarski ,"Wave Propagation in a Turbulent Medium," Translated by R.A.Silverman, McGraw-Hill,New York,N.Y., 1961.

$$\underline{m} = \frac{\underline{r}' - \underline{s}}{|\underline{r}' - \underline{s}|}$$

$$\underline{n} = \frac{\underline{r} - \underline{r}'}{|\underline{r} - \underline{r}'|}$$

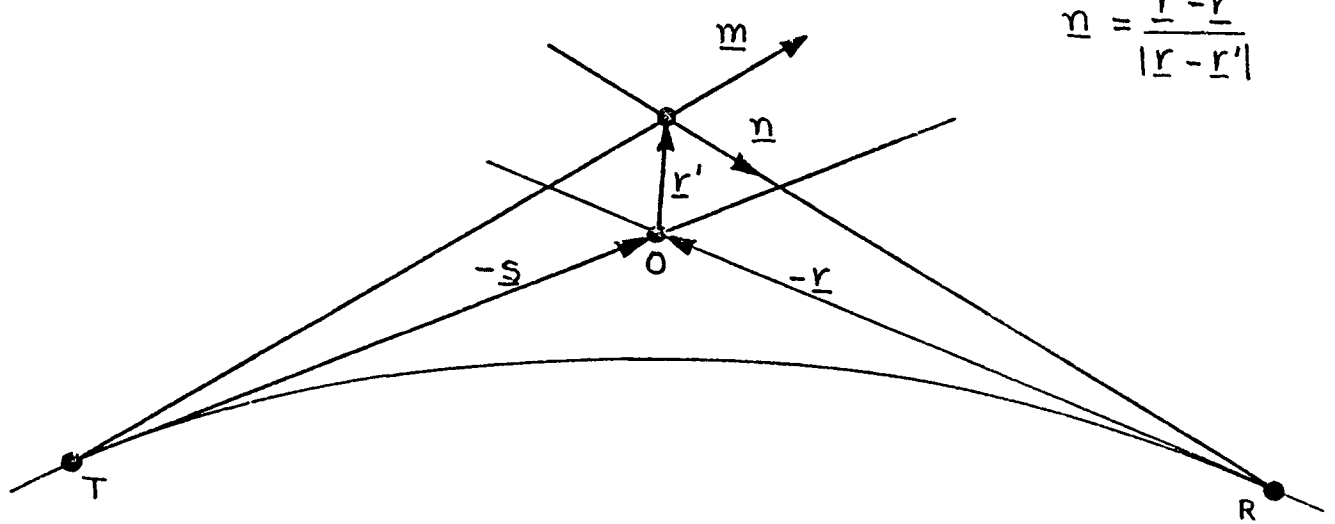

Fig. A.1 Troposcatter Geometry

by $k\bar{n}$ in the final results. We assume an $e^{-j\omega t}$ time dependence and thus Maxwell's equations in CGS units take the form

$$\nabla \times \underline{E} = jk\underline{H} \tag{A.1}$$

$$\nabla \times \underline{H} = -jk\epsilon\underline{E} \tag{A.2}$$

$$\nabla \cdot \epsilon\underline{E} = 0 \quad . \tag{A.3}$$

The permittivity ϵ because of its random component must be considered as a spatial variable. Using the identity

$$\nabla \times (\nabla \times \underline{E}) = -\nabla^2\underline{E} + \nabla(\nabla \cdot \underline{E})$$

and the first of Maxwell's equations, we obtain

$$-\nabla^2\underline{E} + \nabla(\nabla \cdot \underline{E}) = \nabla \times (jk\underline{H}) = k^2\epsilon\underline{E} \; . \tag{A.4}$$

From the divergence equation

$$0 = \nabla \cdot \epsilon\underline{E} = \epsilon\nabla \cdot \underline{E} + \underline{E} \cdot \nabla\epsilon \tag{A.5}$$

or

$$\nabla \cdot \underline{E} = -\frac{1}{\epsilon}\,\underline{E} \cdot \nabla\epsilon = -\underline{E} - \nabla \ell n \epsilon .$$

Combining (A.4) and (A.5) we have

$$-\nabla^2\underline{E} - \nabla(\underline{E} \cdot \nabla \ell n \epsilon) = k^2\epsilon^2\underline{E}$$

or

$$\nabla^2\underline{E} + 2\nabla(\underline{E} \cdot \nabla \ell n n) + k^2 n\underline{E} = 0 \tag{A.6}$$

where we have substituted $\epsilon = n^2$. We assume that the fluctuations of the refractive index are small compared to the mean, i.e.,

$$\overline{n_1^2} \ll 1$$

so that we can make an expansion of the electric field of the form

$$\underline{E} = \underline{E}_o + \underline{E}_1 + \underline{E}_2 + \ldots$$

where

E_i is the order smallness of n_1^i.

Keeping only the first two terms of the electric field, and using the first order approximation $\ell n(1+n_1) \doteq n_1$, the expression in terms of the first two field component becomes

$$\nabla^2(\underline{E}_o + \underline{E}_1) + 2\nabla\left[(\underline{E}_o + \underline{E}_1)\cdot\nabla n_1\right] + k^2(1+2n_1)(\underline{E}_o + \underline{E}_1) = 0.$$

If we group terms of order 1 and n_1, we have

$$\nabla^2\underline{E}_o + k^2\underline{E}_o = 0 \tag{A.7}$$

$$\nabla^2\underline{E}_1 + k^2\,\underline{E}_1 + 2k^2 n_1\underline{E}_o + 2\nabla(\underline{E}_o\cdot\nabla\underline{n}) = 0 \tag{A.8}$$

The solution to (A.7) at a field point $\underline{r}$ is the spherical wave

$$\underline{E}_o = \underline{A}_o(\underline{r})\; e^{j\underline{k}\cdot\underline{r}}$$

which is taken as the incident wave with propagation vector $\underline{k}=k(\underline{r}/r)$. The cartesian components of (A8) are of the form

$$\nabla^2 u + k^2 u = f(\underline{r})$$

which has the Green's function solution

$$u(\underline{r}) = -\frac{1}{4\pi}\int_V f(\underline{r}')\;\frac{e^{jk|\underline{r}-\underline{r}'|}}{|\underline{r}-\underline{r}'|}\;d^3r' \tag{A.9}$$

where $\underline{r}'$ is a variable vector ranging over the scatter volume V. Since the receive antenna is much farther away than the linear dimension of the scattering volume, the denominator in (A.9) can be approximated by $|\underline{r}|=r$. The solution for the scattered field is then

$$\underline{E}_1(\underline{r}) = \frac{k^2}{2\pi r} \int_v \underline{E}_o(\underline{r}')\ n_1(\underline{r}')\ e^{jk(|\underline{r}-\underline{r}'|)}\ d^3r'$$

$$+ \frac{1}{2\pi r} \int_v e^{jk|\underline{r}-\underline{r}'|}\ \nabla(\underline{E}_o \cdot \nabla n_1)\ d^3r' \triangleq I_1 + I_2.$$

The second integral can be integrated by parts (using Gauss's Theorem)

$$\int_v x\ \nabla y = \int_s xy - \int_v y \nabla x$$

and the surface integral disappears since the volume can be made large enough that the integrand is negligible. Thus

$$I_2 = -\frac{1}{2\pi r} \int_v (\underline{E}_o \cdot \nabla n_1)\ \nabla e^{jk|\underline{r} - \underline{r}'|}\ d^3r'$$

$$= -\frac{jk}{2\pi r} \int_v (\underline{E}_o \cdot \nabla n_1)\ e^{jk|\underline{r} - \underline{r}'|}\ \frac{-\underline{r}+\underline{r}'}{|\underline{r}-\underline{r}'|}\ d^3r'$$

$$\doteq \frac{jk}{2\pi r}\ \underline{a}r \int_v (\underline{E}_o \cdot \nabla n_1)\ e^{jk|\underline{r}-\underline{r}'|}\ d^3r'$$

where $\underline{a}_r$ is the unit vector $\underline{r}/r$. Integrating by parts again and neglecting the surface integral gives

$$I_2 = \frac{-jk}{2\pi r}\ \underline{a}_r \int_v n_1\ \nabla \cdot \underline{E}_o\ e^{jk|\underline{r}-\underline{r}'|}\ d^3r'$$

and

$$\nabla \cdot \underline{E}_o \, e^{jk|\underline{r}-\underline{r}'|} = e^{jk|\underline{r}-\underline{r}'|} \, \nabla \cdot \underline{E}_o + \underline{E}_o \cdot \nabla e^{jk|\underline{r}-\underline{r}'|}$$

$$= 0 + jke^{jk|\underline{r}-\underline{r}'|} \, \underline{E}_o \cdot \frac{-\underline{r}+\underline{r}'}{|\underline{r}-\underline{r}'|}$$

$$\doteq -jke^{jk|\underline{r}-\underline{r}'|} \underline{E}_o \cdot \underline{a}_r$$

where we have used the fact that the divergence of the incident field is zero. The two integrals are now seen to be identical except for their vector direction. The scattered field is thus

$$\underline{E}_1 = \frac{k^2}{2\pi r} \int_v \left[\underline{E}_o - \underline{a}_r (\underline{E}_o \cdot \underline{a}_r) \right] n_1 \, e^{jk|\underline{r}-\underline{r}'|} \, d^3r' \, .$$

The vector $\underline{E}_1$ is easily seen to be perpendicular to the unit vector $\underline{a}_r$. Let $\underline{a}_1$ be any unit vector satisfying $\underline{a}_1 \cdot \underline{a}_r = 0$, then

$$\underline{E}_1 \cdot \underline{a}_1 = \frac{k^2}{2\pi r} \int_v (\underline{a}_1 \cdot \underline{E}_o) \, n_1 \, e^{jk|\underline{r}-\underline{r}'|} d^3r'$$

$$\underline{E}_1 \cdot \underline{a}_r = 0.$$

The incident field $\underline{E}_o$ has a vector direction which makes an angle with the unit vector to the source $\underline{a}_r$ of $90^o - \theta$. where θ is the scattering angle. For small scattering angles, the dot product $\underline{a}_1 \cdot \underline{E}_o$ is approximately equal to the incident field function $A_o(\underline{r}') \, e^{jk\underline{m}\cdot\underline{r}'}$. Thus the electric field at the receiving antenna is a transverse plane wave with amplitude

$$E_1(r) = \frac{k^2}{2\pi r} \int_v A_o(\underline{r}') n_1(\underline{r}') \, e^{jk(|\underline{r}-\underline{r}'| + \underline{m}\cdot\underline{r}')} \, d^3r'$$

which is the expression used in Section 2 to derive the cross-channel multipath profile.

Distribution List
Interim Technical Report - Adaptive Antenna Control

No. Copies	Code	Address
3	W15P8E	Commander US Army Electronics Command ATTN: DRSEL-NL-RM-3 Fort Monmouth, N.J. 07703
2	CCM-RD	Commander US Army Communications Systems Agency ATTN: CCM-RD Fort Monmouth, N.J. 07703
2	DCEC Code R220	Director Defense Communications Engineering Center ATTN: Code R220 1860 Wiehle Avenue Reston, VA 22099
12		Defense Documentation Center ATTN: DDC-TCA Cameron Station (Bldg. 5) Alexandria, VA 22314